[redacted]

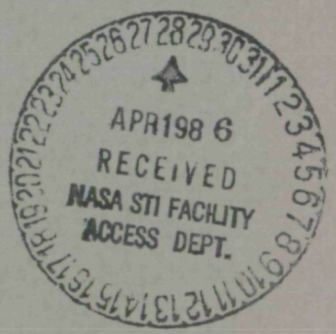

SRS

TECHNOLOGIES

SRS/STD-TR86-014
535

BEARING TESTER DATA COMPILATION, ANALYSIS, AND REPORTING AND BEARING MATH MODELING

ANNUAL REPORT

JANUARY, 1986

PARPARED BY

SRS TECHNOLOGIES
Systems Technology Division
Aerospace and Commercial Systems Department
555 Sparkman Drive; Suite 1406
Huntsville, AL 35805

Under Contract NAS8-36183

FOR THE

George C. Marshall Space Flight Center
National Aeronautics and Space Administration

SYSTEMS TECHNOLOGY DIVISION

555 SPARKMAN DRIVE/SUITE 1406
HUNTSVILLE, ALABAMA 35816-3425
(205) 830-0375

FOREWORD

This report was prepared by SRS Technologies - Systems Technology Division under Contract No. NAS8-36183 entitled "Bearing Tester Data Compilation, Analysis, and Reporting and Bearing Math Modeling" for the George C. Marshall Space Flight Center of the National Aeronautics and Space Administration. The work was administered under the technical direction of the Materials and Processes Laboratory, Engineering Physics Division of the George C. Marshall Space Flight Center with Mr. Fred J. Dolan acting as project manager.

This report describes the work performed during the January, 1985 - December, 1985 period. Joseph C. Cody served as the SRS Technologies Project Manager. The project technical support staff included:

Dr. Ashoke Ghosh
Dr. Alok K. Majumdar
Dr. D. David Marshall
David E. Marty
M. Anthony Stone
Bruce K. Tiller
Glen P. Westrich.

CONTENTS

LIST OF EXHIBITS

LIST OF EXHIBITS (Continued)

LIST OF EXHIBITS (Continued)

1.0 INTRODUCTION

This report describes the work accomplished during the contract period January - December, 1985 in support of the MSFC Bearing and Seal Materials Tester (BSMT) Program. The objective of this activity is to support the development and operation of the BSMT, including data reduction and evaluation. Since the Space Shuttle Main Engine (SSME) turbopump bearings operate in an environment considerably more severe than conventional bearing systems, traditional analysis methods and bearing life models are not directly applicable.

The MSFC BSMT Program is therefore directed toward a better understanding of the various parameters that effect or determine the SSME turbopump bearing operational characteristics and service life and to develop and verify design tools applicable to these systems. Support of this program involves a broad spectrum of engineering analysis activities including static analysis of the BSMT Shaft Bearing System, high-speed bearing system analysis, contact stress evaluation, bearing failure mode evaluation, and thermal modeling of the bearing and cryogenic flow system. The tasks described in this report do not represent the total analysis effort for the design and development of the BSMT. The enclosed work was done to support the development of the BSMT in specialized areas as problems occurred and to support the stated objectives. BSMT test data are reduced, evaluated, and correlated with analyses where applicable. Since test data applicable to the turbopump bearing system is limited and the system and operating conditions are of such complexity that theoretical modeling requires unprecedented extrapolations, additional data from the BSMT are required to fully substantiate turbopump bearing analysis results and bearing life predictions.

2.0 SUMMARY

During this annual reporting period, a test condition data base has been developed for the BSMT program which permits rapid retrieval of test data for trend analysis and evaluation. The data base has been used to update several trend analyses relating heat generation to shaft speed and coolant flow, and bearing outer race temperatures to run time and coolant flow.

Approximately 1.2 hours of run time was accumulated in LN_2 for the turbine-end bearing (57 mm bearing). These bearings were operated at a shaft speed of 30,000 RPM, axial load of approximately 1,700 lbs, and a coolant flow of 4.6 lbs/sec. At the end of this period surface distress was evident for bearing Number 2, and outer race temperature spikes indicated intermittent ball skidding which was confirmed by borescope inspection. Subsequent to the above tests, the coolant flow was increased to 9 lbs/sec which eliminated the temperature spikes and lowered the average outer race temperature rise by about 20°F.

The complex two phase rotational flow field within the bearing, and lack of comparible test data, makes estimates of heat transfer coefficients inexact at best. The operation of the BSMT has shed considerable light on the magnitude of heat generation due to viscous shear, and the relation of this quantity to shaft speed and coolant flow. It is expected that bearing temperature measurements at different flow conditions will lead to a similar advancement in the understanding of the surface to fluid heat transfer coefficient.

A model was developed for the SSME Liquid Oxygen (LOX) turbopump shaft/bearing system. The model includes the turbine-end and pump-end bearings, bearing isolators, and the shaft. A detailed nodal network is used for thermally modeling the Number 2 pump-end bearing. An automated iteration method was developed to allow iteration between the shaft/bearing model and the thermal model until the models converge to a solution. The model was used to perform parametric analyses to determine the sensitivity of bearing operating characteristics and temperatures to variations in: axial preload, contact friction, coolant flow and subcooling, heat transfer coefficients, outer race misalignments, and outer race to isolator clearances. The bearing operating characteristics and temperatures are very sensitive to preload,

contact friction, and heat transfer coefficients. The heat transfer coefficients had to be increased by factors as large as 3.43 to achieve converged solutions for the more severe cases of preloads and high contact friction. Outer race misalignments greater than 29 minutes caused thermally unstable operating conditions. Misalignment produced the highest bearing temperatures of any stable operating condition investigated. Although the bearing temperatures were not as sensitive to coolant flow and subcooling, these parameters became important for marginal operating conditions. The analysis predicts less sensitivity to coolant flow than has been determined by BSMT data. Further work is underway to resolve the disagreement between analysis and test. Operational outer race-to-isolator clearance was lost for initial clearances below 1.7 mils with improved heat transfer coefficients. For an initial clearance of 2.6 mils, operational outer race-to-isolator clearance was lost for nominal heat transfer and contact friction factor of 0.2.

The bearing program ADORE (Advanced Dynamics of Rolling Elements) has been installed on the MSFC UNIVAC 1100/80 computer system and is operational. ADORE is an advanced FORTRAN computer program for the real time simulation of the dynamic performance of rolling bearings. A model of the 57 mm turbine-end bearing is currently being checked out.

Analyses were conducted to estimate flow work energy for several flow diverter configurations and coolant flow rates for the LOX BSMT. These analyses show that for a given coolant flow, coolant type, and shaft speed, there is a configuration that minimizes the heat generated by flow work. A bearing shaft model of the LOX BSMT was used to generate bearing friction heat loads for several radial and axial load conditions. Radial loading resulted in the inboard bearings sharing more load than the outboard. Viscous energy terms were also estimated.

3.0 WORK PERFORMED DURING 1985

3.1 DEVELOPMENT AND USE OF A TEST CONDITION DATA BASE

A computerized data base of BSMT test conditions has been developed. This data base permits quick retrieval of test data for use in trend analysis and prediction. This section describes the development of the system, some of its major features, and includes trend analysis plots that were generated with data from the data base.

Exhibit 3.1.1 shows the original design of the test condition data base system. The inputs to the system are a set of test conditions that classify the test data desired. The output is then a list of test numbers and times of tests that were run under those conditions. The contents of the data base were initially to include only the set of independent test conditions shown in Exhibit 3.1.2. Then any other data is dependent on these conditions and could be retrieved from the original tapes once the proper time segments were determined from the data base program. These time segments are those during which the tester was operating under the set of conditions input to the data base program.

The test measurement values contained in the data base are average values over time. To determine these average values, several methods have been tried. A program to average BSMT test data was written and installed on the MSFC UNIVAC 1100. This program utilized the ACCESS data retrieval subroutine and gave mean values along with the data's standard deviation about that mean. However, we have found that for most trend analysis plots, we can manually average the data from the test data plots with good accuracy.

The use and the contents of the data base have been expanded since its initial design. Several dependent temperature measurements have been added to the data base. A list of these measurements is shown in Exhibit 3.1.3. These temperatures were used for several trend analysis plots and they are updated after each test. The data base has been set up so that it will be easy to add new measurements when necessary. While the data base system has a flexible query language that allows various types of searches, it can also be used to produce a formatted report like the one shown in Exhibit 3.1.4. (Note that this is only a sample report and some of the data is incomplete.)

The data stored in the data base has been used to update several trend analysis plots of BSMT data. These plots now include data from tests since

Exhibit 3.1.1 General Design of Test Condition Data Base

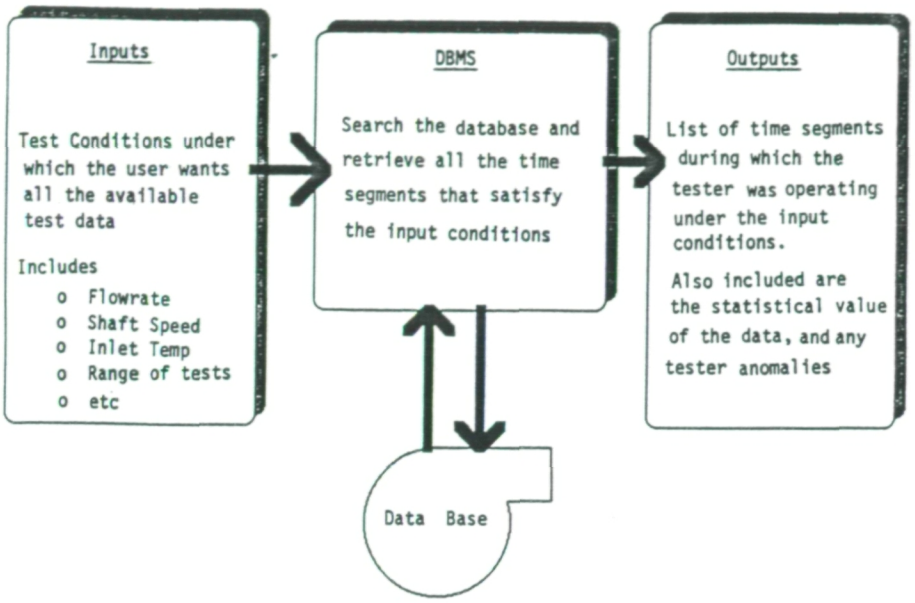

Exhibit 3.1.2 Independent BSMT Test Variables

	MSID	
1	FC1	Flow Rate #1
2	FC2	Flow Rate #2
3	T1001	Flow Inlet Temp #1 (Load Side)
4	T1002	Flow Inlet Temp #2 (Drive Side)
5	P1001	Pressure LOX Inlet Cavity #1 (Load Side)
6	P1002	Pressure LOX Inlet Cavity #2 (Drive Side)
7	RPM4	Shaft Speed
8	L1002	Axial Load
9	____	Radial Load
10	Fluid Type (LOX, LN2)	
11	Tester Build	
12	Tester Facility	

SRS TECHNOLOGIES

Exhibit 3.1.3 Dependent BSMT Test Variables

MSID	DESCRIPTION
P33	Delta Pressure, Bearings 1 and 2
P36	Delta Pressure, Bearings 3 and 4
T1018	Temperature Inlet, Bearing 3
T1019	Temperature Outlet, Bearing 4
T1004	Temperature Outer Race, Bearing 1
T1005	Temperature Outer Race, Bearing 2
T1006	Temperature Outer Race, Bearing 3
T1007	Temperature Outer Race, Bearing 4

Exhibit 3.1.4 Example Data Report

BEARING TESTER REPORT #1 DATE OF REPORT: 01/13/86

RUN NUMBER	SHAFT SPEED	FLOW RATE	TEMPERATURE OF OUTER RACE				TEMPERATURE OF INLET		PRESSURE OF INLET	
			BRG #1	BRG #2	BRG #3	BRG #4	LOAD SIDE	DRIVE SIDE	LOAD SIDE	DRIVE SIDE
201N0407	14400.00	0.00	-293.80	-292.50	-293.00	-295.07	-301.10	-300.66	490.30	491.00
201N0501	18000.00	6.30	-287.80	-285.20	-285.20	-288.50	-296.50	-297.00	497.00	500.00
201N0501	21000.00	6.29	-287.30	-281.50	-281.50	-288.00	-296.00	-297.00	500.00	508.00
201N0501	25000.00	6.28	-286.50	-275.80	-275.80	-284.00	-294.50	-296.50	506.00	515.00
201N0702	15200.00	11.20	-292.50	-289.00	-290.80	-290.50	-297.60	-297.70	505.00	505.00
201N0702	20000.00	11.20	-292.00	-286.50	-287.00	-290.20	-297.40	-297.60	508.00	508.00
201N0801	21000.00	11.10	-286.00	-283.00	-284.00	-286.50	-294.00	-294.30	511.00	509.00
201N0801	30000.00	11.08	-285.50	-271.50	-271.00	-285.50	-293.50	-293.80	526.00	526.00
201N0902	21000.00	0.00	-290.00	-283.00	-284.00	-290.00	-298.20	-298.90	500.00	495.00
201N0902	30000.00	0.00	-288.00	-270.00	-271.50	-287.00	-296.20	-298.10	512.00	510.00
201N1001	29000.00	6.39	-290.00	-270.00	-270.00	-290.00	-296.00	-299.00	520.00	520.00
201N1102	30200.00	6.40	-292.00	-272.00	-271.00	-287.50	-295.00	-301.00	530.00	520.00
22N101R	30000.00	9.15	-297.00	-261.00	-272.50	-299.00	-296.50	-297.00	530.00	521.00
22N21	15000.00	6.20	-303.00	-300.00	0.00	-293.00	-300.00	0.00	490.00	510.00
22N21	15000.00	6.20	-303.00	-298.50	0.00	-294.00	-300.00	0.00	490.00	520.00
22N33R	30000.00	4.60	-296.00	-265.00	-263.00	-295.50	-265.00	-296.00	505.00	513.00
22N41R	30000.00	4.35	-296.00	-268.00	-260.00	-298.00	-295.00	-295.00	510.00	520.00
22N51R	30063.39	4.56	-292.03	-269.45	-264.97	-296.02	-294.10	-295.33	505.00	515.66
22N61R	0.00	4.60	-295.00	-264.00	-270.00	-295.00	-293.00	-295.00	510.00	680.00
22N71R	0.00	0.00	-294.00	-258.00	-263.00	-294.00	-292.00	-294.00	510.00	520.00
22N72R	0.00	0.00	-297.00	-257.00	-266.00	-295.00	-292.00	-295.00	510.00	520.00
22N81R	30000.00	4.60	-297.00	-261.50	-267.00	-298.00	-294.00	-297.50	520.00	520.00
22N82R	30000.00	4.60	-301.00	-255.00	-268.00	-301.00	-296.50	-300.00	520.00	530.00
22N91R	30000.00	9.15	-295.50	-275.50	-275.00	-301.00	-298.20	-298.70	535.00	541.00

SRS TECHNOLOGIES

May, 1984. They are shown in Exhibits 3.1.5, 3.1.6, and 3.1.7. The most recent tests, 22N91 and 22N101, were conducted with a coolant flow rate of 9 lbs/sec. Exhibit 3.1.5 shows the pressure difference across Bearings 1 and 2 increasing over time for the tests that have a flow rate of 4.6 lbs/sec. The pressure difference measured during the latest tests (30,000 rpm, 9 lbs/sec) are considerably higher than the curve drawn from earlier tests would predict for this flow rate. (This is the curve labeled "30,000 RPM (ACTUAL)".) An explanation for this may be the increased heating due to bearing deterioration, which would decrease the density of the fluid. Exhibit 3.1.6 shows the bearing heat generation on the drive end of the tester as a function of tester shaft speed. The heat generation data for the latest 9 lbs/sec coolant flow tests agree fairly well with the previous data on this plot. Exhibit 3.1.7 shows the temperature difference between the outer races and the coolant inlet temperature as a function of coolant flow rate and illustrates the approximate 10° to 18°F drop in outer race temperature as the flow is increased from 4.6 to 9.0 lbs/sec for the 30,000 RPM tests. Exhibit 3.1.8 shows how this same temperature difference has changed over the age of the bearing.

Exhibits 3.1.9, 3.1.10, and 3.1.11 are outer race temperature time plots for the tester bearings. Exhibit 3.1.9 is data from the first test at 4.6 lbs/sec and 3.1.10 is data from the last test. Notice that the initial temperature for the first test is about 5° higher than for the last test. If this bias is included, the difference in average temperature for Bearing Number 2 between the two tests is approximately 12°F indicating the deterioration of the bearing with run time. Also observe the 5 to 10°F temperature spikes for the last 4.6 lb/sec test which indicate severe ball skidding. These temperature spikes are not observable in Exhibit 3.1.11 for the first test with 9 lbs/sec coolant flow. Also observe that the average temperature difference, for Bearing No. 2, between the last test at 4.6 lbs/sec and the first test at 9 lbs/sec is approximately 18°F. This leads to the conslusion that increasing the coolant flow from 4.6 to 9 lbs/sec has a significant effect in reducing bearing operating temperatures and is especially effective in bearings with surface distress.

Exhibit 3.1.5 BSMT (LN2) Pressure Difference vs Flow Rate

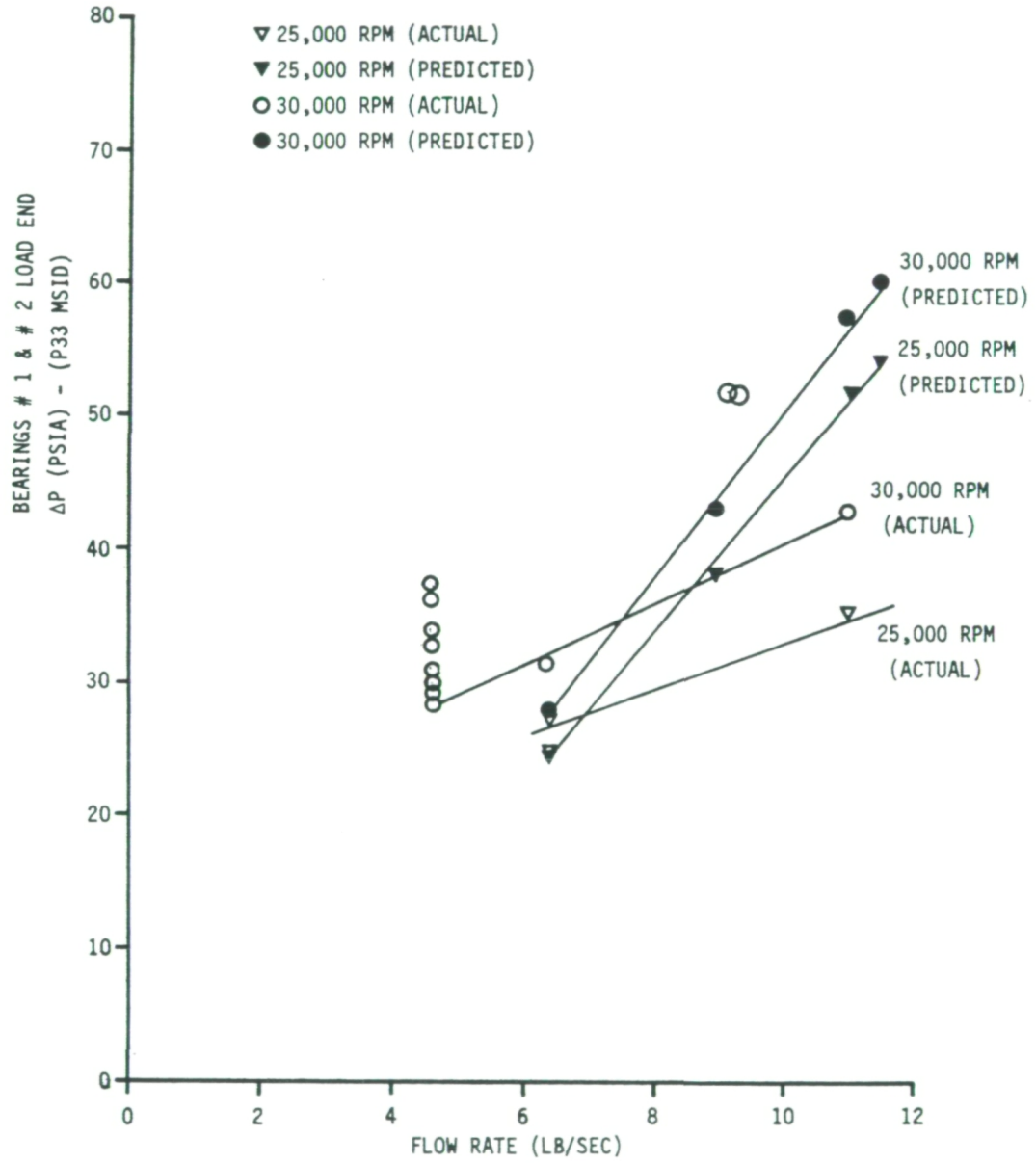

SRS TECHNOLOGIES

Exhibit 3.1.6 BSMT (LN2) Bearing Heat Generation vs. Tester Speed

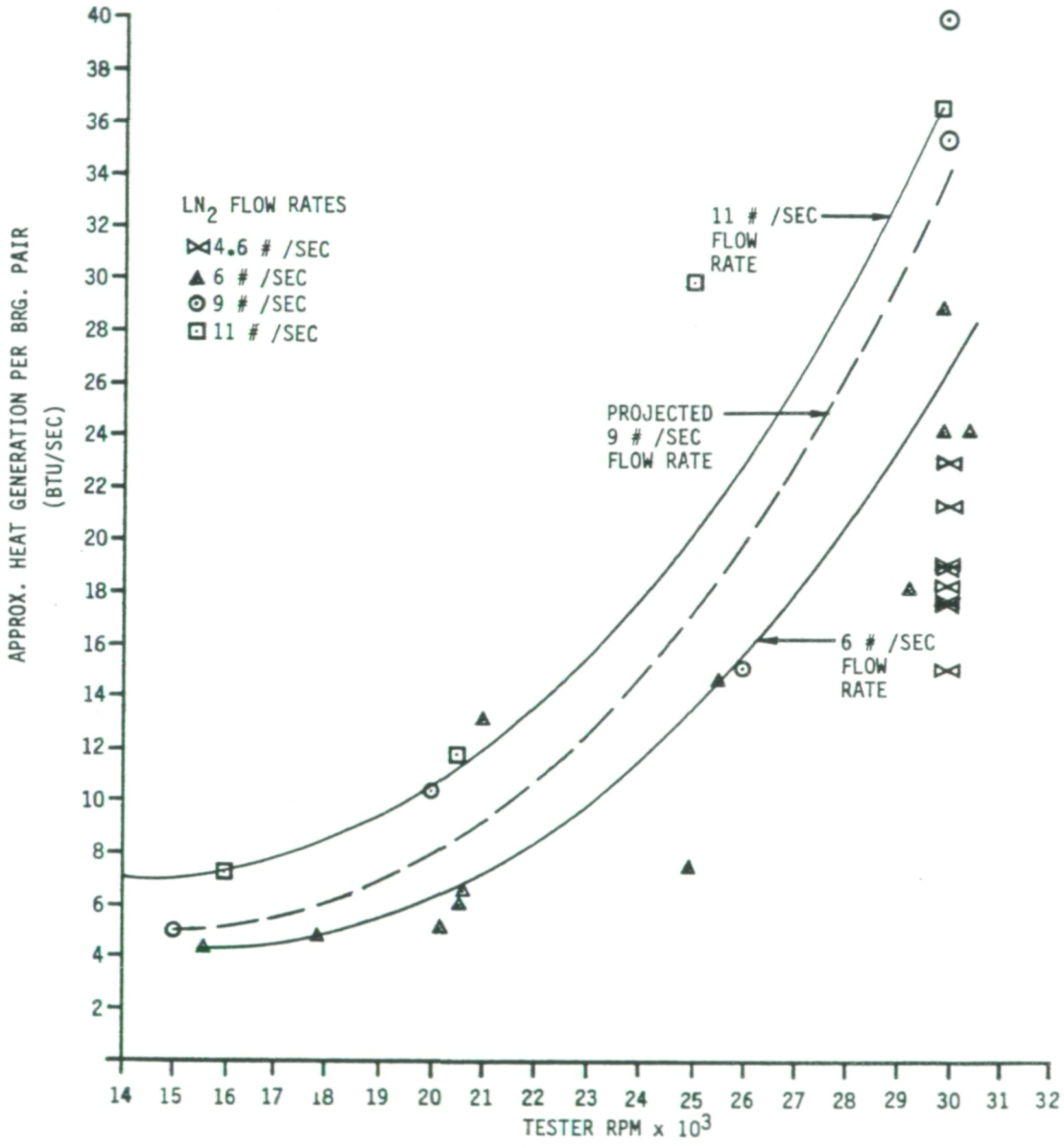

Exhibit 3.1.7 LN2 Test Data Flow Rate vs. Bearing Temperature

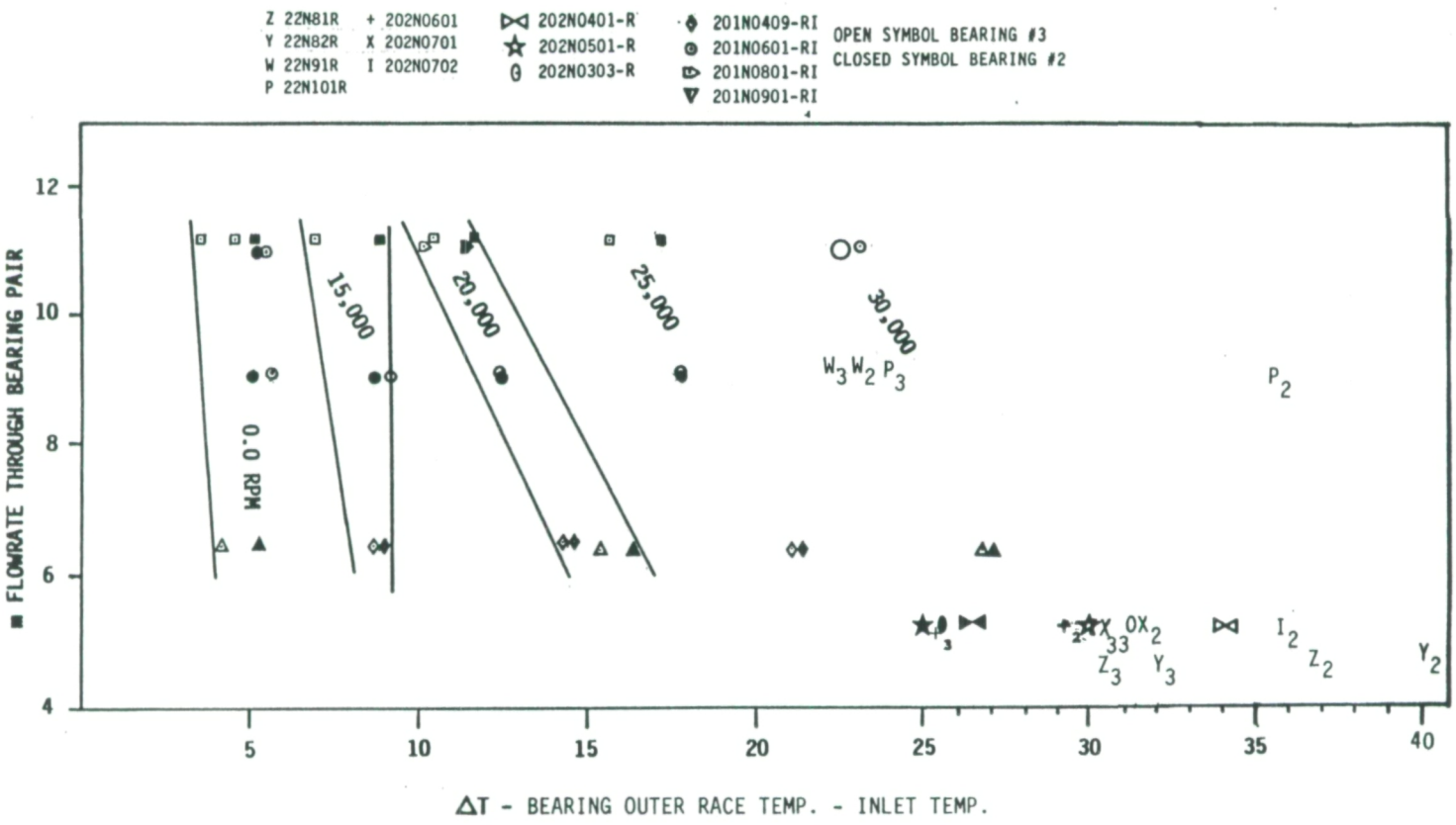

SRS TECHNOLOGIES

Exhibit 3.1.8 Temperature Difference vs. Accumulated Run Time

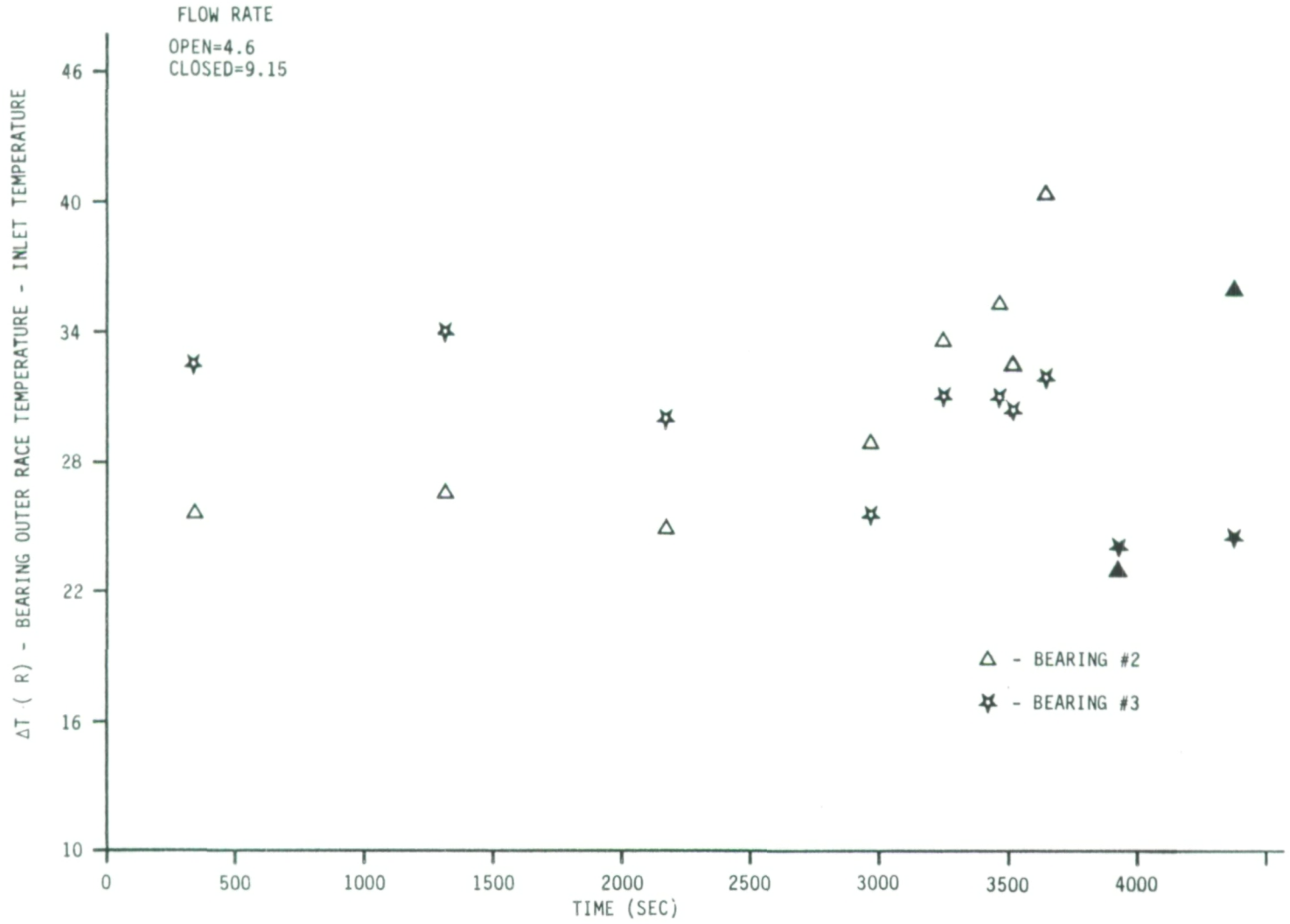

SRS TECHNOLOGIES

Exhibit 3.1.9 Outer Race Temperature - Test No. 22N33

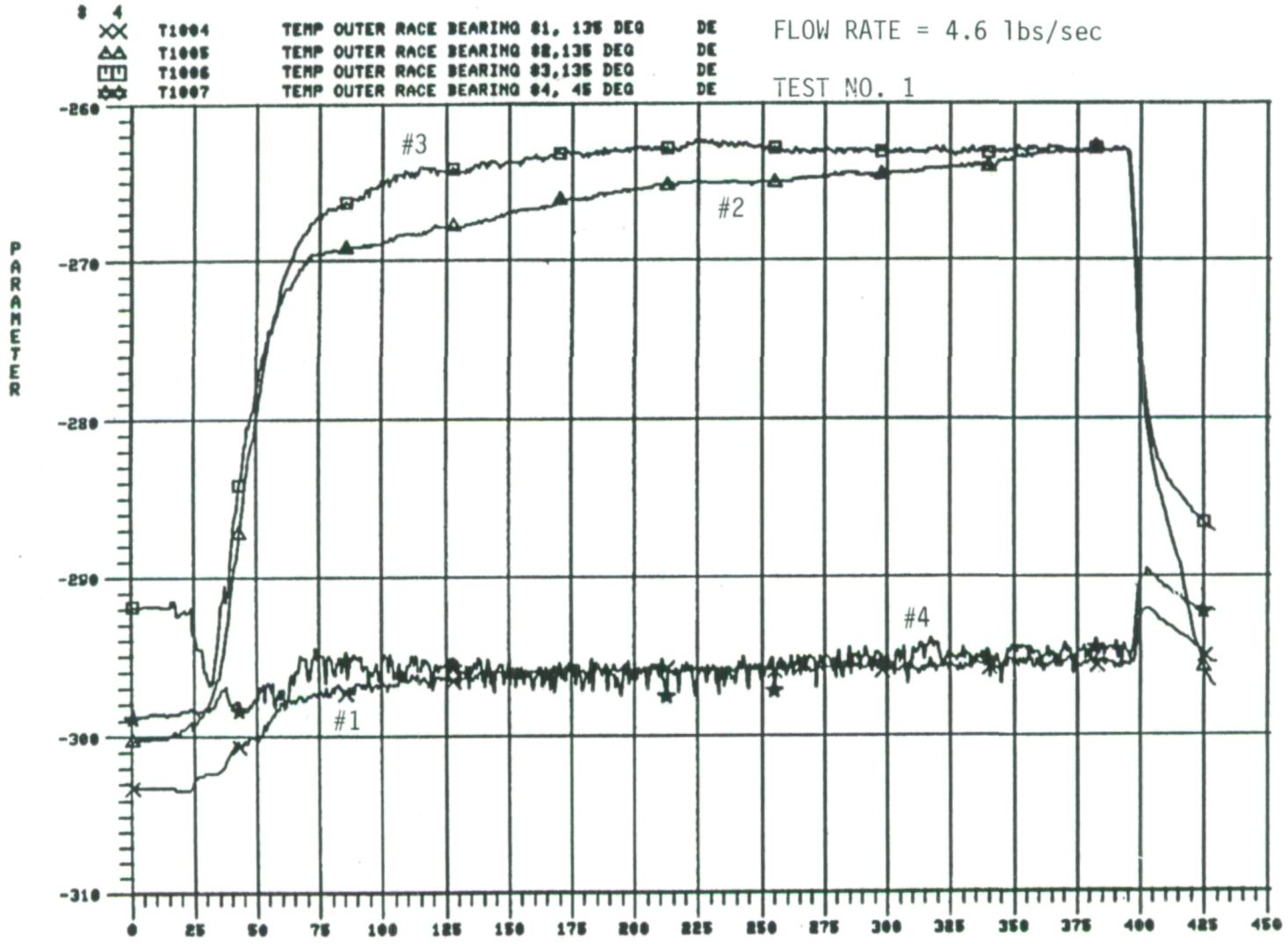

SRS TECHNOLOGIES

Exhibit 3.1.10 Outer Race Temperature - Test No. N2282RDB

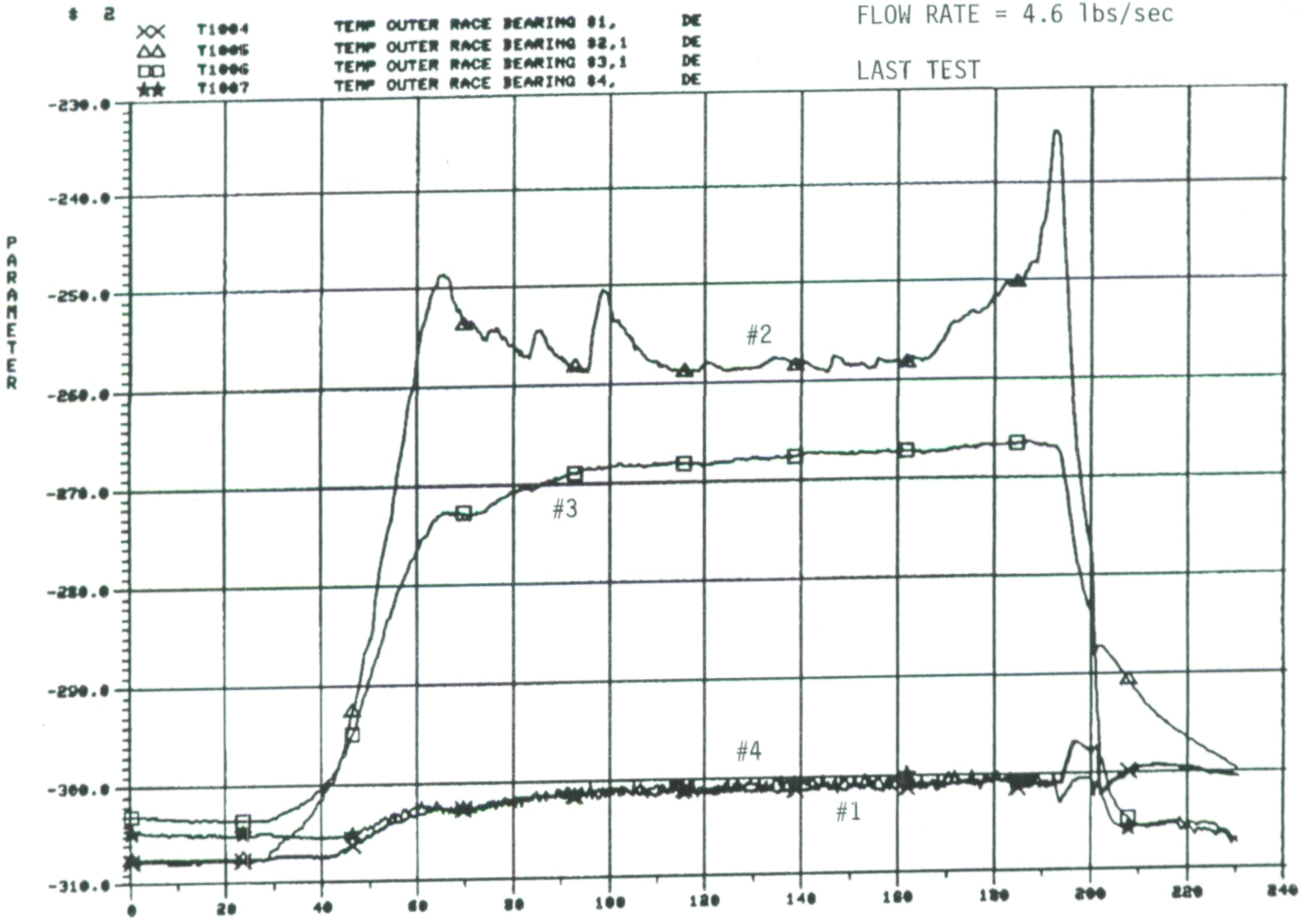

ORIGINAL PAGE
COLOR PHOTOGRAPH

SRS TECHNOLOGIES

Exhibit 3.1.11 Outer Race Temperature - Test No. N2291RDB

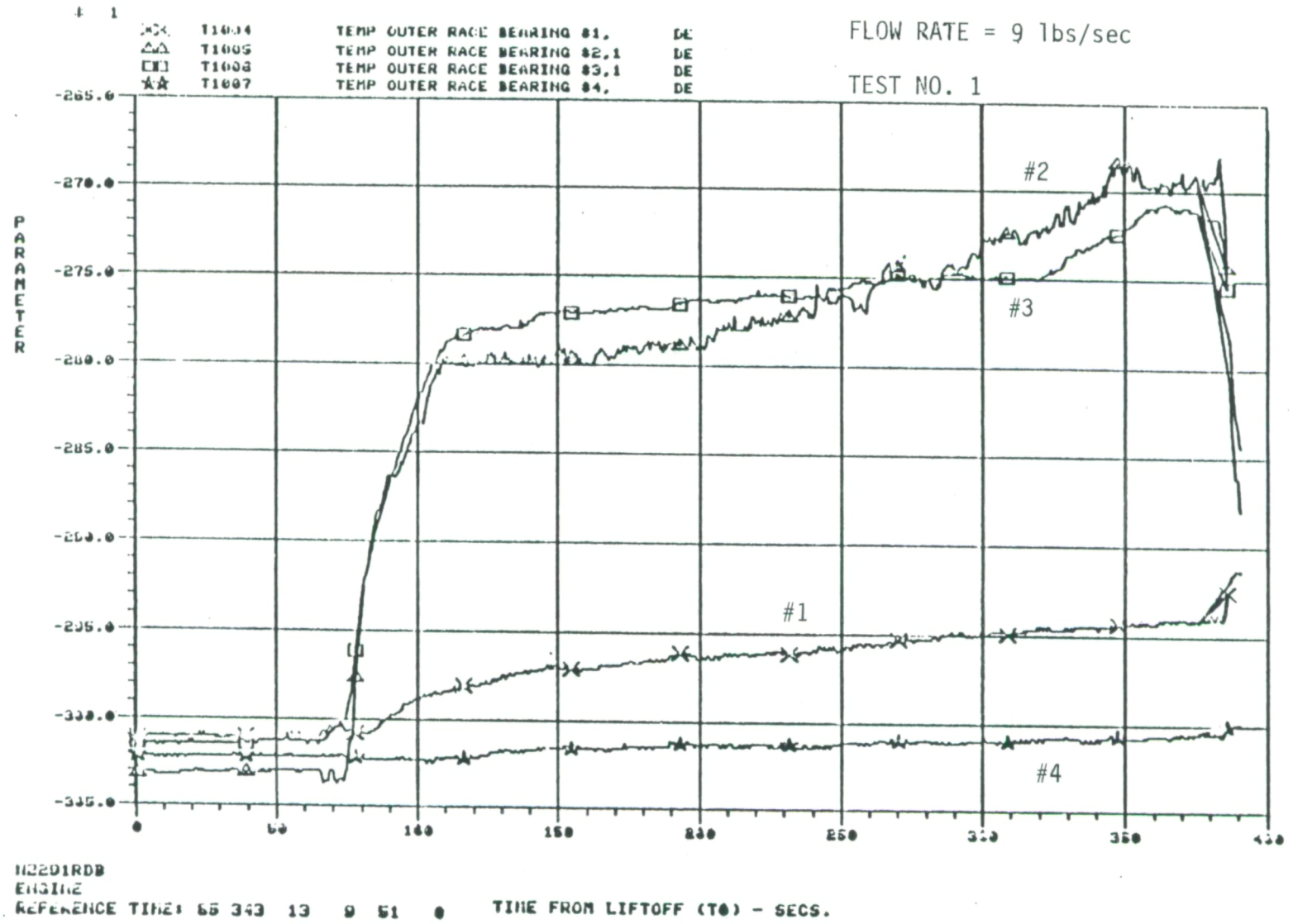

SRS TECHNOLOGIES

3.2 DEVELOPMENT AND USE OF A 45 MM BEARING MECHANICAL/THERMAL MODEL

3.2.1 SHAFT/BEARING MODEL DESCRIPTION

A shaft/bearing system model was developed to represent the SSME LOX turbopump shaft and bearing configuration using the SHABERTH computer program. A thermal model was developed specifically for the 45 mm pump-end bearing using the Systems Improved Numerical Differencing Analyzer (SINDA) program.

SHABERTH SHAFT/BEARING MODEL

The SHABERTH model for the SSME LOX turbopump consists of the turbopump shaft, turbine-end and pump-end bearings. The major components of the shaft/bearing model are shown in Exhibit 3.2.1. The complete shaft/bearing system was modeled so that the effects of preload and shaft deflection on bearing load sharing could be studied. Variations in outer race clearance, outer race tilt, and contact friction could also be investigated using this model. The model used a shaft speed of 30,000 RPM and shaft loading conditions presented in Exhibit 3.2.1. These radial loads were used to produce the reactions reported for pump build number 2606R1. The SHABERTH model predicts the frictional heat generation at the contact points in the bearing and the load distribution for each bearing set.

SINDA THERMAL MODEL OF 45 MM BEARING

The SINDA thermal model is a detailed nodal division of the SSME LOX turbopump Number 2 bearing. The SINDA thermal model, using the nodal representation of the bearing components (inner race, ball, outer race, etc.), is able to predict component temperature profiles and average component temperatures. The thermal model uses the energy conservation equation to obtain the temperature distribution in the bearing components. The model solves the conservation equation using the bearing frictional heat generation, predicted by the SHABERTH model, and fluid stirring heat generation. The thermal model also accounts for the heat generated by pump-end bearing Number 1.

The SINDA thermal model is able to simulate different coolant flow rates and inlet coolant temperatures. The model is capable of simulating saturated

EXHIBIT 3.2.1 SSME LOX TURBOPUMB BEARING/ SHAFT LOAD CONFIGURATION

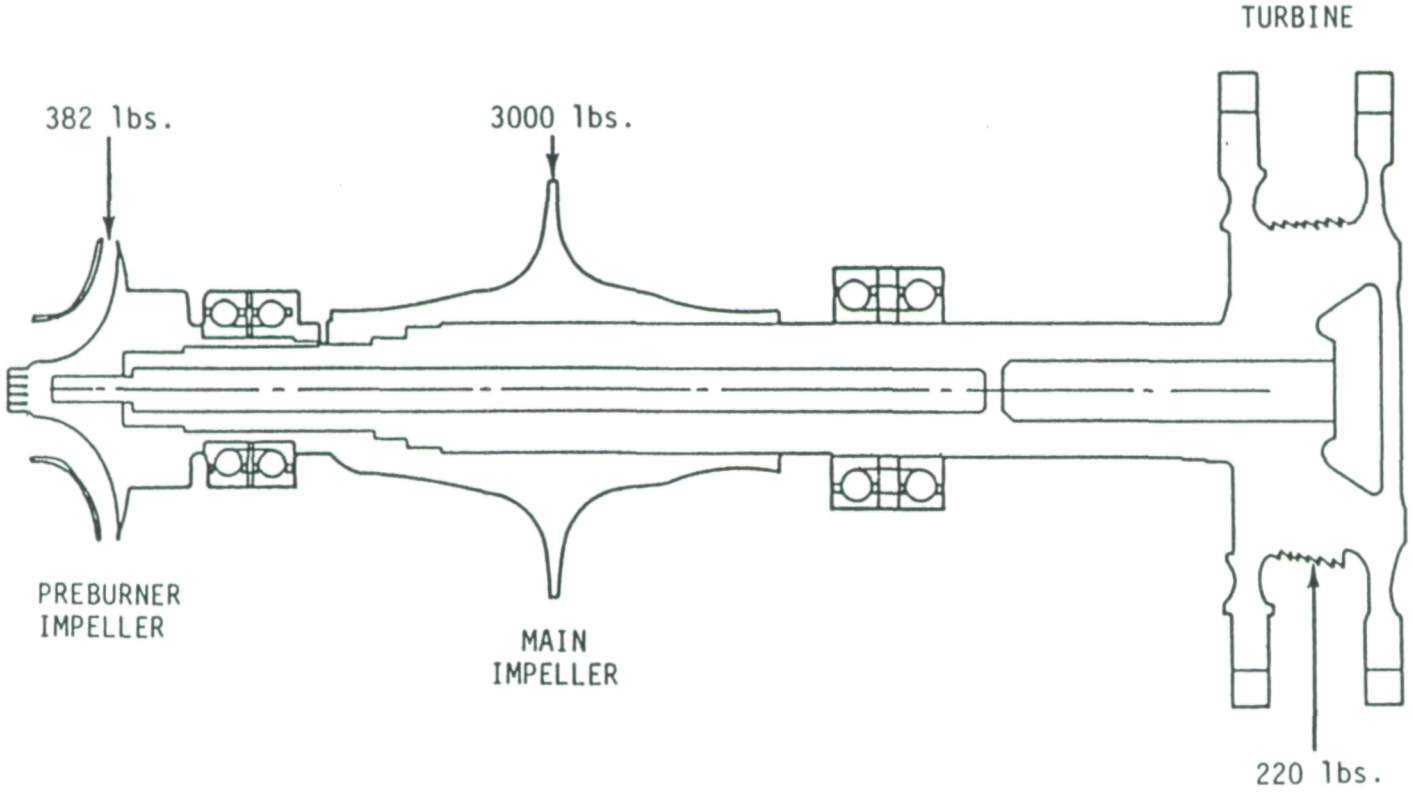

SRS
TECHNOLOGIES

coolant entering bearing Number 2. Also, thermal isolation of specific components in the bearing can be performed with this model.

MODEL ITERATION PROCESS

The SHABERTH shaft/bearing model and the SINDA thermal model are used in an interactive iteration process to determine the steady state operating conditions for a specific case. The iteration process can also predict if a case is thermally unstable.

The iteration process is totally automated. The user supplies an initial guess for the bearing component temperatures and the models iterate until a solution is determined. The models are first set up to simulate a specific case. The user then supplies an initial guess for the component temperatures to the SHABERTH shaft/bearing model. The SHABERTH model then analyzes the shaft/bearing system and calculates the frictional heat generation rates of the contact points in the bearing. These heat generation rates are placed in the SINDA thermal model. SINDA then solves the energy conservation equation to predict the temperature distribution in the bearing components. The average component temperatures are calculated from the temperature profiles and are used in a comparison with the average component temperatures used by the SHABERTH model. If all the temperatures compare to within 2°C, the steady state solution has been reached. If the comparison fails, the SHABERTH model uses the new temperatures to predict new frictional heat rates. The thermal model uses the new heat rates to predict another set of average component temperatures. The temperature comparison is again made.

The iteration process is continued in this manner until the temperatures used by the SHABERTH model are within 2°C of the temperatures predicted by the thermal model or the predicted temperatures exceed an upper limit of 2000°F. 2000°F was chosen as the approximate ignition temperature of 440C in liquid oxygen. A case is considered thermally unstable if an average component temperature exceeds the 2000°F limit. Exhibit 3.2.2 illustrates the iteration process between the SHABERTH shaft/bearing model and the SINDA thermal model for a converged case. In this case the friction heat from SHABERTH and the average component temperature from SINDA increase to a converged point. Exhibit 3.2.3 shows a diverged (thermally unstable) case which has no converged point.

EXHIBIT 3.2.2 ITERATION PROCESS BETWEEN SHABERTH AND SINDA

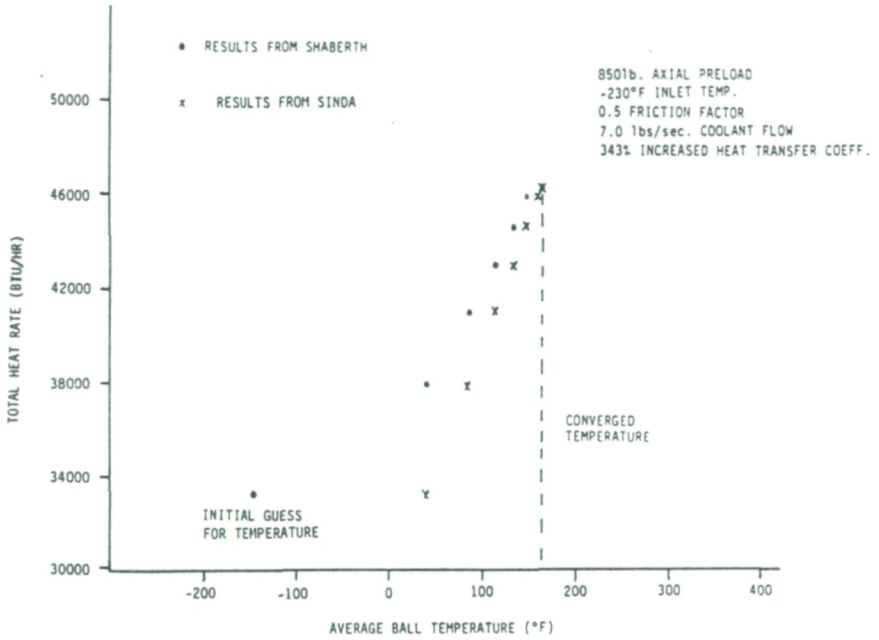

EXHIBIT 3.2.3 EXAMPLE OF A DIVERGED ITERATION PROCESS (DIVERGED CASE)

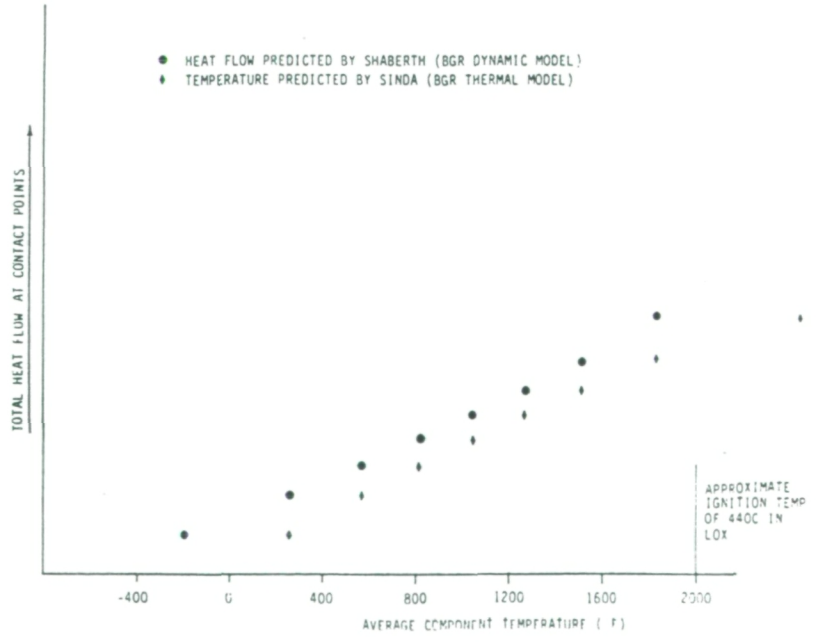

3.2.2 ANALYSIS OBJECTIVES AND APPROACH

The objectives of the SSME LOX turbopump pump-end bearing analysis were to investigate the sensitivity of bearing operating characteristics to variations in operating parameters. The operating parameters that were considered are listed below with the values investigated.

1.	Coolant Flow Rate (lbs/sec)	3.6, 7.0
2.	Contact Friction Factor	0.2, 0.3, 0.5
3.	Inlet Coolant Temperature to Bearing #1 (°F)	-240, -230, -218
4.	Axial Preload (lbs)	350, 480, 850
5.	Outer Race Clearance (mils)	2.6, 1.7, 1.0
6.	Outer Race Tilt (minutes)	0 through 42
7.	Heat Transfer Between Outer Race and Isolator	With, Without

The flow rate, friction factor, inlet temperature, and preload were investigated in all combinations while holding the remaining parameters at their initial values. This resulted in 54 initial cases to be simulated. These cases are represented in the parameter data tree of Exhibit 3.2.4. This figure shows that 42 of the 54 cases were thermally unstable (diverged). It was not necessary to run computer simulations for all the cases to determine thermal instability. For example, if a case with an inlet coolant temperature of -218°F, flow rate of 7.0 lbs/sec, preload of 850 lbs, and friction factor of 0.2 was unstable, then cases for friction factor of 0.3 and 0.5 with the other parameters the same would obviously not be stable.

The effects of changes in coolant flow rate and inlet coolant temperature were evaluated using the 12 converged cases. However, more converged cases, over the full range of parameter values, were needed to properly evaluate changes in the remaining operating parameters. Thus, it was decided to increase the boundary heat transfer coefficient to obtain more cases that are thermally stable.

Changing the boundary heat transfer coefficient introduced heat transfer as a new parameter into the sensitivity analysis. A second parameter data tree was developed for the increased heat transfer coefficients and unevaluated parameters. Exhibit 3.2.5 shows this parameter data tree, which has 18

EXHIBIT 3.2.4 PARAMETER DATA TREE WITH NOMINAL HEAT TRANSFER COEFFICIENT

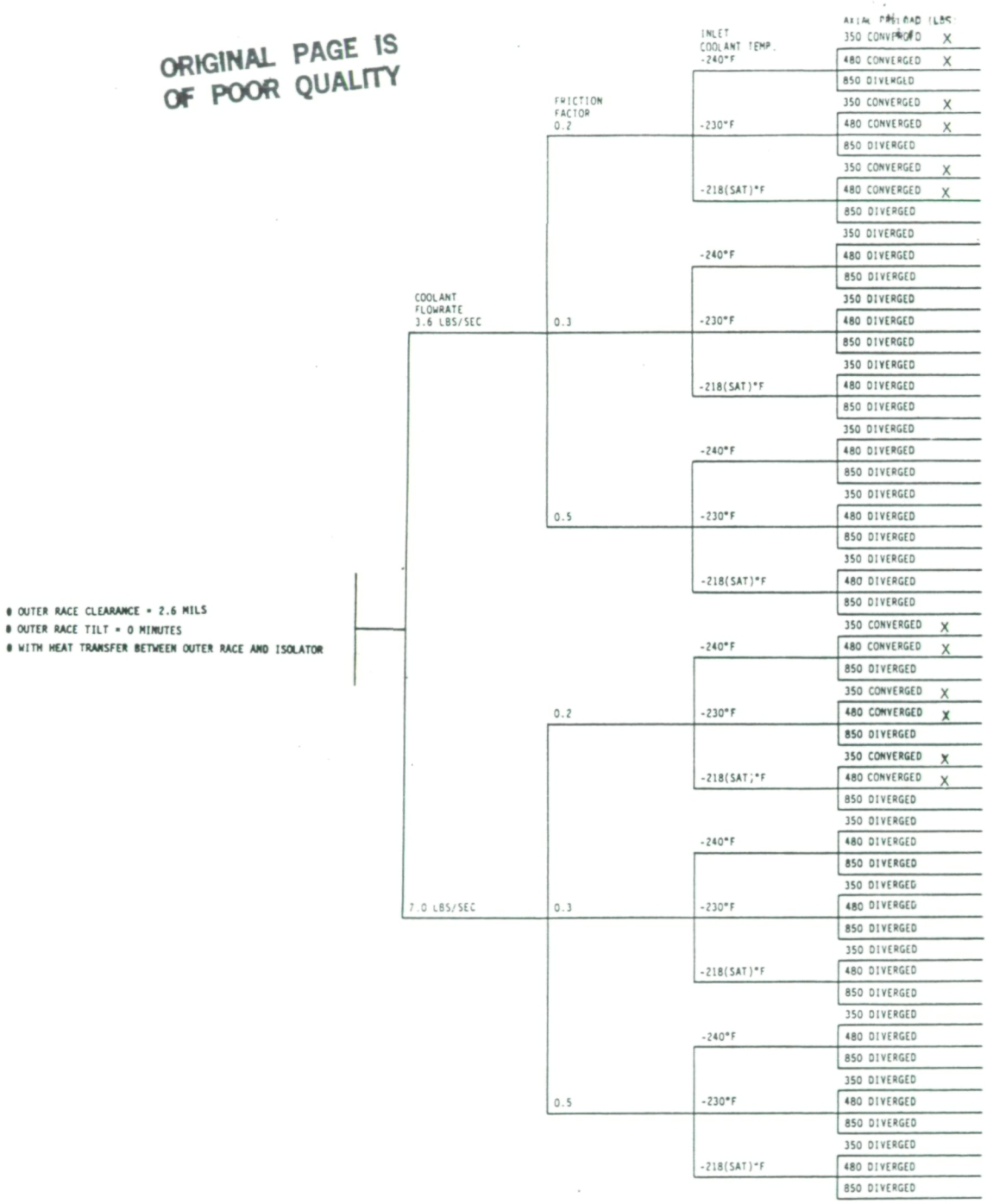

EXHIBIT 3.2.5 PARAMETER DATA TREE WITH ENHANCED HEAT TRANSFER COEFFICIENT

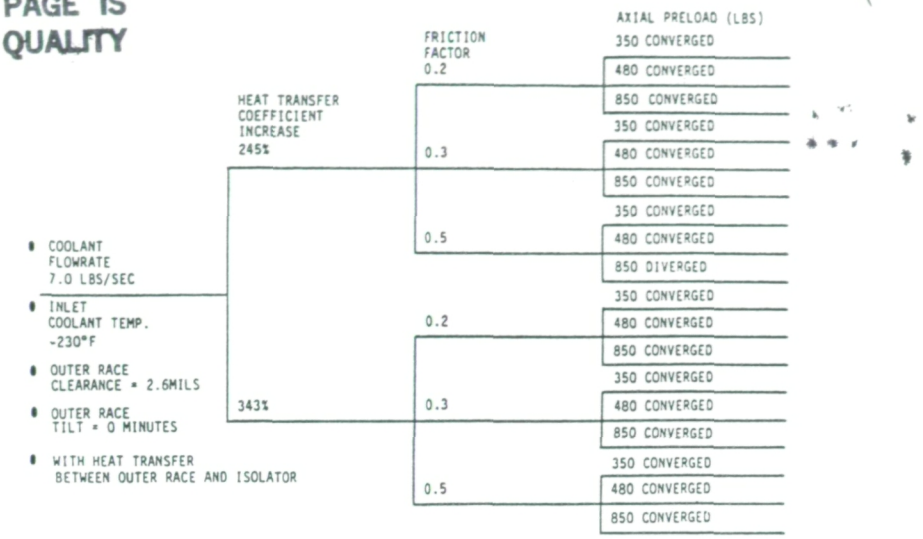

EXHIBIT 3.2.6 BEARING OPERATING CHARACTERISTICS WITH UNIFORM TEMP. PROFILE

BEARING NO.	REACTION FORCES(lbs)		MOMENTS (ft/lbs)	MAX. HERTZ STRESSES (kpsi)	DEFLECTIONS (inches)
	RADIAL	AXIAL			
1	618.7	941.5	-32.2	377	0.00080
2	1572	-1042	84.8	469	0.00114
3	1292	114.3	-10.0	382	0.00053
4	-320.8	-14.32	-3.55	300	-0.00014

480 LBS AXIAL PRELOAD
6.3 MILS DIAMETRICAL CLEARANCE
2.6 MILS OUTER RACE CLEARANCE

EXHIBIT 3.2.7 BEARING OPERATING CHARACTERISTICS CONSIDERING THERMAL EFFECTS

BEARING NO.	REACTION FORCES(lbs)		MOMENTS (ft/lbs)	MAX. HERTZ STRESSES (kpsi)	DEFLECTIONS (inches)
	RADIAL	AXIAL			
1	530.8	1040	-26.6	374	0.00074
2	1650	-1170	88.6	486	0.00116
3	1495	145.4	-12.9	402	0.00058
4	-513.5	-15.13	-4.76	327	0.00021

480 LBS AXIAL PRELOAD
6.3 MILS DIAMETRICAL CLEARANCE
2.6 MILS OUTER RACE CLEARANCE

SRS TECHNOLOGIES

more cases. The effect of varying friction factor and axial preload were properly evaluated using these cases.

The heat transfer coefficient was increased to obtain converged cases over the range of parameter values. A thermally stable solution was obtained for a coolant flow rate of 7.0 lbs/sec, inlet temperature of -230°F, friction factor of 0.5, and preload of 480 lbs with a 245 percent increase in heat transfer coefficient. An increase in heat transfer coefficient of 343 percent was needed for the 850 lb preloaded case.

The variation of outer race clearance, outer race tilt, and thermal isolation of the isolator were evaluated separately, holding all other parameters constant. A nominal case with a flow rate of 7.0 lbs/sec, inlet temperature of -230°F, friction factor of 0.2, and preload of 480 lbs was used to evaluated these parameters. The 245 percent increased heat transfer coefficient was needed for the evaluation of outer race clearance changes. The 343 percent increased heat transfer coefficient was needed to evaluate the effects of changing outer race tilt.

3.2.3 ANALYSIS RESULTS

The analysis of the SSME LOX turbopump included different loading conditions and bearing temperature profiles. A mechanical analysis of the shaft/bearing system was performed using the SHABERTH computer model. The thermal analysis of the pump-end Number 2 (inboard) bearing was performed using the SINDA thermal model. The use of these computer models, in an interactive manner, enabled the comprehensive evaluation of the bearing performance.

MECHANICAL CHARACTERISTICS

The mechanical analysis was performed using a shaft speed of 30,000 RPM and radial loads on the preburner impeller, main impeller, and turbine of 382, 3000, and -220 lbs, respectively. These radial loads, illustrated in Exhibit 3.2.1, were used to produce the reaction loads measured for pump build 2606R1. The model used an unmounted diametrical clearance of 6.3 mils, inner race curvature of 0.55, and outer race curvature of 0.52 for the 45 mm inboard (Number 2) bearing. The model also simulates the outer races sliding

with axial load. This was done by manipulating the turbine-end bearings so that they transmit very small axial loads to the pump-end bearings.

The bearing operating characteristics were determined for a case using 480 lbs preload, 7.0 lbs/sec coolant flow rate, and friction factor of 0.2. Exhibit 3.2.6 shows the bearing operating characteristics for a uniform temperature profile of -230°F. Exhibit 3.2.7 shows the same case at its steady state (converged) temperature profile. As can be seen from these tables, the pump-end bearings (Numbers 1 and 2) do not share an equal amount of the load. This is primarily due to the shaft deflecting from the large radial load placed between the pump-end bearings and the turbine-end bearings (Numbers 3 and 4). Bearing 2 received about 72 percent of the load to the pump-end bearings with a uniform temperature profile. The bearing received about 76 percent of the load, considering thermal effects. Bearing 2 received a greater portion of the load with the steady state temperature profile because of thermal growth of the ball, with respect to the races. The thermal growth of the ball decreased the internal clearances in the bearing which increased the axial load. The increased axial load caused the bearing to become "stiffer" and thus able to support a larger radial load.

THERMAL ANALYSIS RESULTS

The SINDA thermal model predicted temperatures for each node of the bearing components. The program then calculated the volume average temperature for the main components. Exhibits 3.2.8 through 3.2.11 show the average component and maximum track temperatures for the cases studying preload, friction factor, inlet temperature, and flow rate.

The calculated results with nominal heat transfer coefficient are shown in Exhibits 3.2.8 and 3.2.9. The effect of preload and inlet coolant temperatures are shown for a friction factor of 0.2 with two flow rates considered. No stable solution was achieved for 850 lbs preload. Therefore, it was necessary to increase the heat transfer coefficient to obtain more stable cases. Exhibit 3.2.10 presents the results for three friction factors and three preloads for cases where the heat transfer coefficient has been increased to 245% of its nominal value. With this increase, it was possible to obtain a thermally stable solution for all cases except the case with 0.5 friction factor and 850 lbs preload. To obtain a thermally stable solution

EXHIBIT 3.2.8 COMPENENT TEMPERATURES FOR DIFFERENT INLET COOLANT TEMPERATURES AT LOW FLOW RATE (3.6 LBS/SEC)

45 MM BEARING

INLET COOLANT TEMPERATURE		BEARING AXIAL PRELOAD (LBS)																	
		350						480						850					
BEARING 1	BEARING 2	AVERAGE TEMPERATURE (°F)			MAXIMUM TRACK TEMPERATURE (°F)			AVERAGE TEMPERATURE (°F)			MAXIMUM TRACK TEMPERATURE (°F)			AVERAGE TEMPERATURE (°F)			MAXIMUM TRACK TEMPERATURE (°F)		
		INNER RACE	BALL	OUTER RACE	INNER RACE	BALL	OUTER RACE	INNER RACE	BALL	OUTER RACE	INNER RACE	BALL	OUTER RACE	INNER RACE	BALL	OUTER RACE	INNER RACE	BALL	OUTER RACE
-240	-232	-144	-23	-125	65	89	102	-106	47	-101	159	182	172	*	*	*	*	*	*
-230	-223	-125	-1	-113	93	115	120	-95	57	-95	177	195	169	*	*	*	*	*	*
-218	-214	-113	8	-105	106	124	128	-88	63	-88	185	200	176	*	*	*	*	*	*

COOLANT FLOWRATE = 3.6 LBS/SEC

FRICTION FACTOR = 0.2

* THERMALLY UNSTABLE

EXHIBIT 3.2.9 COMPONENT TEMPERATURES FOR DIFFERENT INLET COOLANT TEMPERATURES AT HIGH FLOW RATE (7.0 LBS/SEC)

45 MM BEARING

INLET COOLANT TEMPERATURE		BEARING AXIAL PRELOAD (LBS)																	
		350						480						850					
BEARING 1	BEARING 2	AVERAGE TEMPERATURE (°F)			MAXIMUM TRACK TEMPERATURE (°F)			AVERAGE TEMPERATURE (°F)			MAXIMUM TRACK TEMPERATURE (°F)			AVERAGE TEMPERATURE (°F)			MAXIMUM TRACK TEMPERATURE (°F)		
		INNER RACE	BALL	OUTER RACE	INNER RACE	BALL	OUTER RACE	INNER RACE	BALL	OUTER RACE	INNER RACE	BALL	OUTER RACE	INNER RACE	BALL	OUTER RACE	INNER RACE	BALL	OUTER RACE
-240	-236	-151	-32	-132	5	79	94	-130	11	-119	118	139	127	*	*	*	*	*	*
-230	-226	-130	-8	-118	85	107	114	-102	49	-101	167	185	162	*	*	*	*	*	*
-218	-214	-113	8	-105	106	124	128	-86	66	-87	188	204	178	*	*	*	*	*	*

COOLANT FLOWRATE = 7.0 LBS/SEC

FRICTION FACTOR = 0.2

* THERMALLY UNSTABLE

SRS TECHNOLOGIES

EXHIBIT 3.2.10 COMPONENT TEMPERATURES FOR DIFFERENT CONTACT FRICTION FACTORS WITH 245% INCREASE IN HEAT TRANSFER COEFFICIENT

45 mm BEARING

FRICTION FACTOR	BEARING AXIAL PRELOAD (LBS)																	
	350						480						850					
	AVERAGE TEMPERATURE (°F)			MAXIMUM TRACK TEMPERATURE (°F)			AVERAGE TEMPERATURE (°F)			MAXIMUM TRACK TEMPERATURE (°F)			AVERAGE TEMPERATURE (°F)			MAXIMUM TRACK TEMPERATURE (°F)		
	INNER RACE	BALL	OUTER RACE	INNER RACE	BALL	OUTER RACE	INNER RACE	BALL	OUTER RACE	INNER RACE	BALL	OUTER RACE	INNER RACE	BALL	OUTER RACE	INNER RACE	BALL	OUTER RACE
0.2	-197	-158	-173	-64	-67	-17	-193	-150	-171	-44	-50	-9	-179	-120	-160	24	8	27
0.3	-176	-110	-139	33	27	106	-164	-96	-133	74	59	123	123	-12	-100	240	205	220
0.5	-98	46	-38	330	307	426	-40	157	6	558	503	560	*	*	*	*	*	*

FLOWRATE = 7.0 LBS/SEC
INLET COOLANT TEMPERATURE = -230°F
INCREASE IN HEAT TRANSFER COEFFICIENT OF 245%
* THERMALLY UNSTABLE

EXHIBIT 3.2.11 COMPONENT TEMPERATURES FOR DIFFERENT CONTACT FRICTION FACTORS WITH 343% INCREASE IN HEAT TRANSFER COEFFICIENT

45 mm BEARING

FRICTION FACTOR	BEARING AXIAL PRELOAD (LBS)																	
	350						480						850					
	AVERAGE TEMPERATURE (°F)			MAXIMUM TRACK TEMPERATURE (°F)			AVERAGE TEMPERATURE (°F)			MAXIMUM TRACK TEMPERATURE (°F)			AVERAGE TEMPERATURE (°F)			MAXIMUM TRACK TEMPERATURE (°F)		
	INNER RACE	BALL	OUTER RACE	INNER RACE	BALL	OUTER RACE	INNER RACE	BALL	OUTER RACE	INNER RACE	BALL	OUTER RACE	INNER RACE	BALL	OUTER RACE	INNER RACE	BALL	OUTER RACE
0.2	-209	-185	-188	-94	-104	-54	-206	-180	-186	-77	-90	-46	-193	-154	-176	-23	-42	-17
0.3	-191	-147	-159	-14	-26	51	-186	-138	-156	14	-4	64	-168	-102	-141	108	73	114
0.5	-149	-62	-92	185	156	292	-132	-32	-81	261	218	328	-28	164	11	719	597	618

FLOWRATE = 7.0 LBS/SEC
INLET COOLANT TEMPERATURE = -230 F
INCREASE IN HEAT TRANSFER COEFFICIENT OF 343

SRS TECHNOLOGIES

for this case, the heat transfer coefficient was increased by 343%. The results of the cases studied with 343% increase in heat transfer coefficient have been reported in Exhibit 3.2.11. The maximum track temperature has been found to be 719°F with a friction factor of 0.5 and a preload of 850 lbs. It should be observed that the higher track temperatures for stable cases occur with the higher heat transfer coefficients and friction coefficients. These conditions allow high local heating while providing the capability to remove sufficient heat to prevent thermal instability.

EFFECT OF AXIAL PRELOAD

The effect of varying axial preload on the 45 mm inboard bearing was determined for friction factors of 0.2, 0.3, and 0.5. Exhibits 3.2.12 through 3.2.14 show the effect of axial preload using the increased heat transfer coefficient of 245%. Exhibits 3.2.15 through 3.2.17 show the effect of preload using the 343% increased heat transfer coefficient. The exhibits show that axial preload does have a significant effect on operating temperatures. The effect of preload is increased as the friction factor is increased. At a friction factor of 0.2, the average ball temperature increases by 31°F with an increase of preload from 350 to 850 lbs. At a friction of 0.5, the average ball temperature increased by 226°F with an increase in preload from 350 to 850 lbs. The dashed line in Exhibit 3.2.14 indicates that the 850 lb preload case did not have a thermally stable solution.

EFFECT OF FRICTION FACTOR

The effect of increasing the friction factor for preloads of 350, 480, and 850 lbs and the two increased heat transfer coefficients are shown in Exhibits 3.2.18 through 3.2.23. The results show that contact friction has a large effect on bearing operating temperatures. An increase in friction factor from 0.2 to 0.5 increased the average ball temperature by 123°F for a preload of 350 lbs and 318°F with a preload of 850 lbs.

EFFECT OF BOUNDARY HEAT TRANSFER COEFFICIENT

The more severe cases involving the higher friction factors and preloads were thermally unstable using the nominal heat transfer coefficient. Thus, the heat transfer coefficient was increased to obtain stable solutions over

EXHIBIT 3.2.12 45mm BEARING OPERATING TEMP. VERSUS AXIAL PRELOAD

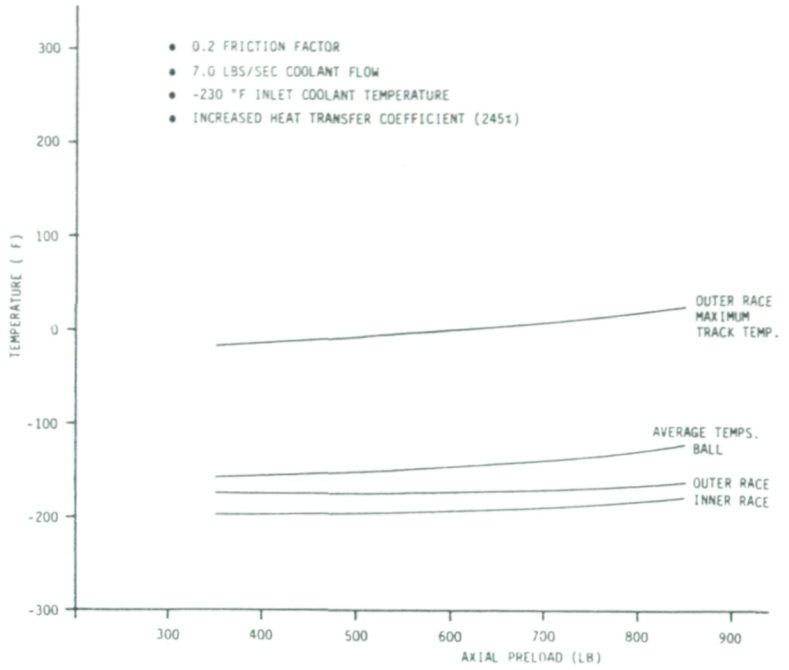

EXHIBIT 3.2.13 45mm PUMP END BEARING OPERATING TEMPERATURES VERSUS AXIAL PRELOAD

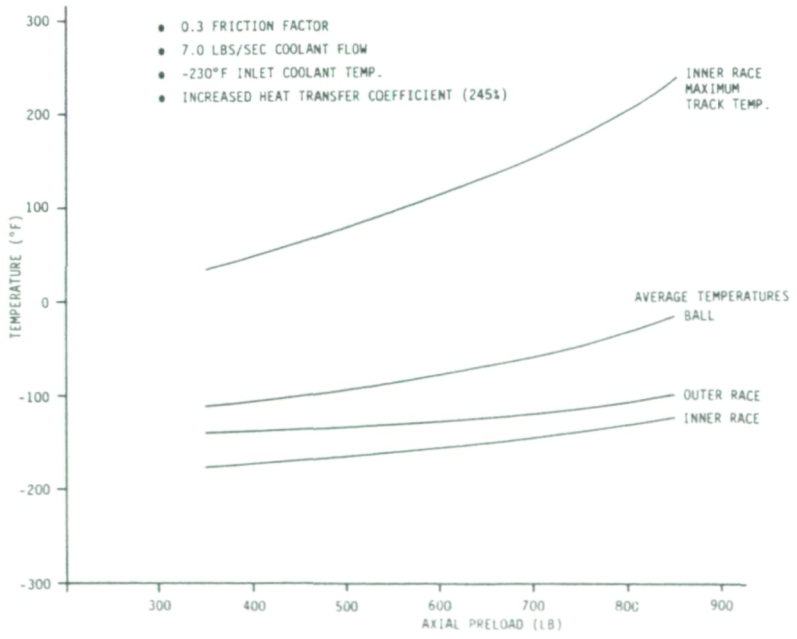

SRS TECHNOLOGIES

EXHIBIT 3.2.14 45mm BEARING OPERATING TEMPERATURES VS. AXIAL PRELOAD

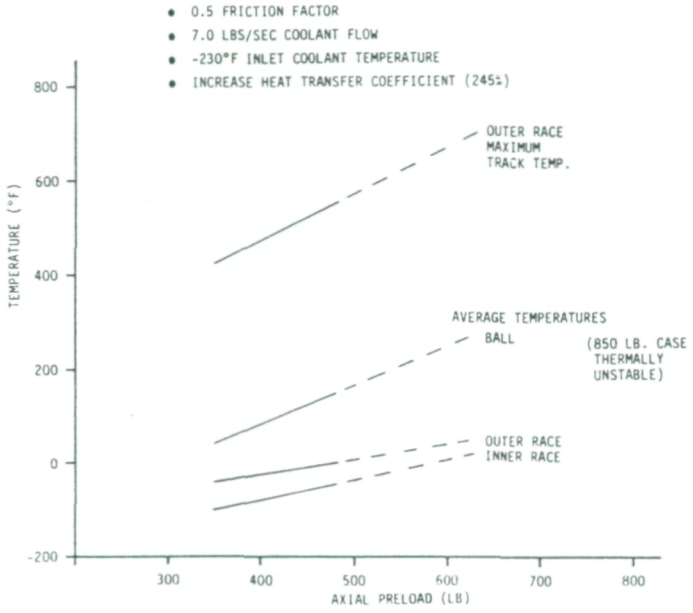

EXHIBIT 3.2.15 45mm BEARING OPERATING TEMP. VERSUS AXIAL PRELOAD

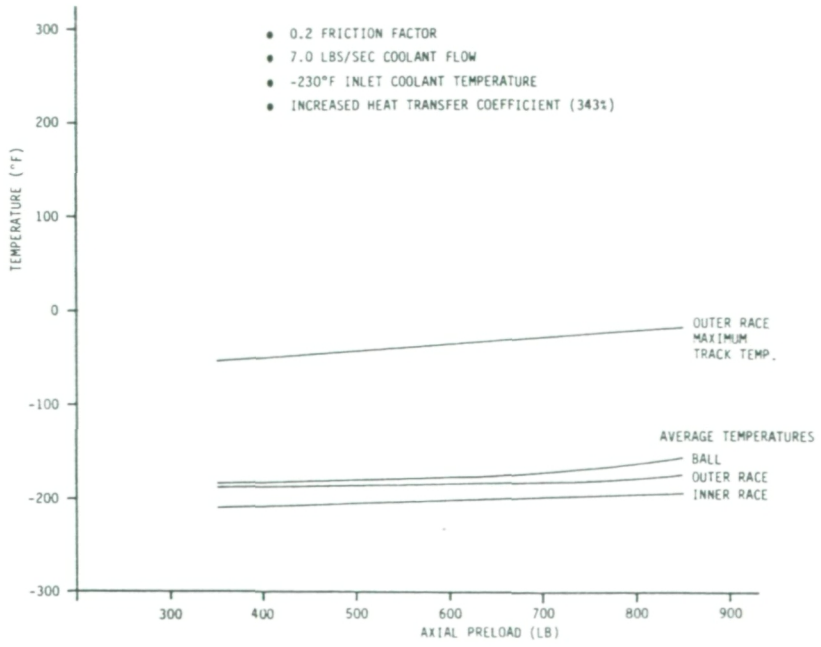

SRS TECHNOLOGIES

EXHIBIT 3.2.16 45mm BEARING OPERATING TEMPERATURES VS. AXIAL PRELOAD

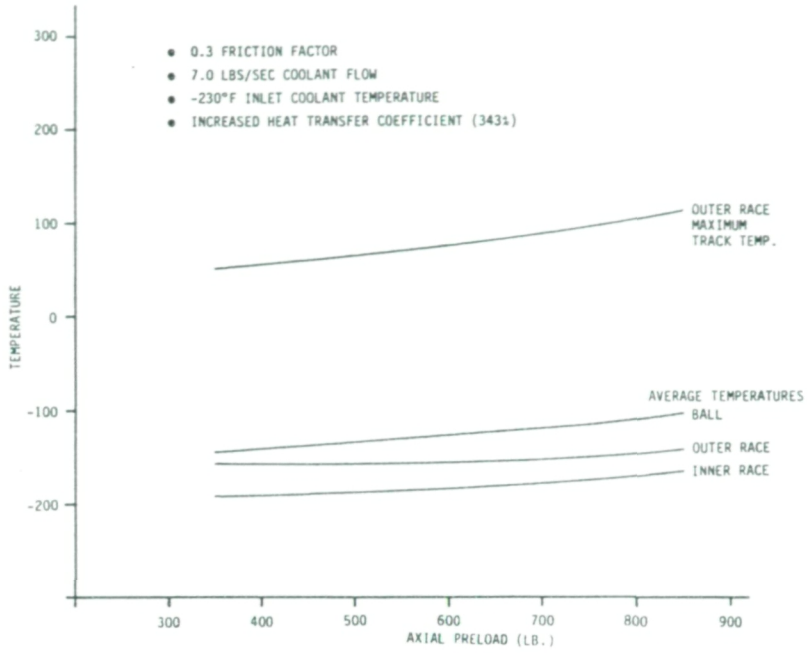

EXHIBIT 3.2.17 45mm BEARING OPERATING TEMPERATURES VS. AXIAL PRELOAD

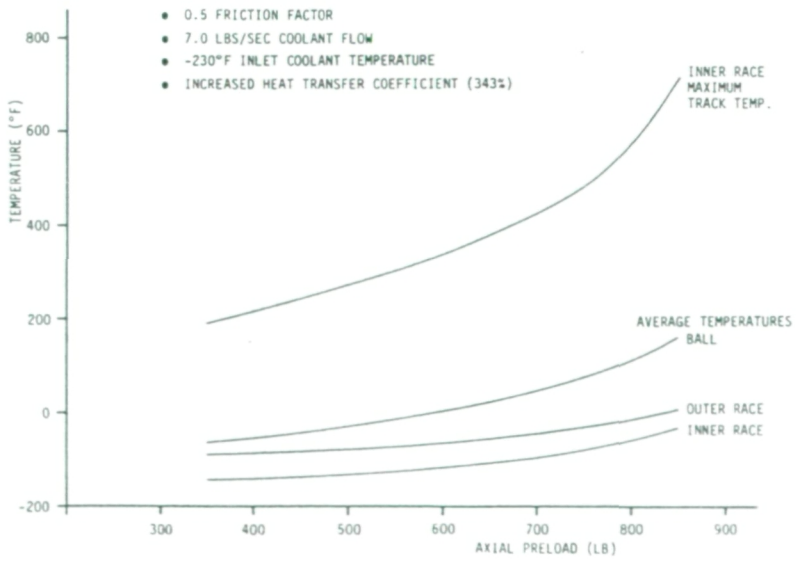

SRS TECHNOLOGIES

EXHIBIT 3.2.18 45mm BEARING OPERATING TEMPERATURES VS. FRICTION FACTOR

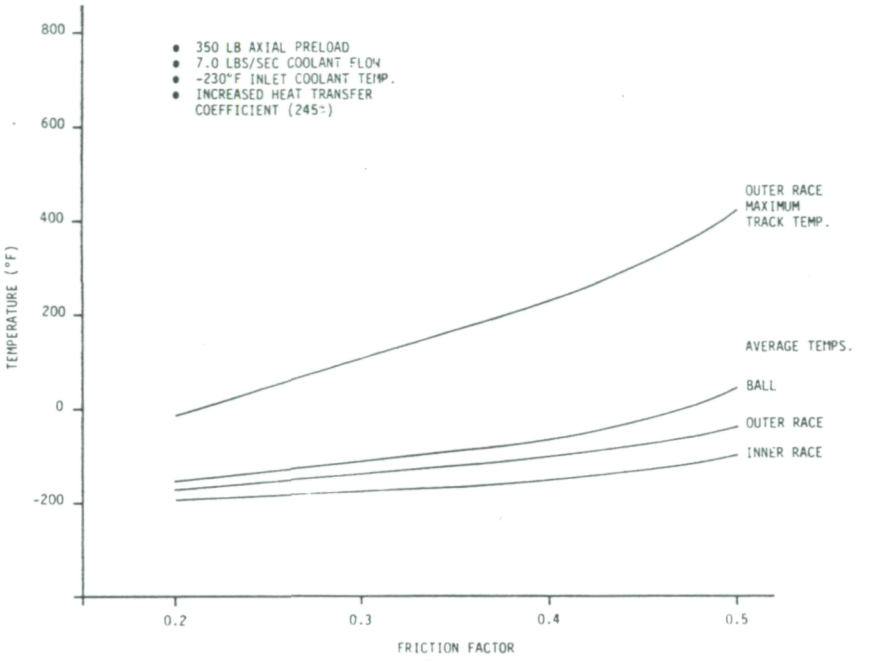

EXHIBIT 3.2.19 45mm BEARING OPERATING TEMPERATURES VS. FRICTION FACTOR

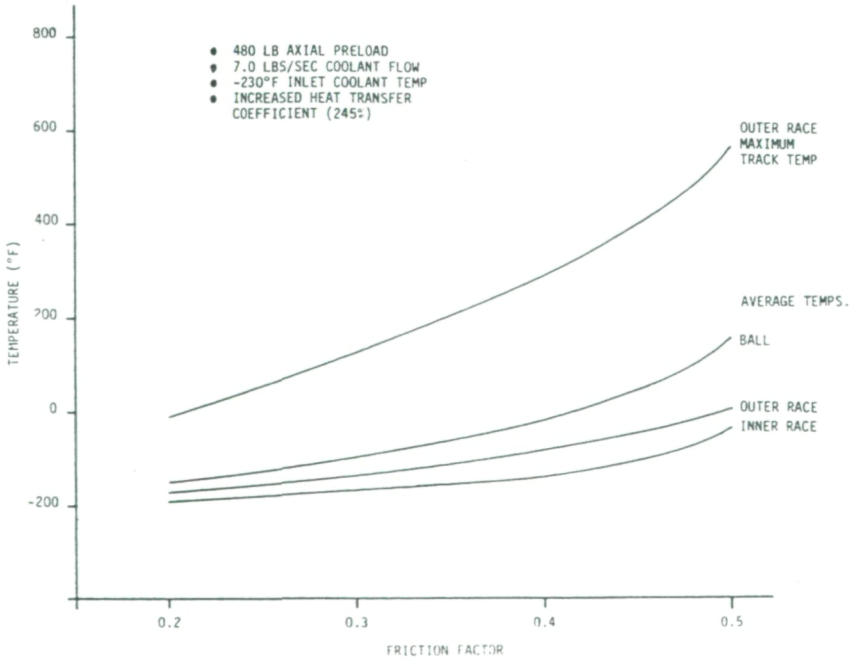

SRS TECHNOLOGIES

EXHIBIT 3.2.20 45mm BEARING OPERATING TEMPERATURES VS. FRICTION FACTOR

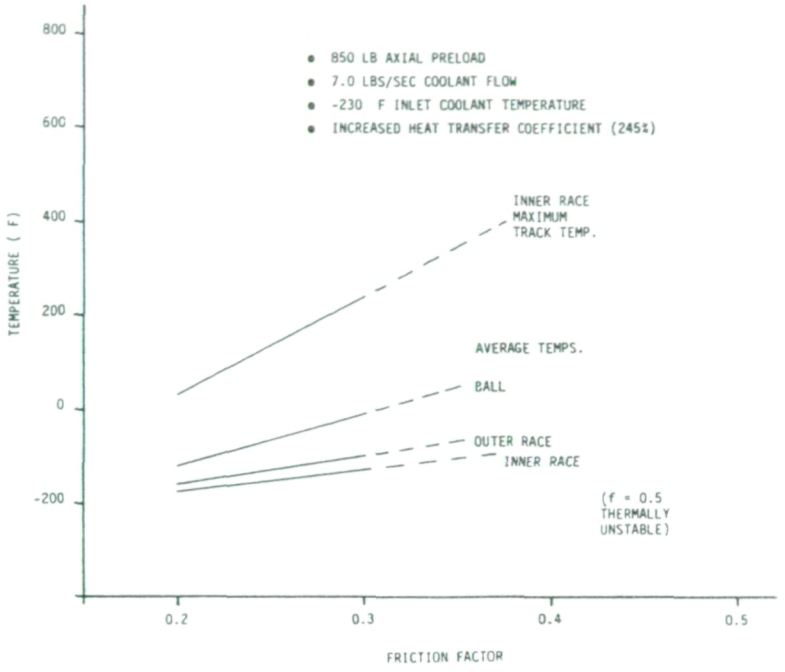

EXHIBIT 3.2.21 45mm BEARING OPERATING TEMPERATURES VS. FRICTION FACTOR

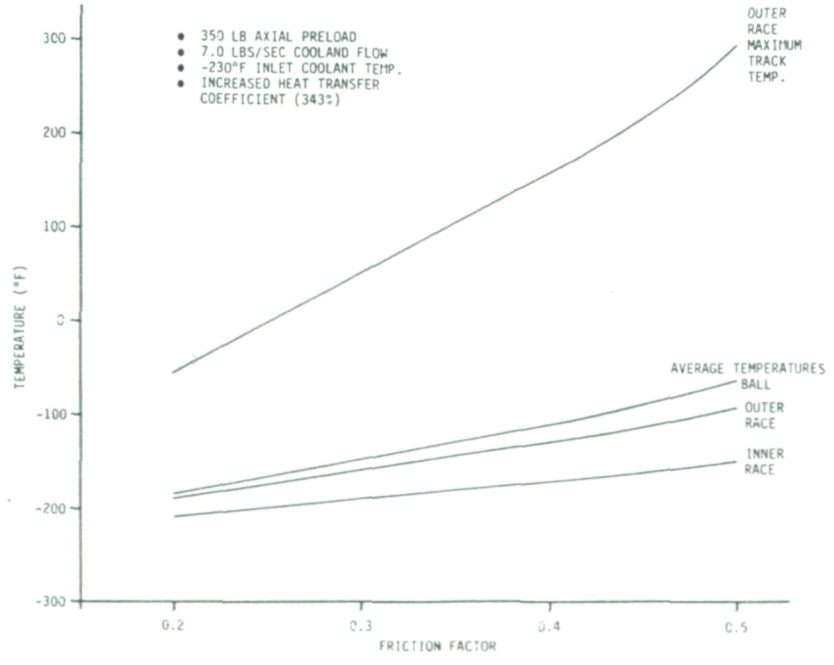

SRS TECHNOLOGIES

EXHIBIT 3.2.22 45mm BEARING OPERATING TEMPERATURES VS. FRICTION FACTOR

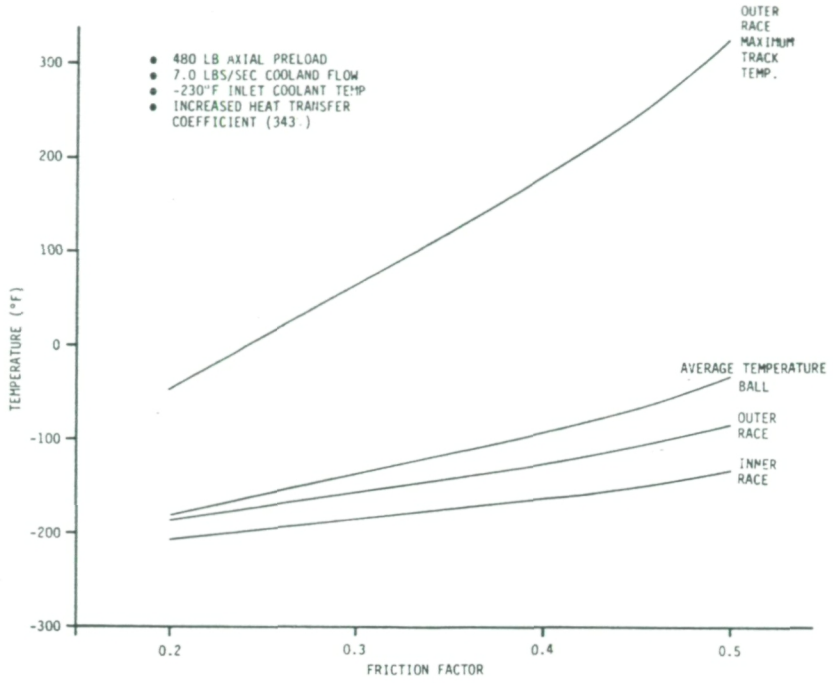

EXHIBIT 3.2.23 45mm BEARING OPERATING TEMPERATURES VS. FRICTION FACTOR

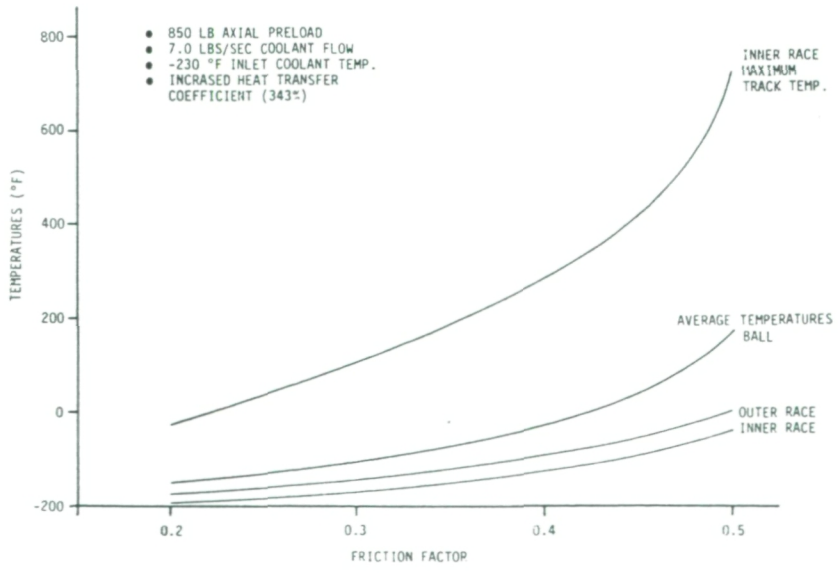

SRS TECHNOLOGIES

the range of friction factors and preloads considered. Exhibits 3.2.24 through 3.2.26 show the results of increasing the heat transfer coefficient. The temperatures decrease with increasing heat transfer coefficient. The heat transfer coefficient had a larger effect on the average ball temperature than it did on the average inner and outer race temperatures. This was because the ball has a larger surface to volume ratio exposed to the fluid than do the inner and outer races. Thus, the ball had a larger heat loss increase than did the inner or outer race as the heat transfer coefficient for surface to fluid increased.

The Dittus Boelter equation was used to determine the heat transfer coefficients for the inner and outer races. The Katsnellson equation was used for the ball. The properties were evaluated at the film temperature which is the average of the surface and saturation temperature.

EFFECT OF COOLANT FLOW RATE

Exhibits 3.2.27 through 3.2.30 show the effect of changing the coolant flow rate. The operating temperatures do not change much over the range of flow rates studied. However, an increase in coolant flow rate could prevent a marginal case from diverging.

EFFECT OF INLET COOLANT TEMPERATURE

The effects of varying inlet temperatures are shown in Exhibits 3.2.31 through 3.2.34. Two subcooled cases (-240°F and -230°F) and a saturated case (T_{sat} = -214°F) were considered. The coolant was introduced at Bearing 1 and was allowed to increase in temperature while passing through the bearing. For the saturated case, the coolant was introduced at -218°F and was allowed to increase to the saturation temperature of -214°F when entering Bearing 2.

The inlet coolant temperature did not have a very significant effect on the bearing operating temperatures. But, lowering the inlet temperature could cause a case that would be thermally unstable to become stable.

EFFECT OF OUTER RACE MISALIGNMENT

Angular misalignments of the outer race up to 31.5 minutes were studied to determine the effect on bearing operating temperatures. The outer race

EXHIBIT 3.2.24 45mm BEARING OPERATING TEMPERATURES VS. HEAT TRANSFER COEFFICIENT

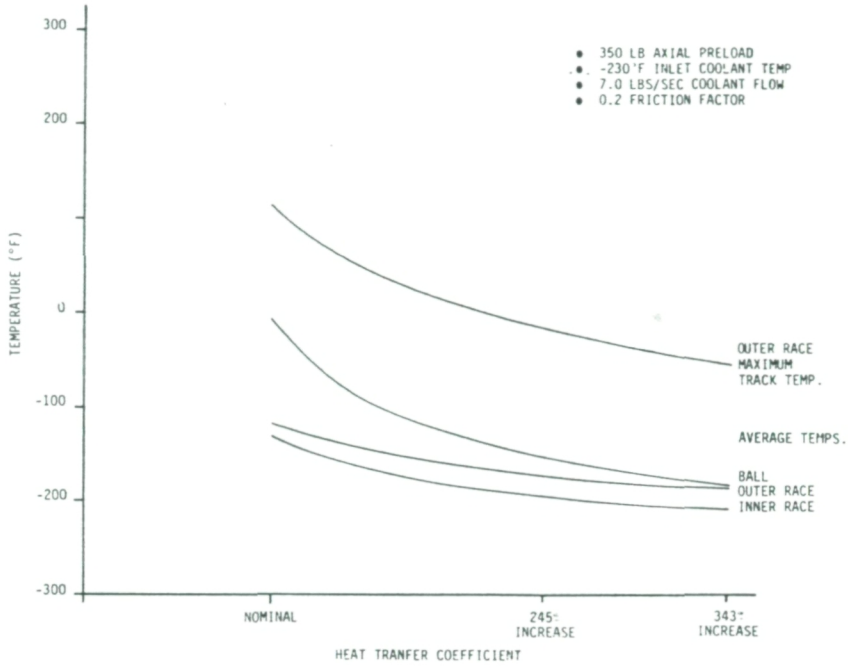

EXHIBIT 3.2.25 45mm BEARING OPERATING TEMPERATURES VS. HEAT TRANSFER COEFFICIENT

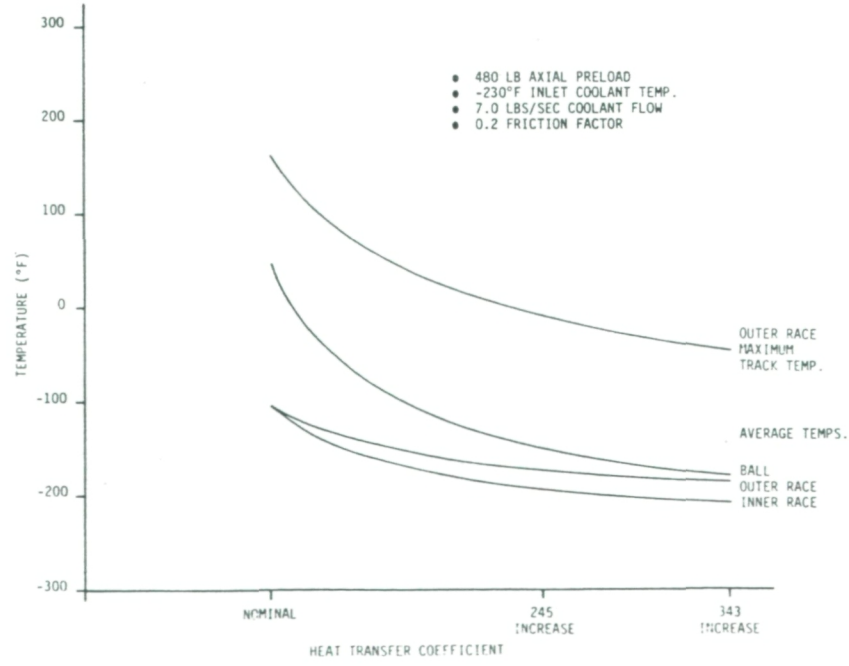

SRS TECHNOLOGIES

EXHIBIT 3.2.26 45mm BEARING OPERATING TEMPERATURES VS. HEAT TRANSFER COEFFICIENT

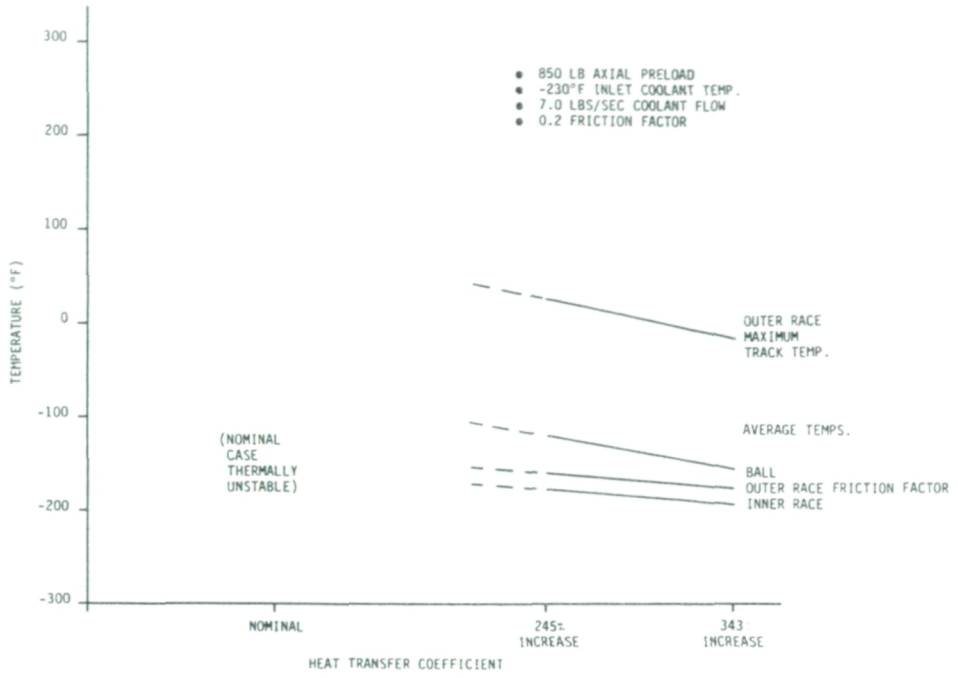

EXHIBIT 3.2.27 45mm BEARING OPERATING TEMPERATURES VS. COOLANT FLOWRATE

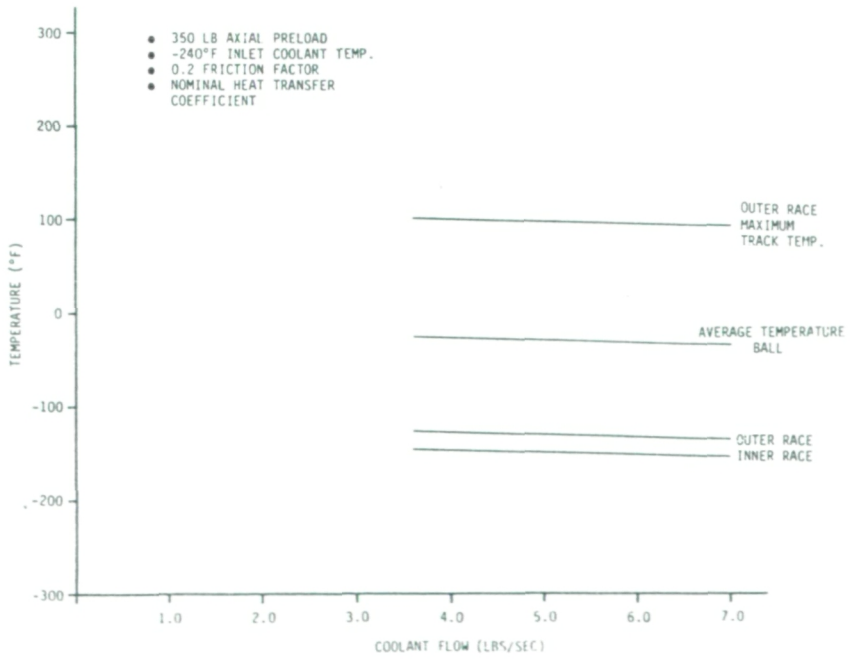

SRS TECHNOLOGIES

EXHIBIT 3.2.28 45mm BEARING OPERATING TEMPERATURES VS. COOLANT FLOWRATE

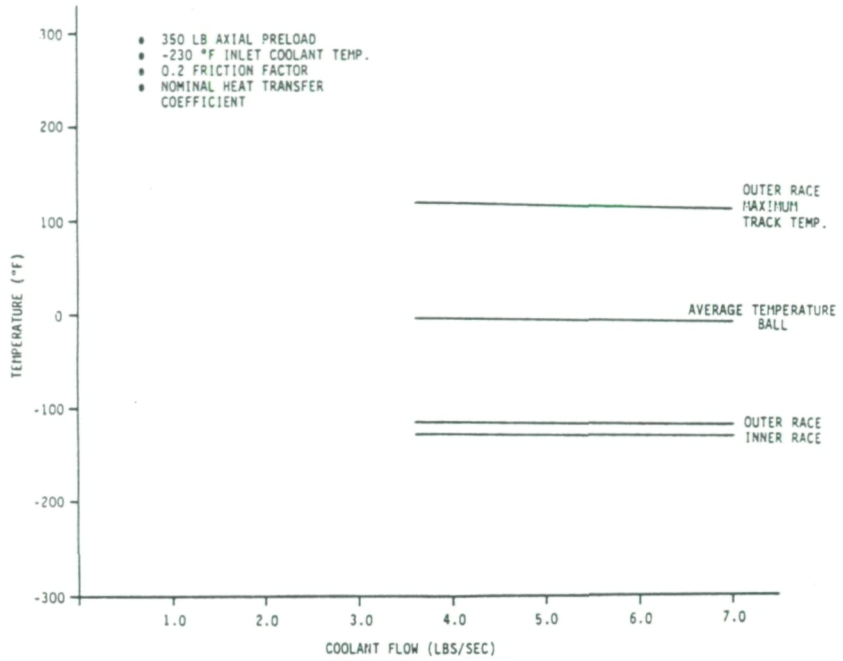

EXHIBIT 3.2.29 45mm BEARING OPERATING TEMPERATURES VS. COOLANT FLOWRATE

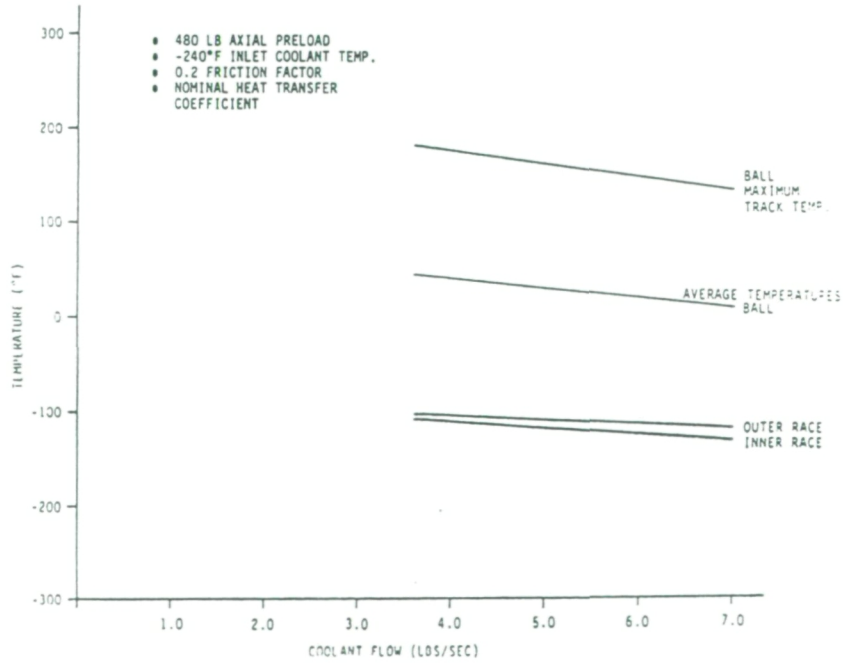

SRS TECHNOLOGIES

EXHIBIT 3.2.30 45mm BEARING OPERATING TEMPERATURES VS. INLET COOLANT FLOWRATE

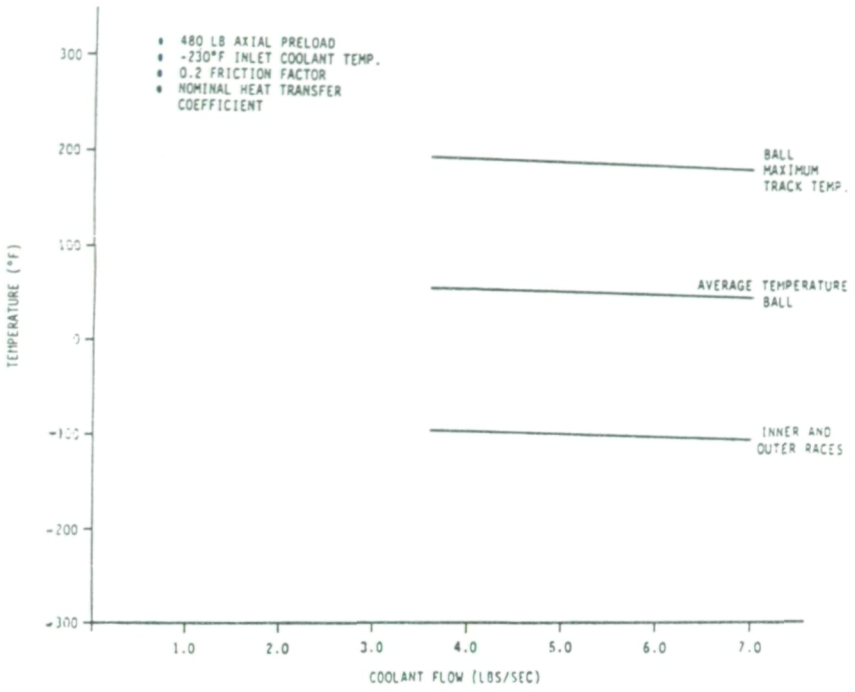

EXHIBIT 3.2.31 45mm BEARING OPERATING TEMPERATURES VS. INLET COOLANT TEMPERATURE

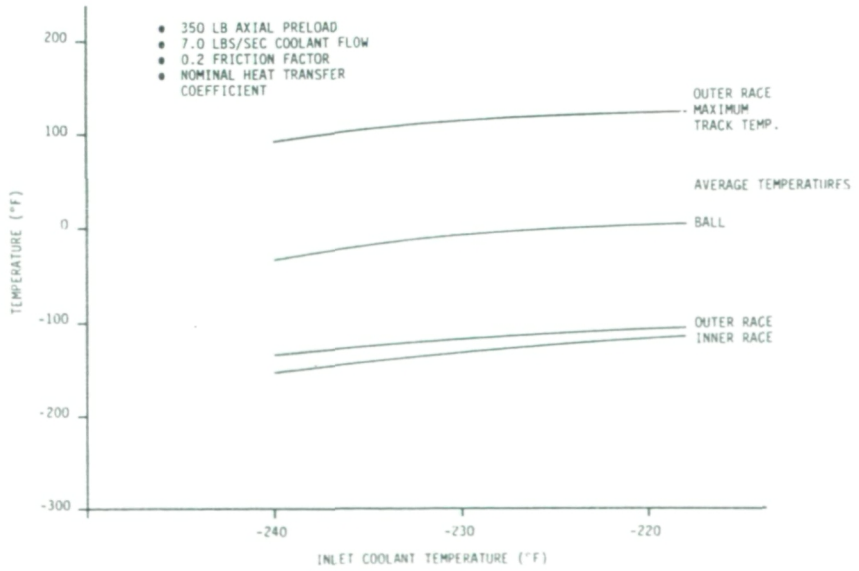

SRS TECHNOLOGIES

EXHIBIT 3.2.32 45mm BEARING OPERATING TEMPERATURES VS. COOLANT TEMPERATURE

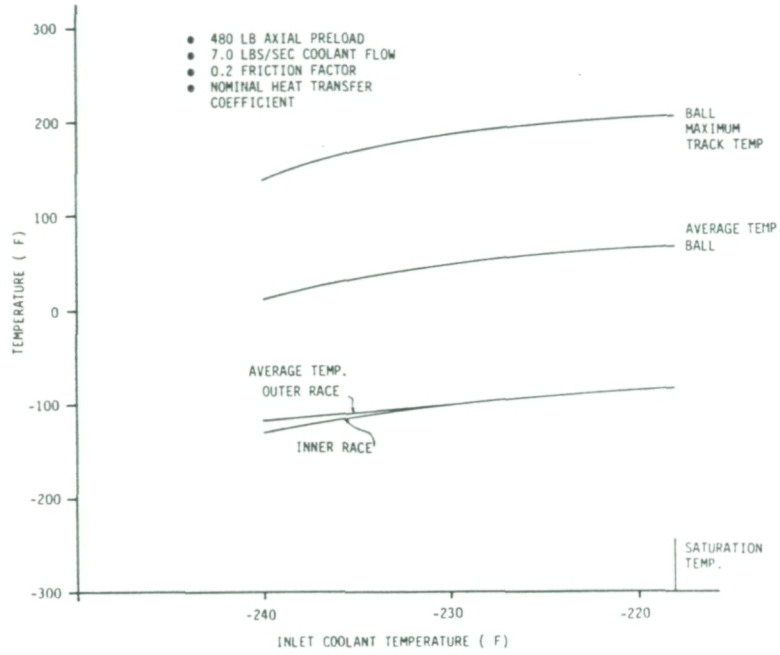

EXHIBIT 3.2.33 45mm BEARING OPERATING TEMPERATURES VS. INLET COOLANT TEMPERATURE

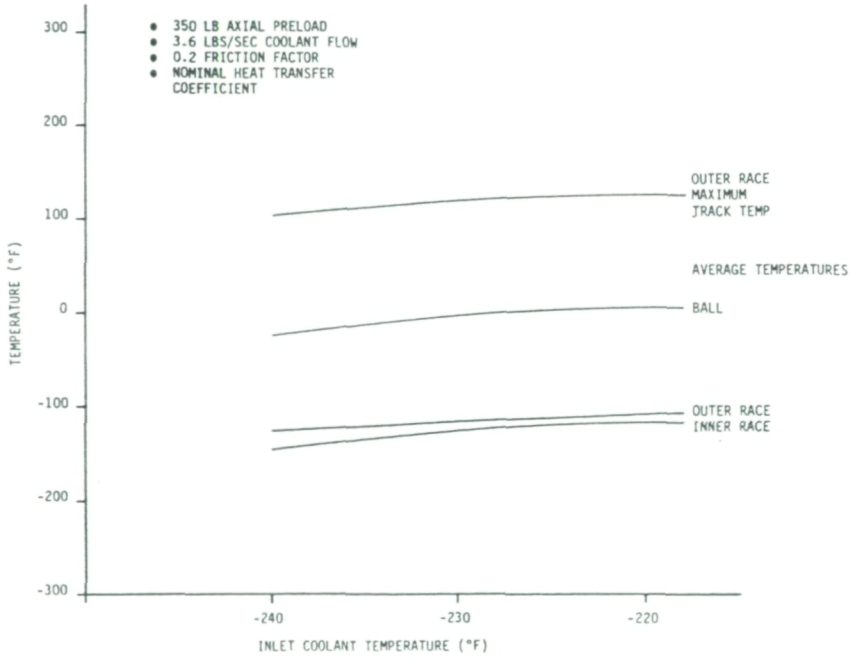

SRS TECHNOLOGIES

EXHIBIT 3.2.34 45mm BEARING OPERATING TEMPERATURES VS. INLET COOLANT TEMPERATURE

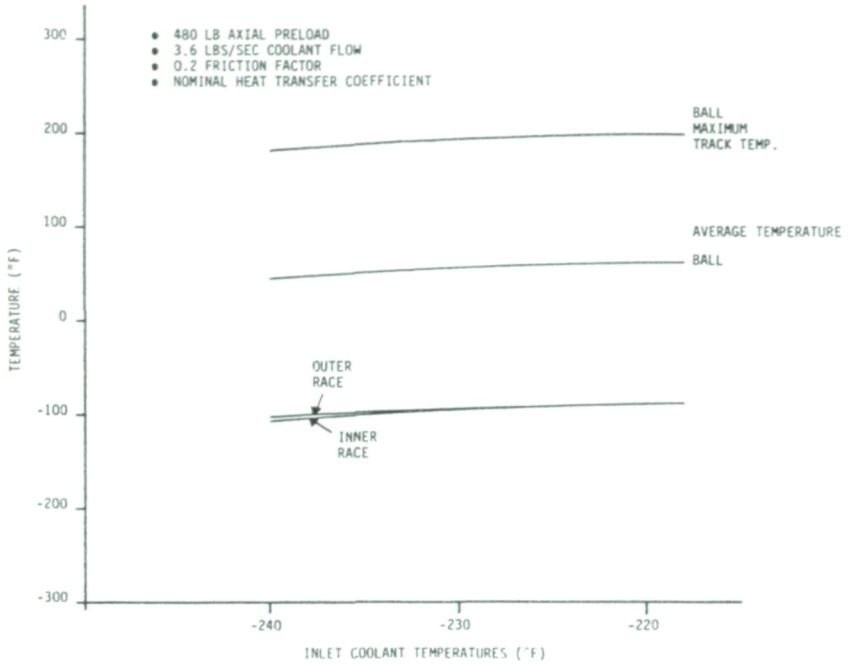

EXHIBIT 3.2.35 45mm BEARING OPERATING TEMPERATURES VS. OUTER RACE MISALIGNMENT

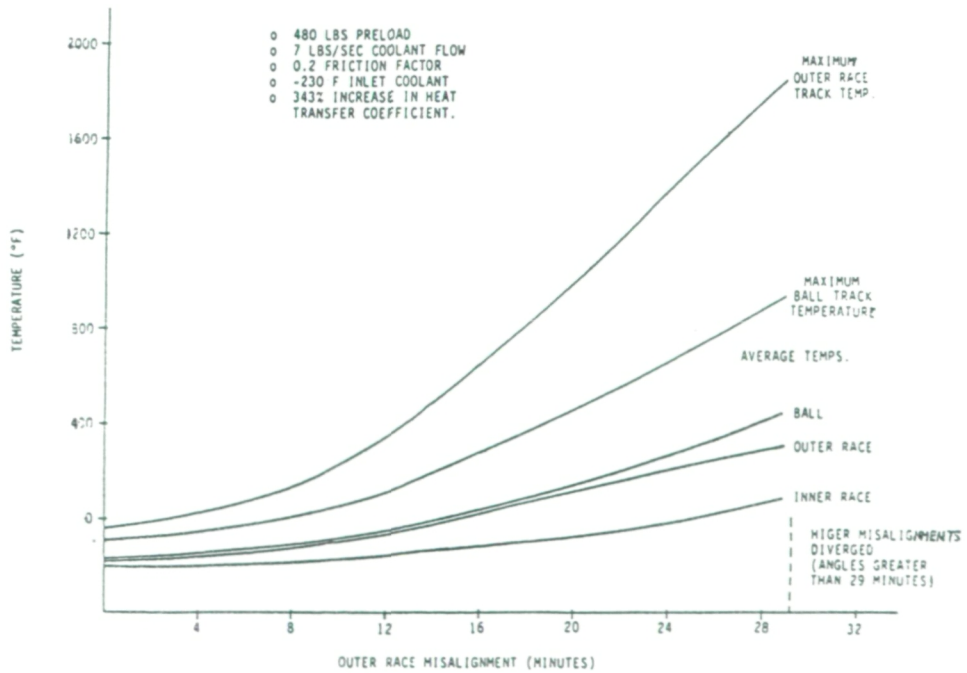

SRS TECHNOLOGIES

was tilted so as to place the heaviest loaded ball in the "pinch point". Consequently, the misalignment contributed to the radial loading of the ball. Exhibit 3.2.35 shows the effect of outer race misalignment for a case using 480 lbs preload, 7.0 lbs/sec flow rate, 0.2 friction factor, -230°F inlet temperature, and 343% increased heat transfer coefficient. The maximum outer race tilt, that produced a stable solution, was about 29 minutes. This tilt caused the highest stable operating temperatures observed in this analysis. The maximum outer race track temperature was found to be 1858°F. The tilt caused the outer race to heat and expand more than the inner race. Thus, the bearing is able to maintain a sufficient operating clearance for higher ball temperatures.

EFFECT OF OUTER RACE-TO-ISOLATOR CLEARANCE

Clearances of 2.6, 1.7, and 1.0 mils between the outer race and isolator were investigated. The heat transfer coefficient was increased by 245% of the nominal value to obtain stable solutions over the range of parameters studied. The results are shown in Exhibits 3.2.36 and 3.2.37. The clearance, over the range studied, had a small effect on the bearing operating temperatures. The average ball temperature increased 46°F for a decrease in clearance of 2.6 to 1.0 mils at a preload of 850 lbs. The effects on operating clearance is shown in Exhibits 3.2.38 and 3.2.39. Fit pressure is an indication of operating clearance. Clearance does not exist for finite values of fit pressure. As shown on Exhibit 3.2.38, there is no operating clearance between the outer race and isolator for initial clearance values of 1 and 1.7 mils. For the nominal value of 2.6 mils, clearances do exist. Note however that these cases were evaluated for a 2.45 increase in nominal heat transfer coefficient. As shown in Exhibit 3.2.39 operational clearance does not exist for the nominal heat transfer case (0% increase) and friction factor of 0.2. Operational clearance is also lost for the higher values of friction over the preload range investigated.

EFFECT OF THERMAL ISOLATION OF THE OUTER RACE

The effect of thermally isolating the outer race from the isolator was determined. The results are shown in Exhibit 3.2.40. The temperature increase was very slight. The small increase indicates that most of the heat

EXHIBIT 3.2.36 EFFECT OF OUTER RACE TO ISOLATOR CLEARANCES (45mm BEARING)

OUTER RACE CLEARANCE	BEARING AXIAL PRELOAD (LBS)																	
	350						480						850					
	AVERAGE TEMPERATURE (°F)			MAXIMUM TRACK TEMPERATURE (°F)			AVERAGE TEMPERATURE (°F)			MAXIMUM TRACK TEMPERATURE (°F)			AVERAGE TEMPERATURE (°F)			MAXIMUM TRACK TEMPERATURE (°F)		
	INNER RACE	BALL	OUTER RACE	INNER RACE	BALL	OUTER RACE	INNER RACE	BALL	OUTER RACE	INNER RACE	BALL	OUTER RACE	INNER RACE	BALL	OUTER RACE	INNER RACE	BALL	OUTER RACE
2.6 mils	-197	-158	-173	-64	-67	-17	-193	-150	-171	-44	-50	-9	-179	-120	-160	24	8	27
1.7 mils	-195	-154	-172	-54	-58	-11	-190	-144	-168	-29	-37	1	-171	-106	-153	62	40	53
1.0 mils	-192	-148	-169	-39	-45	-2	-184	-130	-164	-1	-13	15	-154	-74	-142	123	94	90

Flowrate = 7.0 lbs/sec
Friction Factor = 0.2
245% Increase in Heat Transfer Coefficient
Inlet Coolant Temperature = -230°F

EXHIBIT 3.2.37 OUTER RACE TO ISOLATOR CLEARANCE VS. COMPONENT TEMPERATURES

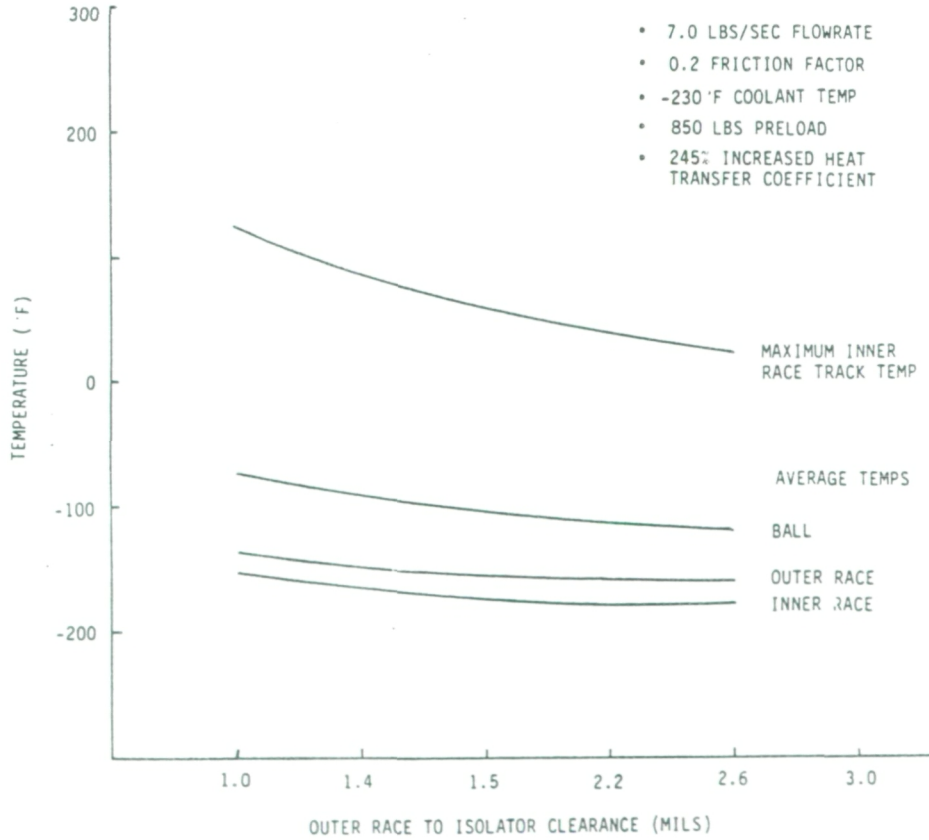

EXHIBIT 3.2.38 THE EFFECT OF CLEARANCE ON THE FIT PRESSURE BETWEEN THE OUTER RACE AND ISOLATOR

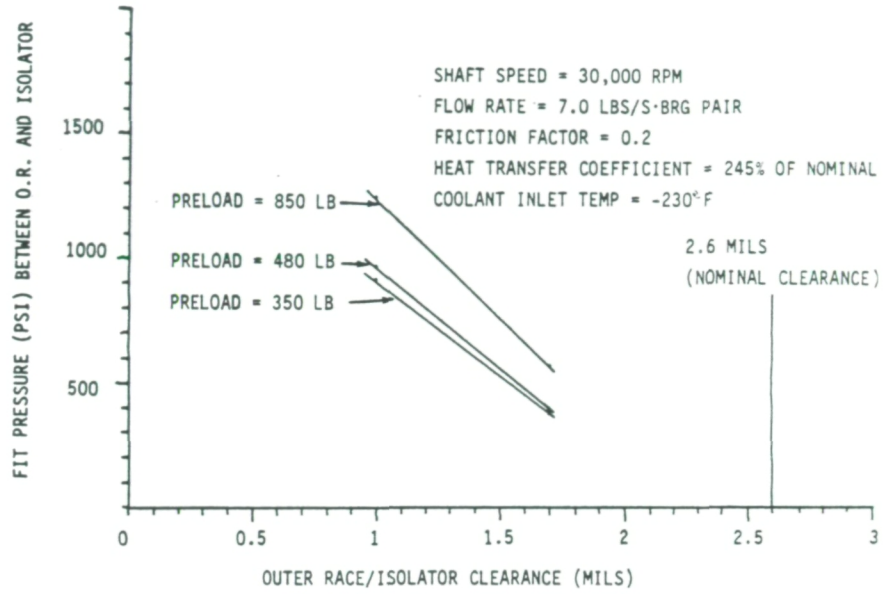

EXHIBIT 3.2.39 THE EFFECT OF PRELOAD ON OUTER RACE/ISOLATOR FIT PRESSURE

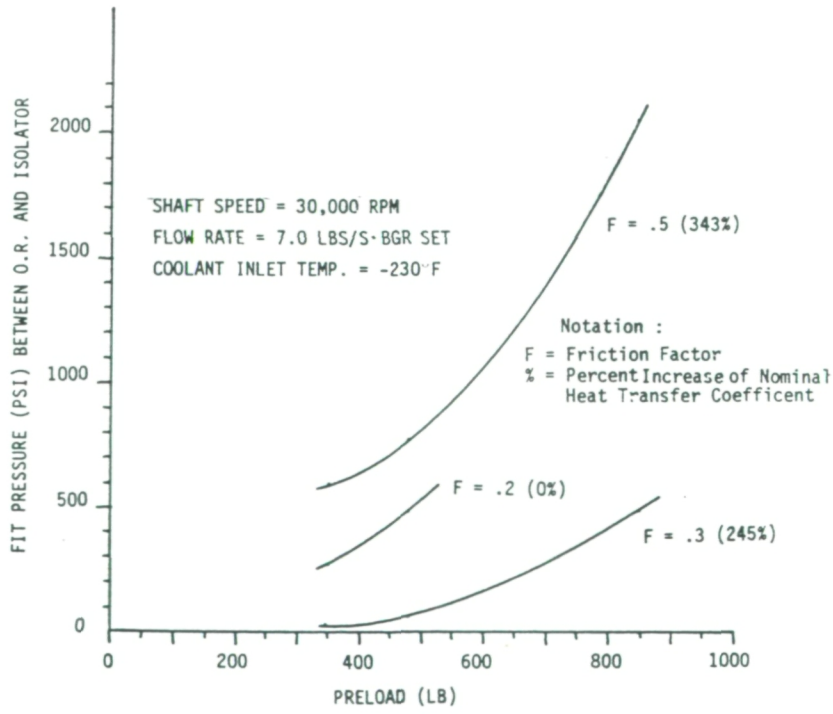

SRS TECHNOLOGIES

EXHIBIT 3.2.40 EFFECTS OF THERMAL ISOLATION OF BEARING ISOLATOR (45mm BEARING)

HEAT TRANSFER BETWEEN ISOLATOR & OUTER RACE	BEARING AXIAL PRELOAD (LBS)																	
	350						480						850					
	AVERAGE TEMPERATURE (°F)			MAXIMUM TRACK TEMPERATURE (°F)			AVERAGE TEMPERATURE (°F)			MAXIMUM TRACK TEMPERATURE (°F)			AVERAGE TEMPERATURE (°F)			MAXIMUM TRACK TEMPERATURE (°F)		
	INNER RACE	BALL	OUTER RACE	INNER RACE	BALL	OUTER RACE	INNER RACE	BALL	OUTER RACE	INNER RACE	BALL	OUTER RACE	INNER RACE	BALL	OUTER RACE	INNER RACE	BALL	OUTER RACE
With	-197	-158	-173	-64	-67	-17	-193	-150	-171	-44	-50	-9	-179	-120	-160	24	8	27
Without	-198	-158	-165	-66	-68	-11	-193	-150	-162	-45	-50	-2	-180	-122	-151	15	1	32

Flowrate = 7.0 lbs/sec
Friction Factor = 0.2
245% Increase in Heat Transfer Coefficient
Inlet Coolant Temperature = 230°F

EXHIBIT 3.2.41 EFFECT OF SATURATED COOLANT ENTERING BEARING 1

INLET COOLANT TEMPERATURE(°F)		AVERAGE TEMPERATURE(°F)			MAXIMUM TRACK TEMPERATURE(°F)		
BEARING 1	BEARING 2	INNER RACE	BALL	OUTER RACE	INNER RACE	BALL	OUTER RACE
-218	-214	-88	63	-88	185	200	176
-214	-214	-87	63	-88	185	200	177

3.6 LBS/SEC COOLANT FLOW
480 LB AXIAL PRELOAD
0.2 FRICTION FACTOR

SRS TECHNOLOGIES

generated is transferred to the coolant and very little is transferred through the bearing isolator.

COOLANT QUALITY

The coolant quality profile was determined for the saturated cases using flowrates of 7.0 and 3.6 lbs/sec. Inlet temperatures of -218°F and -214°F were used for the inlet to bearing 1. For the case using a -214°F inlet temperature, the fluid is assumed to have a quality of zero percent before entering bearing 1. Lowering the inlet temperature of bearing 1 to saturation had little affect on bearing 2 operating temperature, as shown in Exhibit 3.2.41. The quality was calculated as the mass of vapor per total mass of coolant. The mass of vapor was determined from the amount of heat transferred to each fluid node. The quality profiles are shown in Exhibit 3.2.42. Fluid node 9 represents the inlet to bearing 1 and node 10 represents bearing 1. The quality was decreased by approximately 70% by increasing the flowrate from 3.6 to 7.0 lbs/sec.

3.3 LOX TURBOPUMP PUMP-END 45MM BEARING OPERATING CHARACTERISTICS

A bearing thermal model of the SSME LOX turbopump turbine-end bearing was used, in conjunction with an overall bearing/shaft SHABERTH model, to evaluate the thermo-mechanical operating characteristics of the LOX turbopump pump-end bearings. The thermal model is described in detail in Reference 1 and the bearing/shaft model is described in Reference 2. This work was done as a precurisor to the previously described analysis and provided a preliminary assessment of the 45 mm bearing operating characteristics. Since at this time, resources and time did not allow for the development of a detailed thermal model of the pump-end bearings, the turbine-end bearing thermal model developed in Reference 1 was used. The close similarity of the bearings justify this approach for preliminary assessment.

The analysis results are reported in Reference 2. This section includes further data from this analysis.

Exhibits 3.3.1 and 3.3.2 show bearing frictional heat generation resulting from the evaluation of loading conditions, clearances, and shaft speed, as noted. Three cases were evaluated for each clearance: 1) the assembled bearing, preloaded, with no thermal gradient across the bearing and no

EXHIBIT 3.2.42 QUALITY OF FLUID FLOWING THROUGH BEARING 2

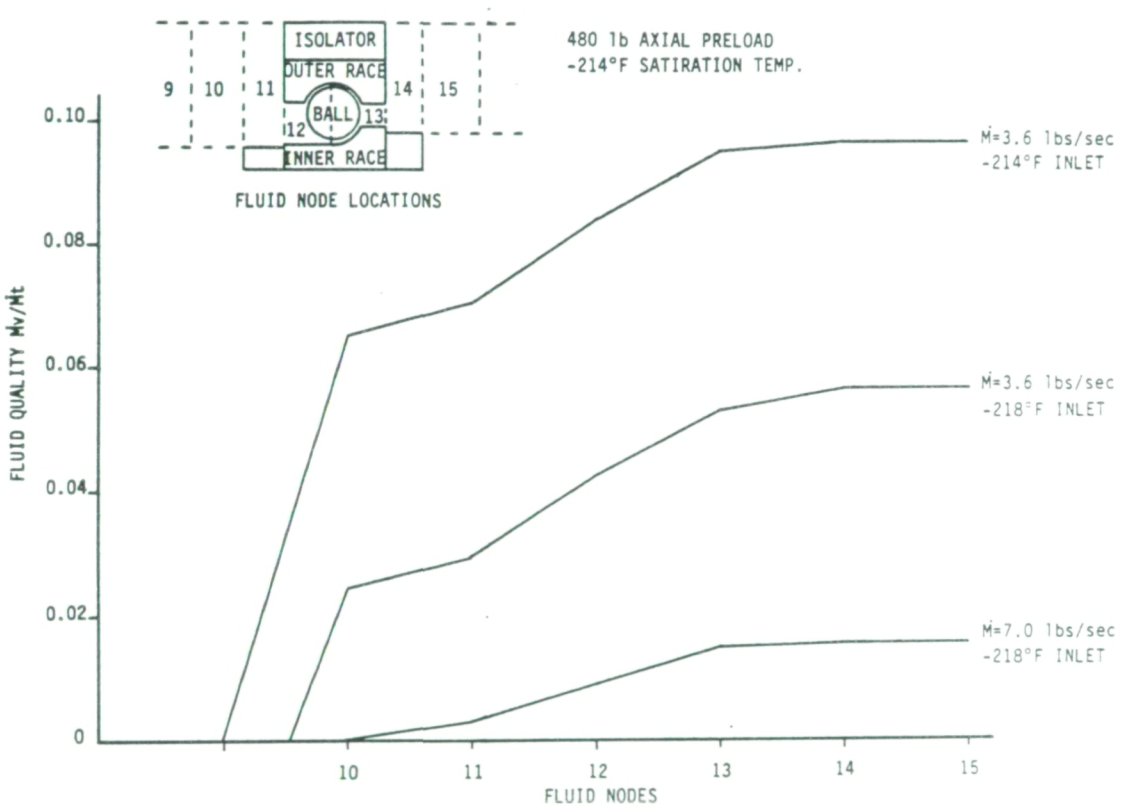

EXHIBIT 3.3.1

PREBURNER PUMP END BEARINGS (45mm.)
BEARING HEAT GENERATION (KW)
4.0 mil CLEARANCE (f_i = 0.53, f_o = 0.52, LOADS FROM BUILD #2606R1)
SHAFT SPEED (30,000 RPM)

	BEARING NO.	MAX PER BALL	MIN PER BALL	AVERAGE PER BALL	TOTAL
ASSEMBLED BEARING, PRELOADED, NO EXTERNAL RADIAL LOADS, NO THERMAL GRADIENT	1	N/A	N/A	.169	2.2
	2			.169	2.2
LOADED BEARING PRELOADED, RADIALLY LOADED NO THERMAL GRADIENT	1	.293	.150	.208	2.7
	2	.941	.036	.338	4.4
LOADED BEARING PRELOADED, RADIALLY LOADED THERMAL GRADIENT	1	.464	.381	.423	5.5
	2	1.202	.115	.546	7.1

EXHIBIT 3.3.2

PREBURNER PUMP END BEARINGS (45mm)
BEARING HEAT GENERATION (KW)
6.3 mil CLEARANCE (f_i = 0.55, f_o = 0.52, LOADS FROM BUILD #2606R1)
SHAFT SPEED (30,000 RPM)

	BEARING NO.	MAX PER BALL	MIN PER BALL	AVERAGE PER BALL	TOTAL
ASSEMBLED BEARING, PRELOADED, NO EXTERNAL RADIAL LOADS, NO THERMAL GRADIENT	1	N/A	N/A	.169	2.2
	2			.169	2.2
LOADED BEARING PRELOADED, RADIALLY LOADED NO THERMAL GRADIENT	1	.287	.134	.208	2.7
	2	.862	.034	.346	4.5
LOADED BEARING PRELOADED, RADIALLY LOADED THERMAL GRADIENT	1	.366	.247	0.300	3.9
	2	1.003	.070	0.423	5.5

SRS TECHNOLOGIES

external radial loads; 2) the loaded bearing, preloaded and with external radial loading, but no thermal gradient considered; and 3) the loaded bearing, preloaded and radially loaded, considering a thermal gradient across the bearing which was determined by a thermal-mechanical evaluation using both a thermal bearing model and a bearing/shaft model. For each radially loaded case the maximum and minimum heat generation is shown corresponding to the most heavily loaded ball and the least heavily loaded ball, as well as the average heat generation per ball and the total heat generation per bearing. This data reflects the unsymmetrical heat generated in the bearing due to radial loading and the influence of clearance and curvature changes.

Exhibits 3.3.3 and 3.3.4 contain various bearing operating characteristics for two clearances and the three cases previously discussed. Radial and axial reactions, bearing deflection, moments, maximum hertz stresses, contact angles and internal clearances for pump-end bearings 1 and 2 are shown.

Bearing inlet and outlet coolant temperatures are shown in Exhibit 3.3.5 for two coolant conditions, subcooled and saturated. The subcooled case provided 16 degrees of subcooling at the bearing 1 inlet with a total ΔT of 13°F across the bearing set. In order to evaluate the effects of two phase flow on the thermal characteristics of the number 2 pump-end bearing, coolant at saturation temperature (-214°F) entering bearing 2 was modeled. The thermal modeling temperature results for each of these cases are reported in Reference 2. These results indicate that no drastic temperature change occurred between the saturated and subcoolant cases. This is because the surfaces of the bearing components were already vapor blanketed before the coolant entering bearing 2 became saturated, and the local fluid heat transfer coefficient did not change significantly due to the increase in bulk coolant temperature from subcooled to saturation (16°F).

The principal difference in the results of this analysis, using the 57 mm bearing thermal model to represent the 45 mm bearing, and the previously discussed analysis is the tendency of the 45 mm model to become thermally unstable at conditions much less severe than those that produced thermal instability in the 57 mm bearing.

EXHIBIT 3.3.3 PREBURNER PUMP END BEARINGS (45mm) OPERATING CHARACTERISTICS

4.0 mil CLEARANCE (f_i = 0.53, f_o = 0.52, LOADS FROM BUILD #2606R1)
SHAFT SPEED (30,000RPM)

	BEARING NO.	REACTIONS (LBS) RADIAL	AXIAL	DEFLECTION (inches)	MOMENTS (ft-lbs)	MAX HERTZ STRESSES (kpsi) OUTER	INNER	CONTACT ANGLES (max loaded ball) OUTER	INNER	INTERNAL CLEARANCE (mils)
ASSEMBLED BEARING PRELOADED, NO EXTERNAL RADIAL LOADS, NO THERMAL GRADIENT	1	0	836	0	0	244	268	18.7	28.8	2.7
	2	0	836	0	0	244	268	-18.7	-28.8	2.7
LOADED BEARING PRELOAD & RADIAL LOADING NO THERMAL GRADIENT	1	398	1004	.00049	-16	280	324	19.7	25.5	2.6
	2	1705	-1385	.00084	89	365	443	-23.3	-26.0	2.5
LOADED BEARING PRELOAD & RADIAL LOADING THERMAL GRADIENT	1	241	1811	.0003	-6	305	362	20.9	25.1	1.6
	2	1886	-2105	.0005	98	377	460	-23.8	-26.0	1.5

EXHIBIT 3.3.4 PREBURNER PUMP END BEARINGS (45mm) OPERATING CHARACTERISTICS

6.3 mil CLEARANCE (f_i = 0.55, f_o = 0.52, LOADS FROM BUILD #2606R1)
SHAFT SPEED (30,000RPM)

	BEARING NO.	REACTIONS (LBS) RADIAL	AXIAL	DEFLECTION (inches)	MOMENTS (ft-lbs)	MAX HERTZ STRESSES (kpsi) OUTER	INNER	CONTACT ANGLES (max loaded ball) OUTER	INNER	INTERNAL CLEARANCE (mils)
ASSEMBLED BEARING PRELOADED, NO EXTERNAL RADIAL LOADS, NO THERMAL GRADIENT	1	0	930	0	0	245	299	19.5	29.0	4.8
	2	0	-930	0	0	245	299	-19.5	-29.0	4.8
LOADED BEARING PRELOAD & RADIAL LOADING NO THERMAL GRADIENT	1	440	981	.0006	-20	279	357	20.88	26.73	4.7
	2	1657	-1397	.0009	92	356	477	-24.31	-27.13	4.6
LOADED BEARING PRELOAD & RADIAL LOADING THERMAL GRADIENT	1	313	1553	.0004	-13	294	382	21.7	26.6	4.1
	2	1811	-1888	.0007	100	369	495	-24.6	-27.2	4.0

SRS TECHNOLOGIES

EXHIBIT 3.3.5
BEARING INLET AND OUTLET COOLANT TEMPERATURES

COOLANT CONDITION	COOLANT TEMPERATURE			
	BEARING 1 INLET	BEARING 1 OUTLET	BEARING 2 INLET	BEARING 2 OUTLET
SUBCOOLED	-230°F	-219°F	-219°F	-217°F
SATURATED	-223°F	-214°F	-214°F	-214°F

- o CLEARANCE = 6.3 mils.
- o BUILD #2606R1
- o SATURATION TEMPERATURE = -214°F
- o SATURATION PRESSURE = 350 psia

3.4 SSME LOX TURBOPUMP BEARING COOLANT FLOW CHARACTERISTICS

Calculation of the temperature distributions in the bearing inner and outer races, and ball, shows that surface temperatures in all of these components exceed the saturation temperature of LOX at certain spots on the surfaces. The fluid in contact with these surfaces will thus be gaseous, resulting in lower heat transfer coefficients than if the fluid were LOX. The lower heat transfer coefficients imply local overheating and consequent degradation of material properties at these surfaces. Exhibits 3.4.1, 3.4.2, and 3.4.3 show calculated temperature distributions for the conditions noted. As shown, these temperatures were estimated for an axial load of 2500 pounds, which is much lower than the loads expected during start and shut down transients.

QUALITATIVE ASSESSMENT OF CURRENT COOLING METHOD

The flow field in the region between the ball, cage, and outer and inner races is fully three dimensional and complex. However, an approximate qualitative assessment of the flow may be carried out to understand some of the features of the real flow. Since the coolant injector is mounted on the rotating shaft, the fluid emerging as a jet will experience a radially outward force, which will tend to "sling" fluid elements in the jet away from the surface of the inner race. Exhibits 3.4.4 and 3.4.5 depict simplified resulting flow fields. In the most favorable case, an assumed "centerline"

EXHIBIT 3.4.1 INNER RACE TEMPERATURE DISTRIBUTION FOR LOX PUMP TURBINE END BEARING

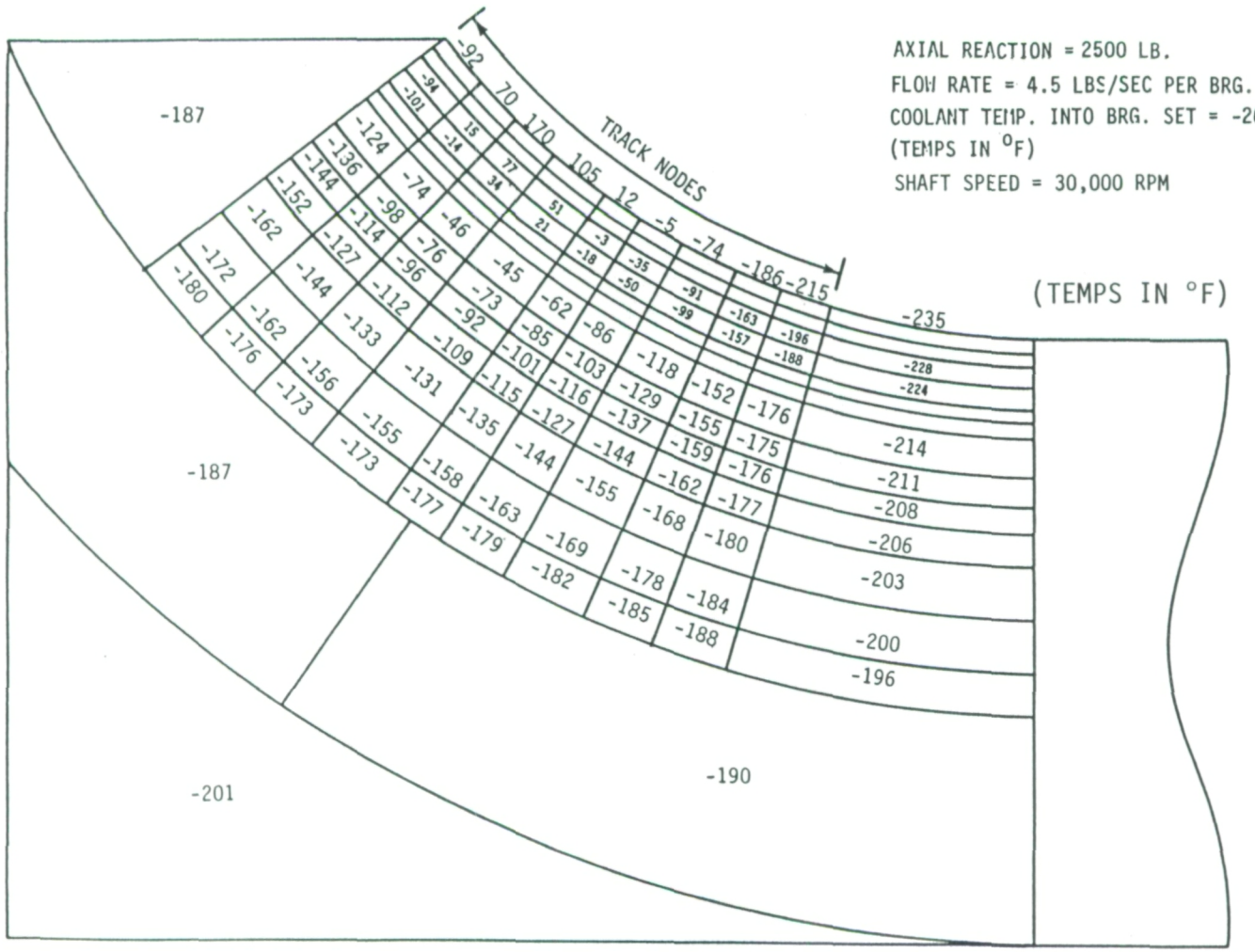

EXHIBIT 3.4.2 ROLLING ELEMENT TEMPERATURE DISTRIBUTION FOR LOX PUMP TURBINE END BEARING

(TEMPERATURES IN DEGREES FARENHEIT)

AXIAL REACTION = 2500 LB.

FLOW RATE = 4.5 LBS/SEC PER BRG. SET

COOLANT TEMP. INTO BRG. SET = -268°F (LOX)

SHAFT SPEED = 30,000 RPM

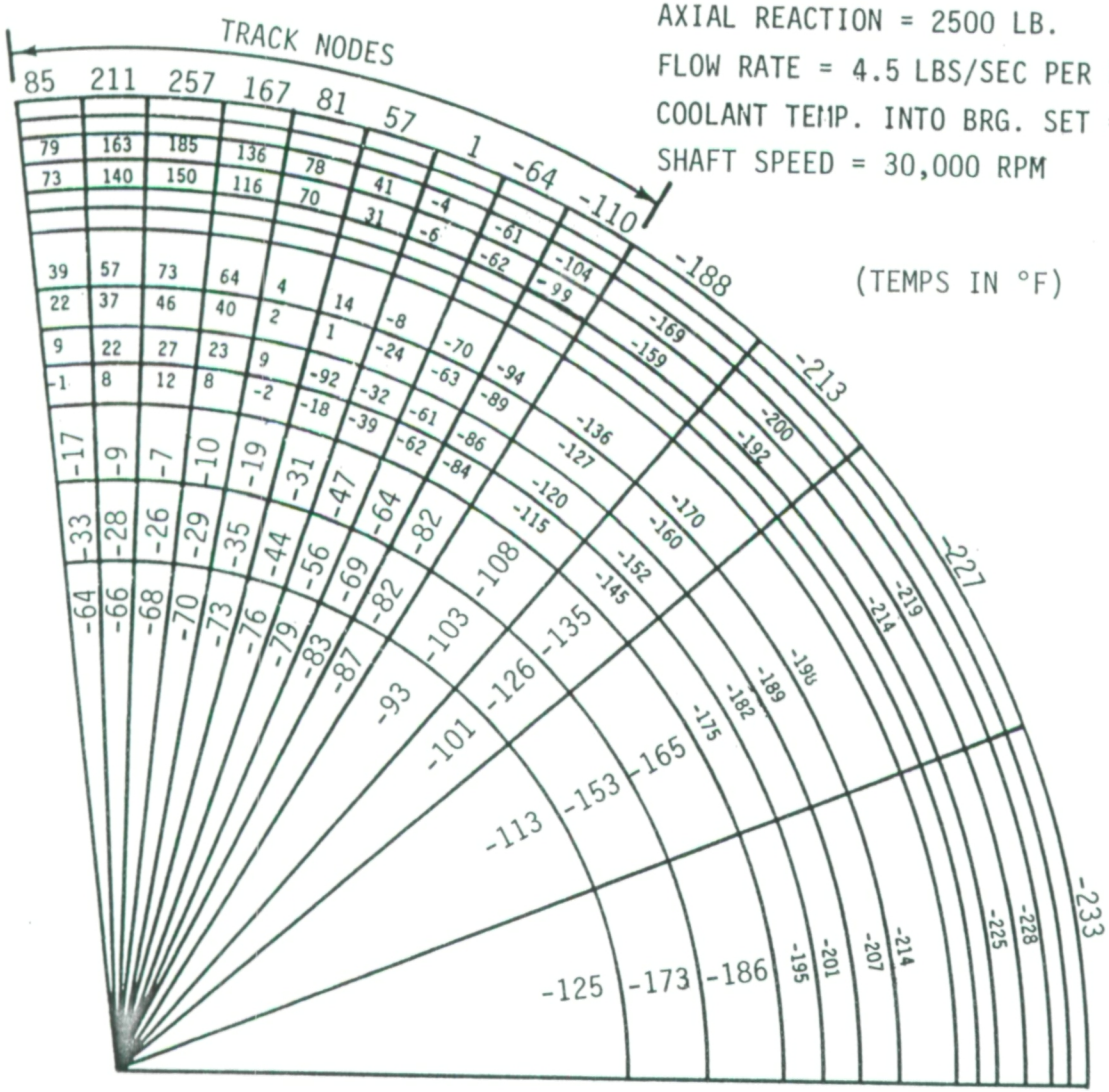

SRS TECHNOLOGIES

EXHIBIT 3.4.3 OUTER RACE TEMPERATURE DISTRIBUTION FOR LOX PUMP TURBINE END BEARING

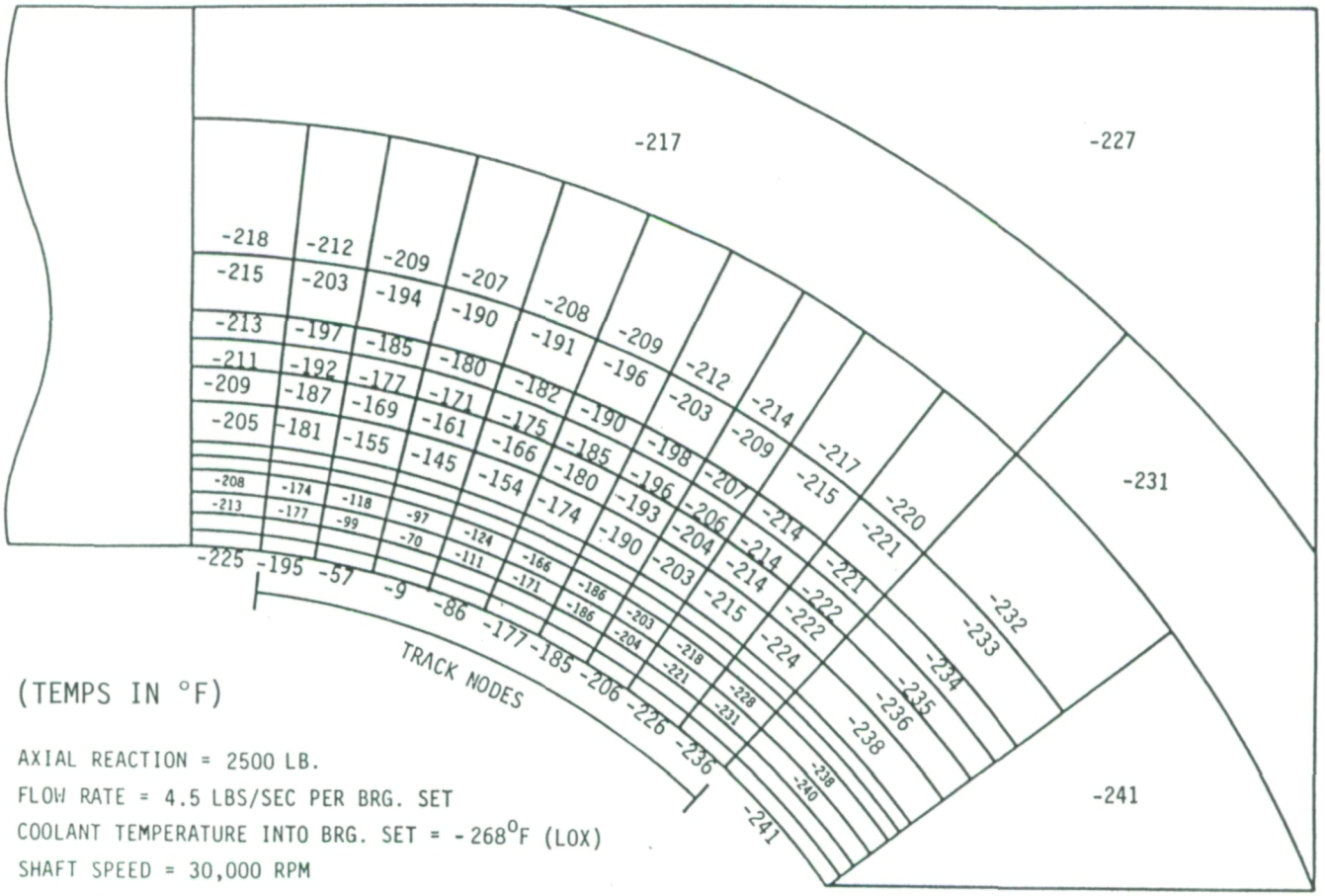

(TEMPS IN °F)

AXIAL REACTION = 2500 LB.

FLOW RATE = 4.5 LBS/SEC PER BRG. SET

COOLANT TEMPERATURE INTO BRG. SET = -268°F (LOX)

SHAFT SPEED = 30,000 RPM

SRS TECHNOLOGIES

of the "turning" jet may be looked upon as impinging on the ball. Part of flow will then be outward (toward the outer race and around the cage) and the remainder inward (toward the inner race). However, any fluid trying to flow radially inward between ball and inner race will be met by other fluid elements (carried there by the action of the spinning ball) moving in an opposite direction due to the centrifugal forces acting on them (due to the inner race rotating at shaft rpm). Thus, a small recirculation zone is expected to be formed near the lower boundary of the jet, as shown in Exhibit 3.4.4. In the most (or nearly the most) unfavorable case, an assumed "centerline" of the "turning" jet may be looked upon impinging on the cage. In this case, the lower boundary of the jet may not touch the surface of the inner race at all, and a large or significant part of the flow may be around the cage, away from the ball. Any fluid brought into the region between ball and inner race will be forced out by centrifugal forces, and will join the jet flow. This is depicted pictorially in Exhibit 3.4.5.

In the absence of the ball, the jet flow is able to expand rapidly. Exhibits 3.4.6 and 3.4.7 show the possible flow configurations. Exhibit 3.4.6 illustrates the expected vapor blanket due to the inner surfaces being above the saturation temperature of the coolant. The turning of the jet is shown as relatively low in Exhibit 3.4.6, and relatively high in Exhibit 3.4.7. The flow "curves" along the surface of the outer race in accordance with the physical boundary condition imposed at that surface.

QUANTITATIVE ASSESSMENT OF CURRENT COOLING METHOD

The effect of rotation of the shaft on the coolant jet and jet boundaries may be calculated approximately by treating an element of fluid in the jet or on the boundary as a solid body obeying the laws of mechanics. Exhibit 3.4.8 shows that for flow rates of 4 and 5 lbs/sec, the lower boundary of the jet completely misses the inner race. It also depicts the point where the lower boundary would have touched the inner race, in the absence of the rotational acceleration field. An identical calculation for the upper boundary of the jet shows that for both 4 and 5 lbs/sec, the upper boundary intersects the cage. Calculations (for the results presented in Exhibits 3.4.8 and 3.4.9) were performed for a fluid rotational velocity of 3141 radians/sec. Results for identical calculations, assuming that the fluid is

EXHIBIT 3.4.4 SIMPIFIED COOLANT FLOW FIELD (CENTER LINE OF JET IMPINGING ON BALL)

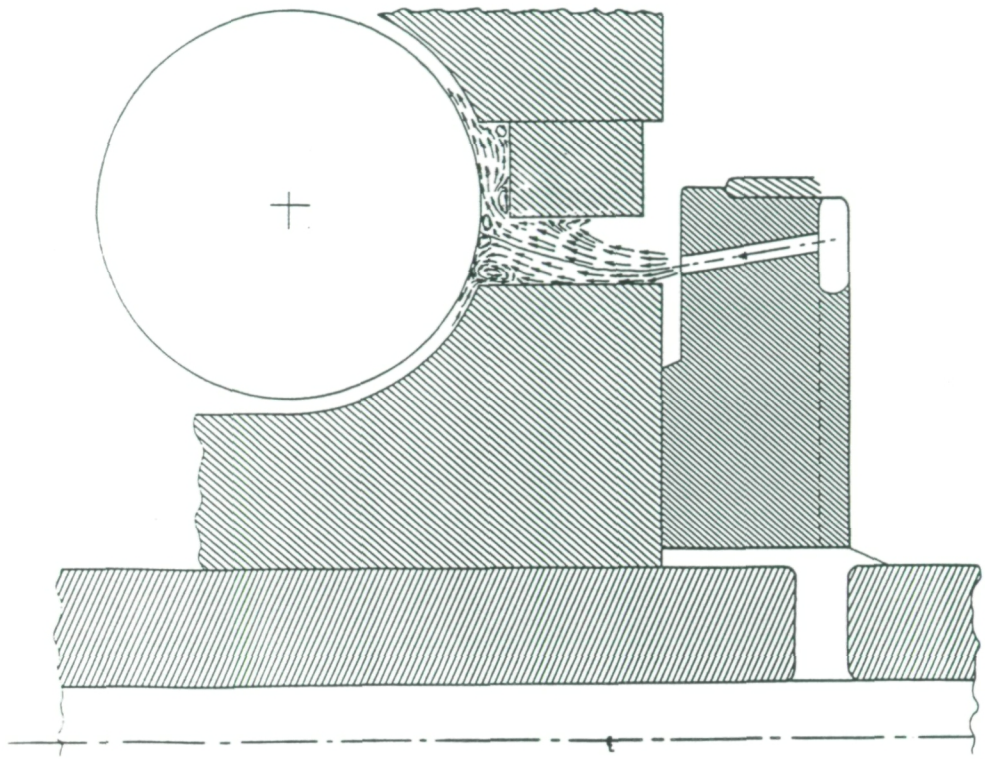

EXHIBIT 3.4.5 SIMPLIFIED COOLANT FLOW FIELD (CENTER LINE OF JET IMPINGING ON CAGE)

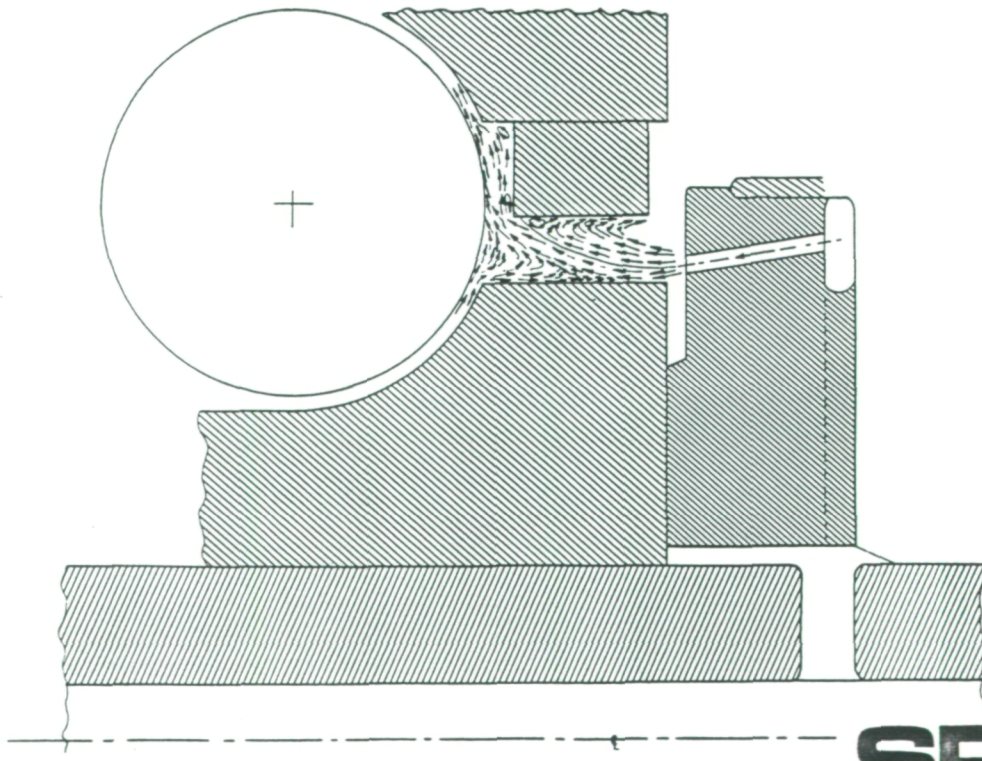

SRS TECHNOLOGIES

EXHIBIT 3.4.6 SIMPLIFIED FLOW FIELD BETWEEN BALLS (LOW JET TURNING ANGLE)

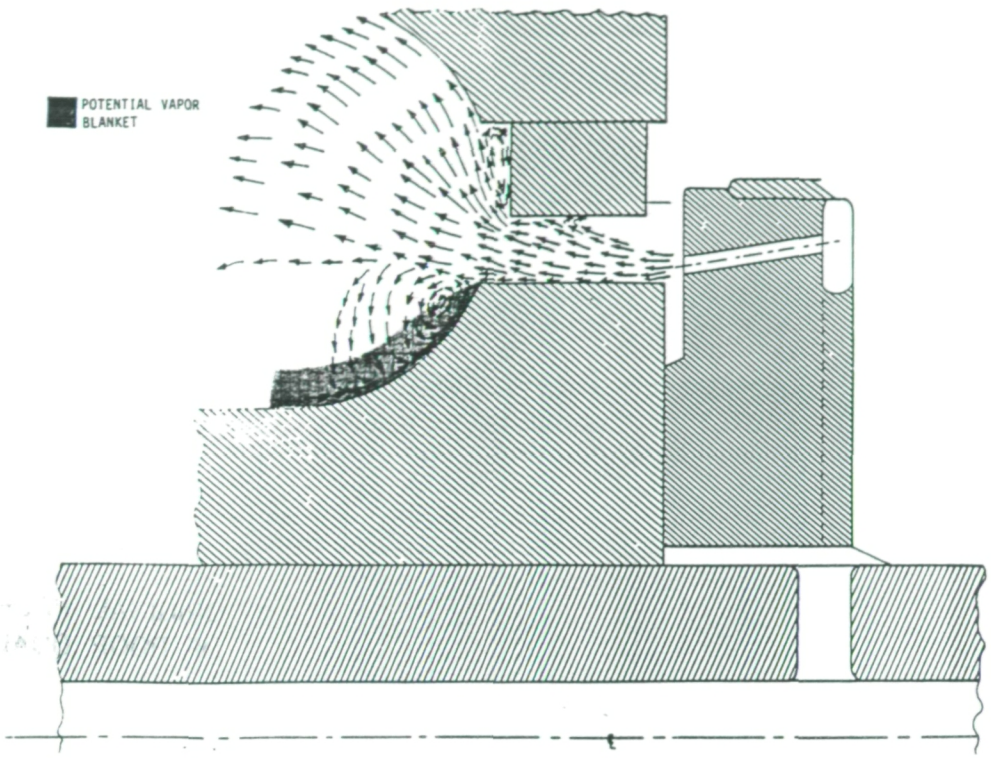

EXHIBIT 3.4.7 SIMPLIFIED FLOW FIELD BETWEEN BALLS (LARGE JET TURNING ANGLE)

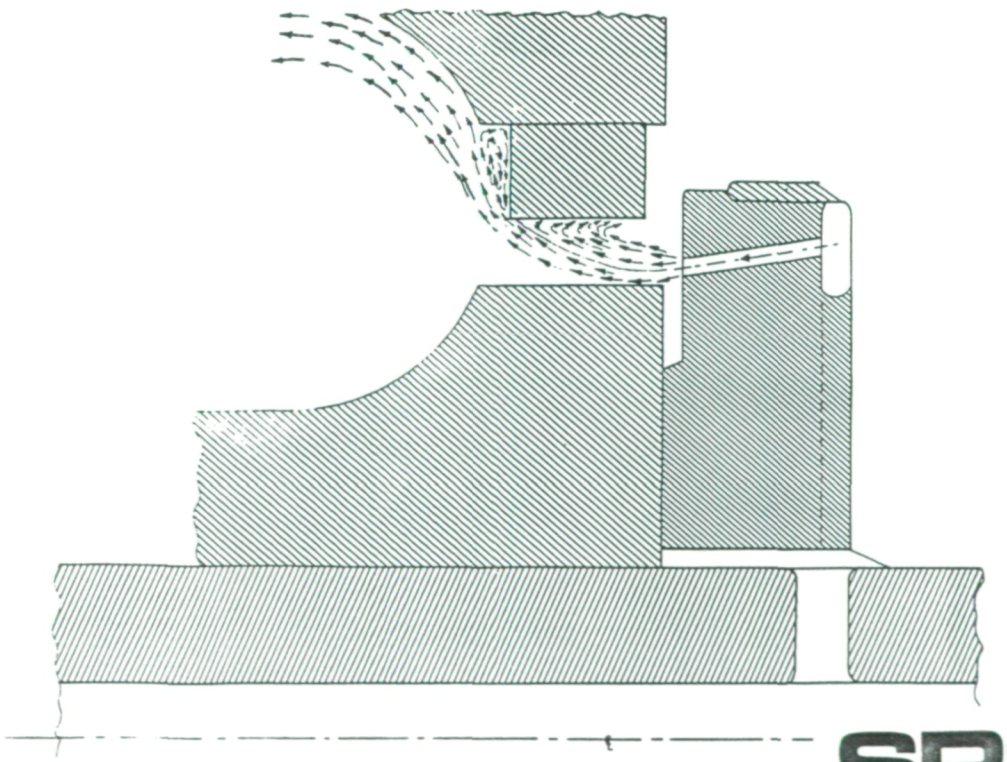

EXHIBIT 3.4.8 LOWER JET BOUNDARY VS. COOLANT FLOW
(FLUID ROTATING AT 3141 rad/sec)

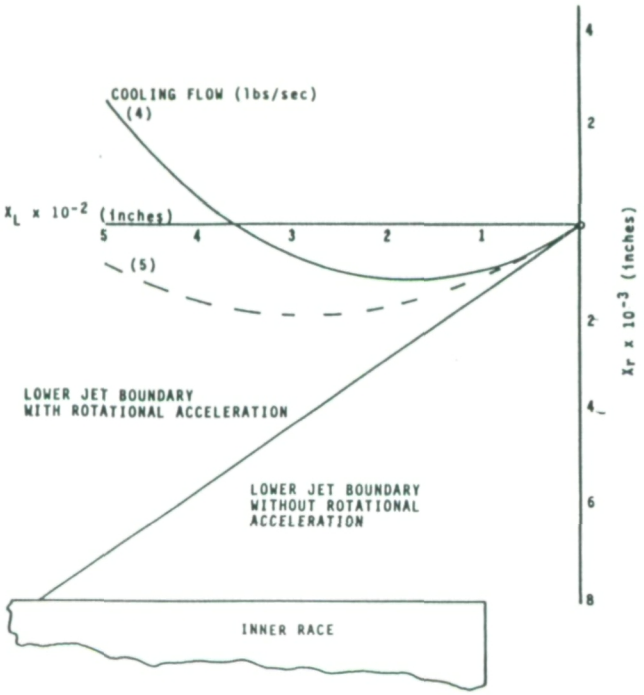

EXHIBIT 3.4.9 UPPER JET BOUNDARY VS. COOLANT FLOW
FLUID ROTATING AT (3141 rad/sec)

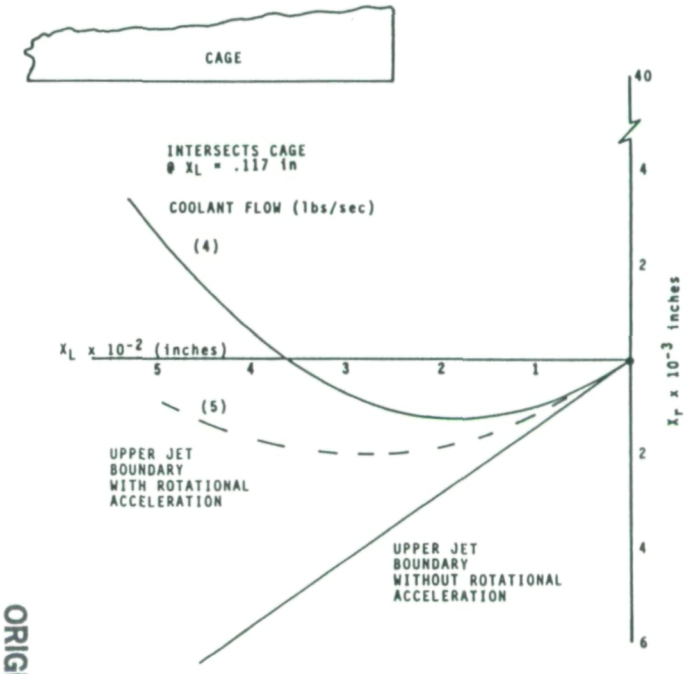

SRS TECHNOLOGIES

rotating at 1360 radians/sec, are presented in Exhibits 3.4.10 and 3.4.11. It is seen from Exhibit 3.4.10 that for a flow rate of 5 lbs/sec, the lower boundary of the jet does intersect the inner race. However, this is not the case for a flow rate of 4 lbs/sec.

SUMMARY OF OBSERVATIONS

1. Fluid elements in the jet flow are "slung" rapidly outward due to centrifugal forces acting on them. A large acceleration field (about 7500 g's) forces high density coolant toward the outer boundary of the bearing cavity.

2. Very little of the fluid in the jet is expected to flow directly into the space between inner race and ball. Most, if any, of the fluid in this region is expected to be carried there by the action of the spinning ball. However, any fluid that is carried there will tend to be slung out by the action of centrifugal forces.

3. In the most favorable case, an assumed "centerline" of the jet may be looked upon as impinging on the ball, the lower boundary of the jet may touch the inner race, and a small part of the fluid near the upper boundary of the jet may flow around the cage away from the ball. In the most unfavorable case, the assumed "centerline" of the jet may be looked upon as impinging on the cage, the lower boundary of the jet may not touch the inner race at all, and a large part of the jet flow may be around the cage away from the ball.

4. A large acceleration field that may potentially force the high density coolant toward the outer boundary of the bearing cavity may result in vapor migrating to the inner race. This will impede cooling. Additionally, the flow may become stratified in the radial direction, with higher temperature vapor at the inner race and cooler fluid at the outer race.

5. Flow over the back side of the inner race must expand against the high g-field to provide coolant to the inner race tracks.

6. The flow field is fully three-dimensional and complex.

EXHIBIT 3.4.10 LOWER JET BOUNDARY VS. COOLANT FLOW (FLUID ROTATING AT 1360 rad/sec)

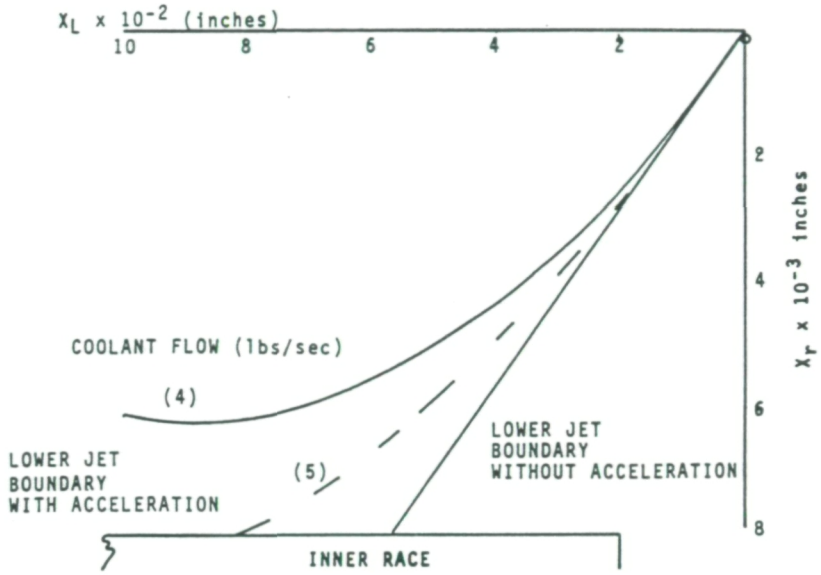

EXHIBIT 3.4.11 UPPER JET BOUNDARY VS. COOLANT FLOW (FLUID ROTATING AT 1360 rad/sec)

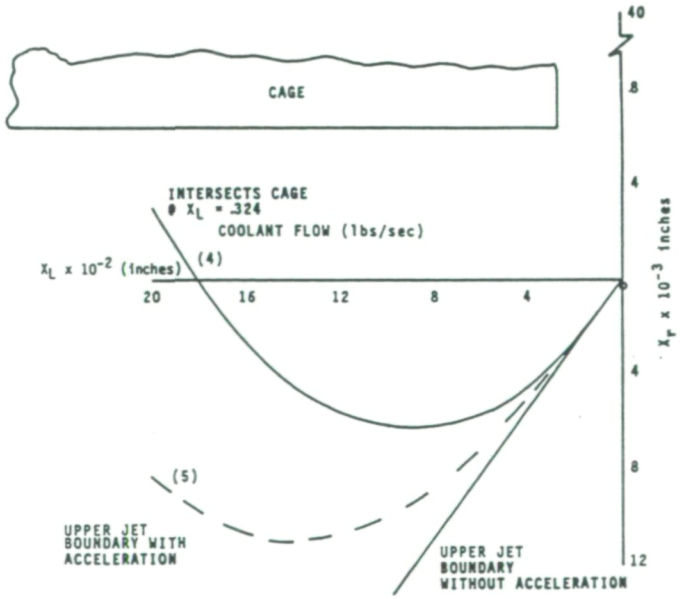

ALTERNATE COOLING CONCEPT

The schematic of an alternate cooling concept, and the expected simplified flow pattern, is shown in Exhibit 3.4.12. With proper placement of the coolant injectors, a significant portion of the coolant may be forced directly into the space between inner race and ball. Principal advantages of this injection and cooling system over the existing one are:

(a) Both bearings may experience identical cooling rates and characteristics.
(b) There is a significant possibility that coolant may be forced between inner race and ball.
(c) Potential for improved cooling of inner race.
(d) High velocity coolant will not impinge directly on the bearing cage.

Disadvantages of the alternate cooling concept are:

(a) The coolant, after passing through bearing #4, will have to be re-routed to the turbopump inlet.
(b) The total coolant flow rate will have to be approximately doubled.
(c) Difficulty in assuring equal coolant flow to each bearing.

The flow, without the ball, is shown in Exhibit 3.4.13.

POTENTIAL FOLLOW-ON INVESTIGATIONS

Alternate cooling concepts that may be defined further and investigated are:

(a) Coolant flow between bearings
(b) Coolant flow under inner races, etc.

The heat transfer characteristics of the postulated flows may then be estimated, as well as the effects on bearing temperatures and operating characteristics, such as sensitivity of heat transfer coefficients and fluid boundary temperatures and loss of internal clearances.

3.5 LOX TESTER BEARING FRICTION AND VISCOUS HEAT ESTIMATES

Heat generation from bearing contact friction and viscous stirring of the coolant was estimated for specific loads and coolant flow for the BSMT LOX Tester. The loading conditions are as follows: 1) no external load,

EXHIBIT 3.4.12 SIMPLIFIED FLOW FIELD FOR ALTERNATE COOLING CONCEPT

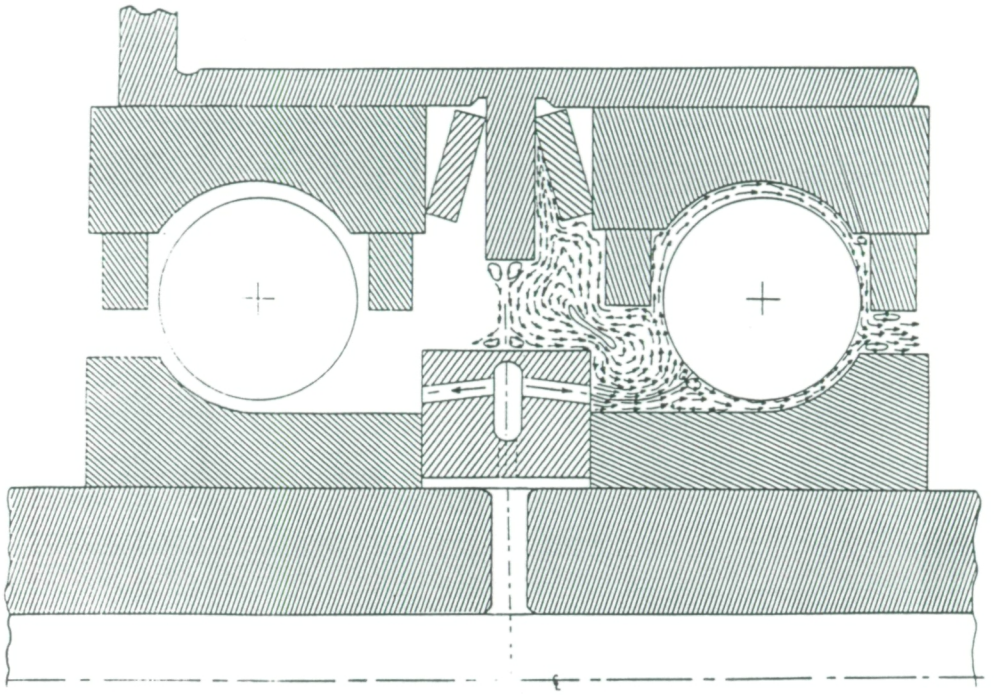

EXHIBIT 3.4.13 SIMPLIFIED FLOW FIELD BETWEEN BALLS FOR ALTERNATE CONCEPT

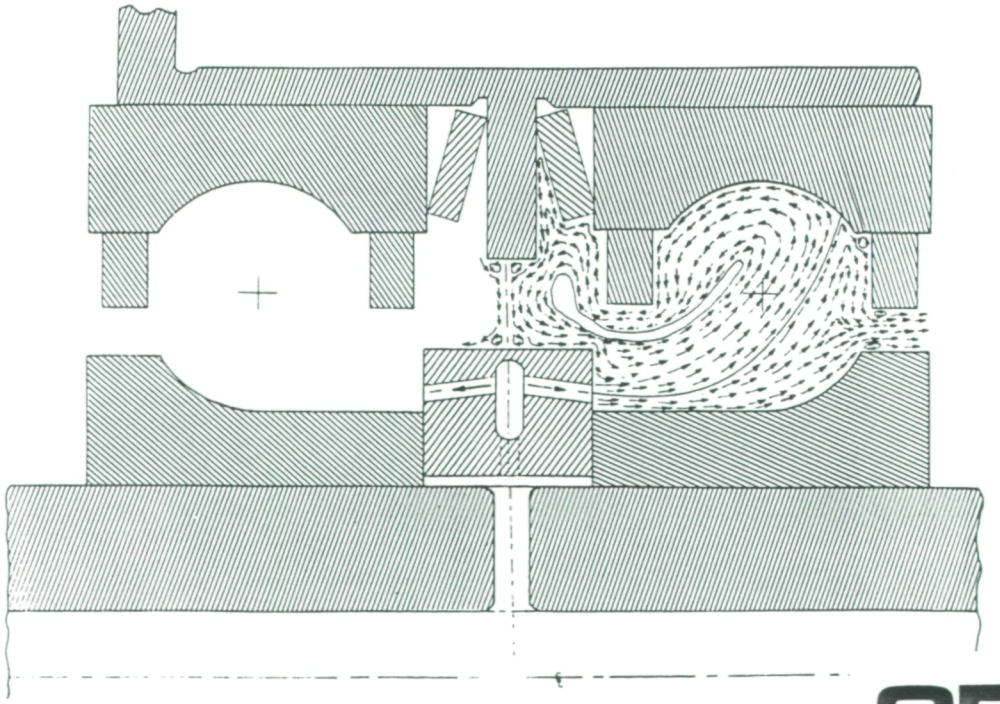

SRS TECHNOLOGIES

bearings preloaded to 1,000 lbs., 2) an 8,000 lb. radial point load imposed between the bearing pairs, 3) an 8,000 lb. radial load and a 5,000 lb. axial load, and 4) 8,000 lb. radial load and a 10,000 lb. axial load. The heat generated due to stirring the coolant was estimated for a 60 hole flow diverter pattern with 0.62" holes and flows of 5.0, 7, and 12 pounds/sec per bearing pair.

BEARING FRICTION HEAT GENERATION ESTIMATES

A bearing/shaft model of the LOX tester was used to compute the frictional heating of each bearing for the loading conditions previously described. These estimates are based on a uniform bearing temperature and do not account for loss of internal clearances due to thermal growth. Furthermore, the values given for the radial load cases are averages. A radially loaded bearing develops a non uniform heat load profile in the circumferential direction; the bearing heat load profile for a radially loaded bearing is not symmetrical about the bearing axis. The bearing friction heat loads are shown in Exhibit 3.5.1 for the conditions noted. The higher heat generation rates for the inboard bearings for the radial load case reflects the higher portion of the total load carried by these bearings.

The combined axial and radial load cases reflect the combined loading on bearing 1 and the unloading of bearing 2. As bearing 1 is loaded axially, the shaft moves, unloading bearing 2. Bearing 2 becomes less stiff in the radial direction while shifting the load to bearing 1. The 10,000 lb. axial load case removes most of the preload from bearing 2 (250 lbs. remain). This could cause increased ball skid and heat generation for bearing 2, which was not accounted for in the analysis.

HEAT GENERATED DUE TO FLUID FRICTION AND PUMPING

Heat is generated in bearings due to fluid friction caused by relatively high velocities between the fluid and bearing components. The fluid circuit of the LOX tester differs from the bearing tester previously run in LN_2. The LOX tester design considered in this analysis provides coolant flow through a hollow shaft and a diverter plate upstream of each bearing pair. The diverter plates attempt to match the tangential velocity of the coolant flow and bearing balls by providing a tangential component to the coolant velocity

EXHIBIT 3.5.1 BEARING FRICTION HEAT LOADS (BTU/SEC)

(57mm BEARING, N = 30,000 RPM, f = 0.2)

No External Load; Preload 1,000 lbs/bearing

COMPONENT	Drive End		Load End	
	Bgr 4	Bgr 3	Bgr 2	Bgr 1
Balls	1.7	1.7	1.7	1.7
Inner Race	1.3	1.3	1.3	1.3
Outer Race	0.4	0.4	0.4	0.4
Total	3.4	3.4	3.4	3.4

8,000 lb. Radial; Preload 1,000 lbs/bearing

COMPONENT	Drive End		Load End	
	Bgr 4	Bgr 3	Bgr 2	Bgr 1
Balls	3.43	8.1	8.1	3.43
Inner Race	2.58	4.4	4.4	2.58
Outer Race	.85	3.67	3.67	.85
Total	6.86	16.17	16.17	6.86

8,000 lb. Radial; 5,000 lb. Axial, Preload 1,000 lbs

COMPONENT	Drive End		Load End	
	Bgr 4	Bgr 3	Bgr 2	Bgr 1
Balls	3.43	8.07	2.17	10.1
Inner Race	2.58	4.4	1.18	6.8
Outer Race	.85	3.67	1.0	3.3
Total	6.86	16.14	4.35	20.2

8,000 lb. Radial; 10,000 lb Axial, Preload 1,000 lbs.

COMPONENT	Drive End		Load End	
	Bgr 4	Bgr 3	Bgr 2	Bgr 1
Balls	3.43	8.07	1.2	22.1
Inner Race	2.58	4.4	.60	14.33
Outer Race	.85	3.67	.61	7.73
Total	6.86	14.14	2.41	44.16

SRS TECHNOLOGIES

equal in magnitude, and opposite in direction, to the difference in the tangential velocity at the exit of the flow passage and ball velocity. An exact match is only possible for a single combination of shaft speed, flow, and diverter flow passage configuration. The diverter configuration analyzed contained 60 .062" diameter holes at an angle of 51° from the diverter axis. The flow energy input to the fluid due to the centrifugal pumping action of the radial coolant passages and flow friction was estimated. The results of these evaluations are shown in Exhibit 3.5.2. The enclosed heat generation data allows several combinations of loads and coolant flows to be selected for overall bearing tester heat loads within the constraints previously discussed.

3.6 HEAT GENERATION FOR THE 60 HOLE DIVERTER - .046" DIAMETER HOLES

Heat generated by fluid friction also was estimated for a 60 .046" diameter hole coolant flow diverter plate. These values are shown in Exhibit 3.6.1 for both LOX and LN_2 Coolant. As shown, the flow friction, pumping, and ball drag energy increases in a non-linear fashion with increased flow rate. This is further emphasized in Exhibit 3.6.2 which shows the increase in total drive-end heat generation as a function of coolant flow rate. The controlling parameters in the viscous fluid energy estimates are the relative velocity between the coolant and the balls, the pump work on the fluid due to shaft rotation, and the friction pressure loss through the coolant passages. When the relative velocity between the fluid and the balls is low, the ball drag energy is low. The friction energy due to pressure loss is directly proportional to the cube of the flow and inversely proportional to the square of the density. Therefore, for this particular diverter configuration there is a better match of ball to fluid relative velocites for the LN_2 at the lower flow rates. However at the higher flows the relative velocity increases and the lower density causes an increase in the LN_2 energy terms over those of LOX. This suggests that there is an optimum diverter configuration for each coolant, coolant flow, and shaft speed.

3.7 ESTIMATE OF BALL TO CAGE HEAT GENERATION

An additional upgrade of the bearing thermal model accounts for the frictional heat generated between the cage and bearing elements, and the

EXHIBIT 3.5.2 SUMMARY OF VISCOUS HEAT GENERATION (BTU/SEC)

Lox BMT 57MM Bgr N = 30,000 f = 0.2
60 hole Flow Diveter with .062 diam holes
Lox Coolant flow = 5 lbs/sec/bgr pair

COMPONENT	Drive End		Load End	
	Brg 4	Brg 3	Brg 2	Brg 1
Balls (Spin & Drag)	24.26	2.07	2.07	24.26
Inner Race & Separator	1.1	1.1	1.1	1.1
Outer Race	3.2	3.2	3.2	3.2
Sub Total	28.56	6.37	6.37	28.56
Fluid Pumping & diverter holes	11.8			11.8
Shaft:				
Hollow Section	6.58			1.76
Sub Total	18.38			13.56

Lox Coolant Flow 7 lbs/sec/brg pair

COMPONENT	Drive End		Load End	
	Brg 4	Brg 3	Brg 2	Brg 1
Balls (Spin & Drag)	18.96	2.07	2.07	18.96
Inner Race & Separator	1.1	1.1	1.1	1.1
Outer Race	3.2	3.2	3.2	3.2
Sub Total	23.26	6.37	6.37	23.26
Fluid Pumping & Diverter Holes	17.2			17.2
Shaft:				
Hollow Section	6.58			1.76
Sub Total	23.78			18.96

SRS TECHNOLOGIES

EXHIBIT 3.5.2 (Cont.) SUMMARY OF VISCOUS HEAT GENERATION (BTU/SEC)

60 hole diverter - .062" diameter holes - LOX

LOX Coolant FLOW 10 lbs./sec/brg pair

Component	Drive End		Load End	
	Brg 4	Brg 3	Brg 2	Brg 1
Balls (Spin & Drag)	13.35	2.07	2.07	13.35
Inner Race & Separator	1.1	1.1	1.1	1.1
Outer Race	3.2	3.2	3.2	3.2
Subtotal	17.65	6.37	6.37	17.65
Fluid Pumping and Diverter Holes	26.57		26.57	
Shaft: Hollow Section	6.58		1.76	
Subtotal	33.15		28.33	

Lox coolant flow = 12 lbs/sec/bgr pair

COMPONENT	Drive End		Load End	
	Brg 4	Brg 3	Brg 2	Brg 1
Balls (Spin & Drag)	13.34	2.07	2.07	13.34
Inner Race & Separator	1.1	1.1	1.1	1.1
Outer Race	3.2	3.2	3.2	3.2
Sub Total	17.64	6.37	6.37	17.64
Fluid Pumping & Diverter holes	34.0		34.0	
Shaft: Hollow Section	6.58		1.76	
Sub Total	40.58		35.76	

Slinger Spacer, 4.71 Btu/sec/Slinger for Lox

SRS TECHNOLOGIES

EXHIBIT 3.5.2 (Cont.) SUMMARY OF VISCOUS HEAT GENERATION (BTU /SEC)

LN_2 Coolant flow = 5 lbs/sec/brg pair

COMPONENT	Drive End		Load End	
	Brg 4	Brg 3	Brg 2	Brg 1
Balls (Spin & Drag)	14.42	1.52	1.52	14.42
Inner Race & Separator	.81	.81	.81	.81
Outer Race	2.35	2.35	2.35	2.35
Sub Total	17.58	4.68	4.68	17.58
Fluid Pumping & Diverter Holes	12.2		12.2	
Shafts: Hollow Section	4.82		1.3	
Sub Total	17.02		13.5	

LN_2 Coolant flow = 7 lbs/sec/brg pair

COMPONENT	Drive End		Load End	
	Brg 4	Brg 3	Brg 2	Brg 1
Balls (Spin & drag)	11.34	1.52	1.52	11.34
Inner Race & Separator	.81	.81	.81	.81
Outer Race	2.35	2.35	2.35	2.35
Sub Total	14.5	4.68	4.68	14.5
Fluid Pumping & Diverter Holes	18.4		18.4	
Shaft: Hollow Section	4.82		1.3	
Sub Total	23.22		19.7	

EXHIBIT 3.5.2 (Con't) SUMMARY OF VISCOUS HEAT GENERATION (BTU/SEC)

60 hole diverter - .062" diameter holes - LN_2

LN_2 Coolant Flow 10 lbs./sec/brg pair

Component	Drive End		Load End	
	Brg 4	Brg 3	Brg 2	Brg 1
Balls (Spin & Drag)	9.30	1.52	1.52	9.30
Inner Race & Separator	.81	.81	.81	.81
Outer Race	2.35	2.35	2.35	2.35
Subtotal	12.46	4.68	4.68	12.46
Fluid Pumping and Diverter Holes	30		30	
Shaft: Hollow Section	4.81		1.3	
Subtotal	34.81		31.3	

LN_2 Coolant flow = 12 lbs/sec/brg pair

COMPONENT	Drive End		Load End	
	Brg 4	Brg 3	Brg 2	Brg 1
Balls (spin & drag)	10.43	1.52	1.52	10.43
Inner Race & Separator	.81	.81	.81	.81
Outer Race	2.35	2.35	2.35	2.35
Sub Total	13.59	4.68	4.68	13.59
Fluid Pumping & Diverter holes	40.0		40.0	
Shaft: Hollow Section	4.82		1.3	
Sub Total	44.82		41.3	

Slinger Spacer, 3.45 Btu/sec/slinger for LN_2

SRS TECHNOLOGIES

EXHIBIT 3.6.1 SUMMARY OF VISCOUS HEAT GENERATION (BTU/SEC)

LOX BMT Tester, 57 mm Bearing, N = 30,000,
60 Hole Diverter .046" Diameter Holes

LOX Coolant Flow 5 lbs/sec bgr pair

COMPONENT	Drive End		Load End	
	Bgr 4	Bgr 3	Bgr 2	Bgr 1
Balls (Spin & Drag)	15.76	2.07	2.07	15.76
Inner Race & Separator	1.1	1.1	1.1	1.1
Outer Race	3.2	3.2	3.2	3.2
Subtotal	20.1	6.37	6.37	20.1
Fluid Pumping & Diverter Holes	12.6		12.6	
Shaft: Hollow Section	6.58		1.76	
Subtotal	19.18		14.36	

LOX Coolant Flow 7 lbs/sec bgr pair

COMPONENT	Drive End		Load End	
	Bgr 4	Bgr 3	Bgr 2	Bgr 1
Balls (Spin & Drag)	13.8	2.07	2.07	13.8
Inner Race & Separator	1.1	1.1	1.1	1.1
Outer Race	3.2	3.2	3.2	3.2
Subtotal	18.1	6.37	6.37	18.1
Fluid Pumping & Diverter Holes	19.55		19.55	
Shaft: Hollow Section	6.58		1.76	
Subtotal	26.13		21.31	

EXHIBIT 3.6.1 (Con't) SUMMARY OF VISCOUS HEAT GENERATION (BTU/SEC)

60 hole diverter - .046" diameter holes - LOX

LOX Coolant Flow 10 lbs./sec/brg pair

Component	Drive End		Load End	
	Brg 4	Brg 3	Brg 2	Brg 1
Balls (Spin & Drag)	15.84	2.07	2.07	15.84
Inner Race & Separator	1.1	1.1	1.1	1.1
Outer Race	3.2	3.2	3.2	3.2
Subtotal	20.11	6.37	6.37	20.11
Fluid Pumping and Diverter Holes	33.49		33.49	
Shaft: Hollow Section	6.58		1.76	
Subtotal	40.07		35.25	

LOX Coolant Flow 12 lbs/sec bgr pair

COMPONENT	Drive End		Load End	
	Bgr 4	Bgr 3	Bgr 2	Bgr 1
Balls (Spin & Drag)	24	2.07	2.07	24
Inner Race & Separator	1.1	1.1	1.1	1.1
Outer Race	3.2	3.2	3.2	3.2
Subtotal	28.3	6.37	6.37	28.3
Fluid Pumping & Diverter Holes	45.85		45.85	
Shaft: Hollow Section	6.58		1.76	
Subtotal	52.43		47.61	

Slinger Spacer, 4.71 BTU/sec - slinger for LOX

SRS TECHNOLOGIES

EXHIBIT 3.6.1 (Con't) SUMMARY OF VISCOUS HEAT GENERATION (BTU/SEC)

LN_2 Coolant Flow = 5 lbs/sec bgr pair

COMPONENT	Drive End		Load End	
	Bgr 4	Bgr 3	Bgr 2	Bgr 1
Balls (Spin & Drag)	9.7	1.52	1.52	9.7
Inner Race & Separator	.81	.81	.81	.81
Outer Race	2.35	2.35	2.35	2.35
Subtotal	12.86	4.68	4.68	12.86
Fluid Pumping & Diverter Holes	13.8		13.8	
Shaft: Hollow Section	4.82		1.3	
Subtotal	18.62		15.1	

LN_2 Coolant Flow - 7 lbs/sec bgr pair

COMPONENT	Drive End		Load End	
	Bgr 4	Bgr 3	Bgr 2	Bgr 1
Balls (Spin & Drag)	11.14	1.52	1.52	11.14
Inner Race & Separator	.81	.81	.81	.81
Outer Race	2.35	2.35	2.35	2.35
Subtotal	14.30	4.68	4.68	14.30
Fluid Pumping & Diverter Holes	22.8		22.8	
Shaft: Hollow Section	4.82		1.3	
Subtotal	27.62		24.1	

SRS TECHNOLOGIES

EXHIBIT 3.6.1 (Con't) SUMMARY OF VISCOUS HEAT GENERATION (BTU/SEC)

60 hole diverter - .046" diameter holes - LN_2

COLLANT FLOW 10 lbs./sec/brg pair

Component	Drive End		Load End	
	Brg 4	Brg 3	Brg 2	Brg 1
Balls (Spin & Drag)	26.05	1.52	1.52	26.05
Inner Race & Separator	.81	.81	.81	.81
Outer Race	2.35	2.35	2.35	2.35
Subtotal	29.21	4.68	4.68	29.21
Fluid Pumping and Diverter Holes	42.88		42.88	
Shaft: Hollow Section	4.81		1.3	
Subtotal	47.69		44.18	

LN_2 Coolant Flow = 12 lbs/sec bgr pair

COMPONENT	Drive End		Load End	
	Bgr 4	Bgr 3	Bgr 2	Bgr 1
Balls (Spin & Drag)	48.3	1.52	1.52	48.3
Inner Race & Separator	.81	.81	.81	.81
Outer Race	2.35	2.35	2.35	2.35
Subtotal	51.46	4.68	4.68	51.46
Fluid Pumping & Diverter Holes	62.1		62.1	
Shaft: Hollow Section	4.82		1.3	
Subtotal	66.92		63.4	

Slinger Spacer, 3.45 BTU sec/slinger for LN_2

SRS TECHNOLOGIES

EXHIBIT 3.6.2 TOTAL HEAT GENERATION (BTU/SEC) LOX BMT DRIVE END VS. COOLANT FLOW

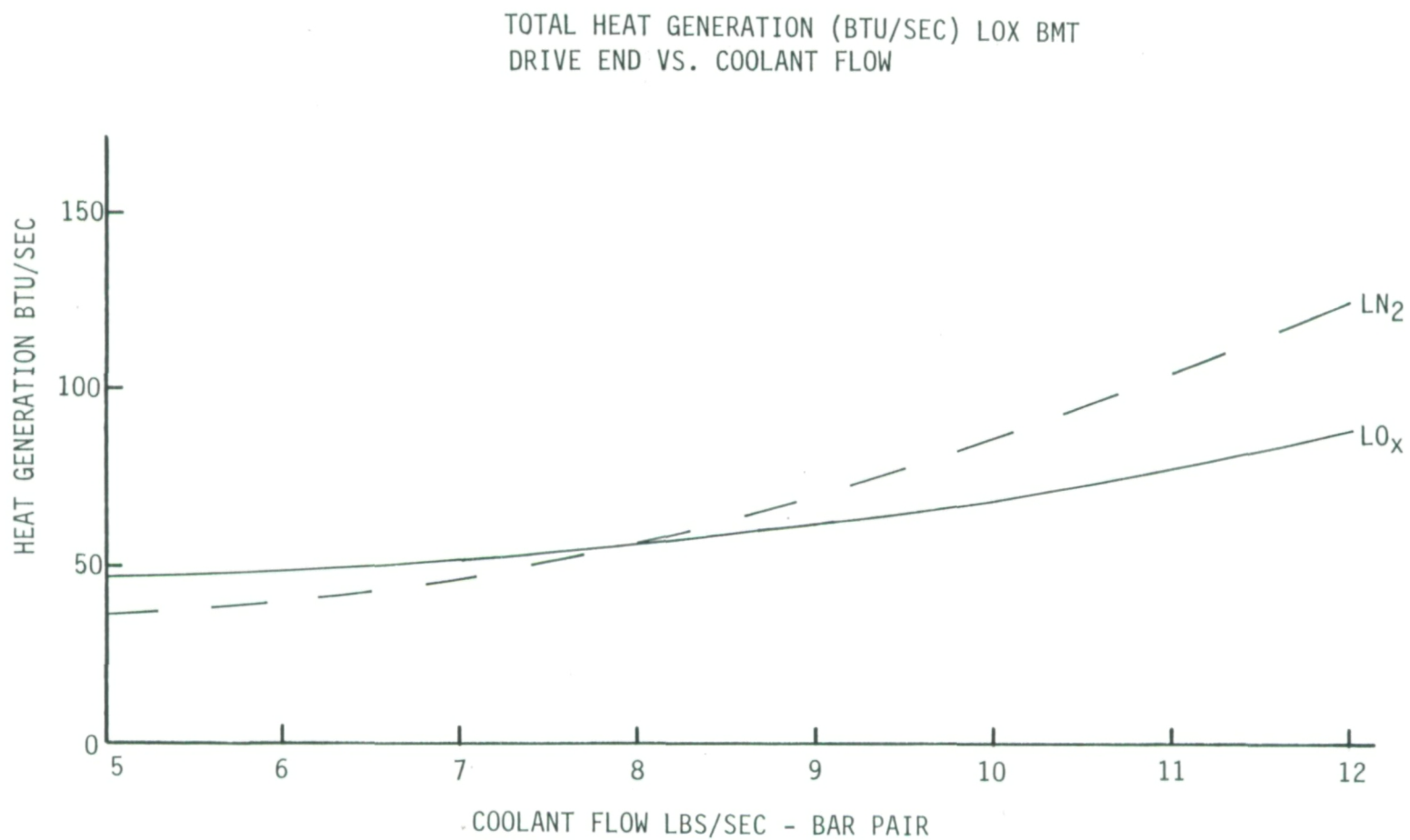

SRS TECHNOLOGIES

associated heat transfer among these components. An analysis was done to determine the ball cage contact area, load distribution in the contacts, and frictional heat generated due to the loads and relative velocity between the ball and cage. Since cage pocket loads are a function of bearing loading, the results are given parametrically as a function of ball pocket loads. The analysis was done for the 45 mm bearing with circular ball pockets.

The estimated contact geometry is shown in Exhibit 3.7.1. Since the contact surface was defined by a Hertz analysis, the resulting contact surface is elliptical and varies with the applied load. This provides the contact area necessary to calculate the thermal conductance between the ball and cage.

The heat generation was estimated by breaking the contact area into finite elements along the major axis, and averaging the normal force along the minor axis for each elemental area. Given the normal force, the relative velocity between ball and cage, and the friction coefficient, the heat produced due to friction can be determined.

Shown in Exhibit 3.7.2 are the results of such an analysis. The results are given for one ball/pocket contact. The influences of load and friction coefficient are illustrated. The cage can affect the ball temperature in two ways. It can block coolant flow and therefore reduce the cooling of the ball surface, and the rubbing between the ball and cage generate heat that must be partially rejected at the surface of the ball. The heating rates shown are significant, and could significantly increase the ball temperature depending on the loading and coefficient of friction between the ball and cage. Since large cage loads are usually associated with large radial loads, the ball and cage pocket loads are not symmetrical about the bearing axis for the expected worst case cage pocket loading. Consequently the bearing components of a heavily loaded radial bearing experience cyclic heating and cooling as they rotate.

The contact surfaces estimated by this analysis should be considered preliminary. A comparison of cage pocket wear patterns should provide additional insight to the actual ball/cage contact areas, and the contact surfaces can be adjusted to agree with the observed conditions.

EXHIBIT 3.7.1 CONTACT GEOMETRY FOR ARMALON CAGE STEEL BALL

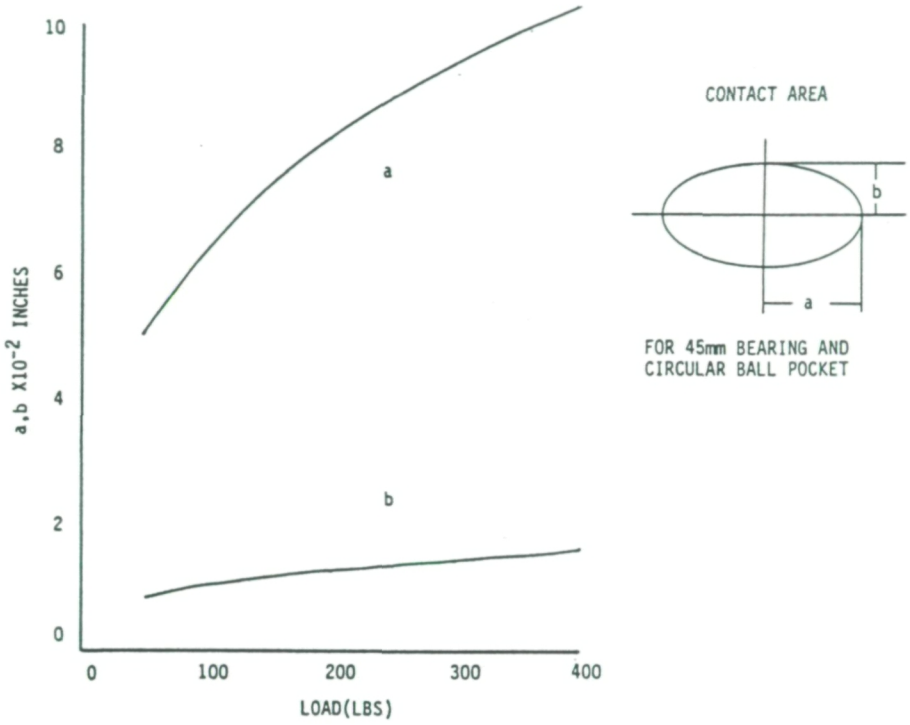

EXHIBIT 3.7.2 BALL POCKET HEAT GENERATION VS. LOAD

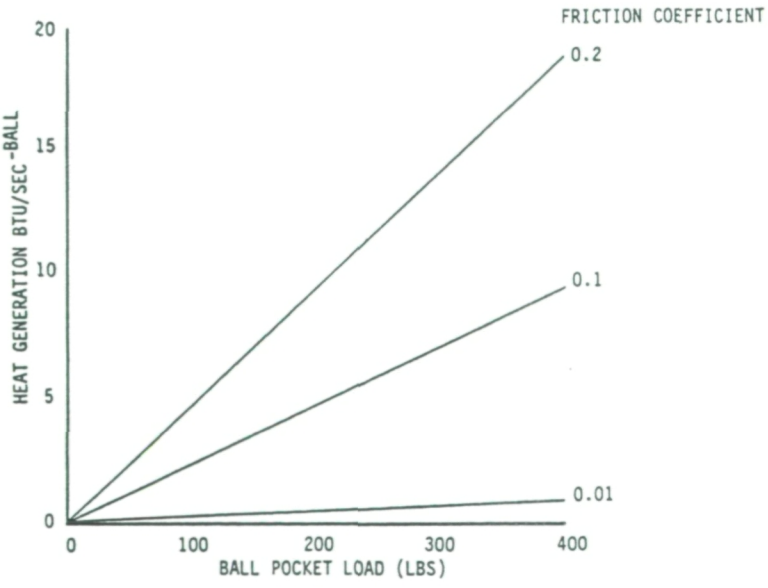

SRS TECHNOLOGIES

3.8 CAGE LOADS FROM COOLANT JETS AND FLUID FRICTION

The 57 mm LOX turbopump turbine-end bearing cage (bearing #4) experiences forces from coolant jets impinging on the cage. These jets are produced by a coolant flow diverter plate that rotates at shaft speed and distributes the coolant through holes in the plate. These holes are angled downward 8° and swept back 51° to direct the jets between the cage and inner race, and to reduce the relative tangential velocity between the cage and fluid. Based on estimates reported in the March, 1985 progress report, the centrifugal forces produced by the high rotational speeds of the shaft are sufficient to bend the jets radially outward such that they impinge on the inner surface of the cage. The tangential component of these jets can act to speed up or slow down the cage, depending on the direction of the relative tangential velocity component with respect to the cage. The relative velocity of the cage and tangential fluid component depends on cage speed, shaft speed, coolant flow rate, and diverter geometry, such as flow area and angles determining the direction of jet flow.

The current coolant flow diverter consists of 30 holes of 0.046" diameter, angled radially inward 8° and swept back 51°. This configuration produces a moment on the cage, due to coolant jet impingement, in a direction to push or increase the cage rotational speed. The principal fluid force or moment in the direction to retard the cage rotation is the viscous drag of the fluid between the cage and outer race. This torque is a function of the clearance between the cage and outer race. Shown in Exhibit 3.8.1 is the cage driving and dragging torque estimated from these two sources.

These estimates are approximate and do not include dissipation of the jets due to surrounding fluid. As a first approximation, the influence of velocity dissipation in the jet due to surrounding fluid can be made as follows. The characteristics of a typical jet discharging into a fluid are shown below.

EXHIBIT 3.8.1 CAGE TORQUE VS. RADIAL CLEARANCE

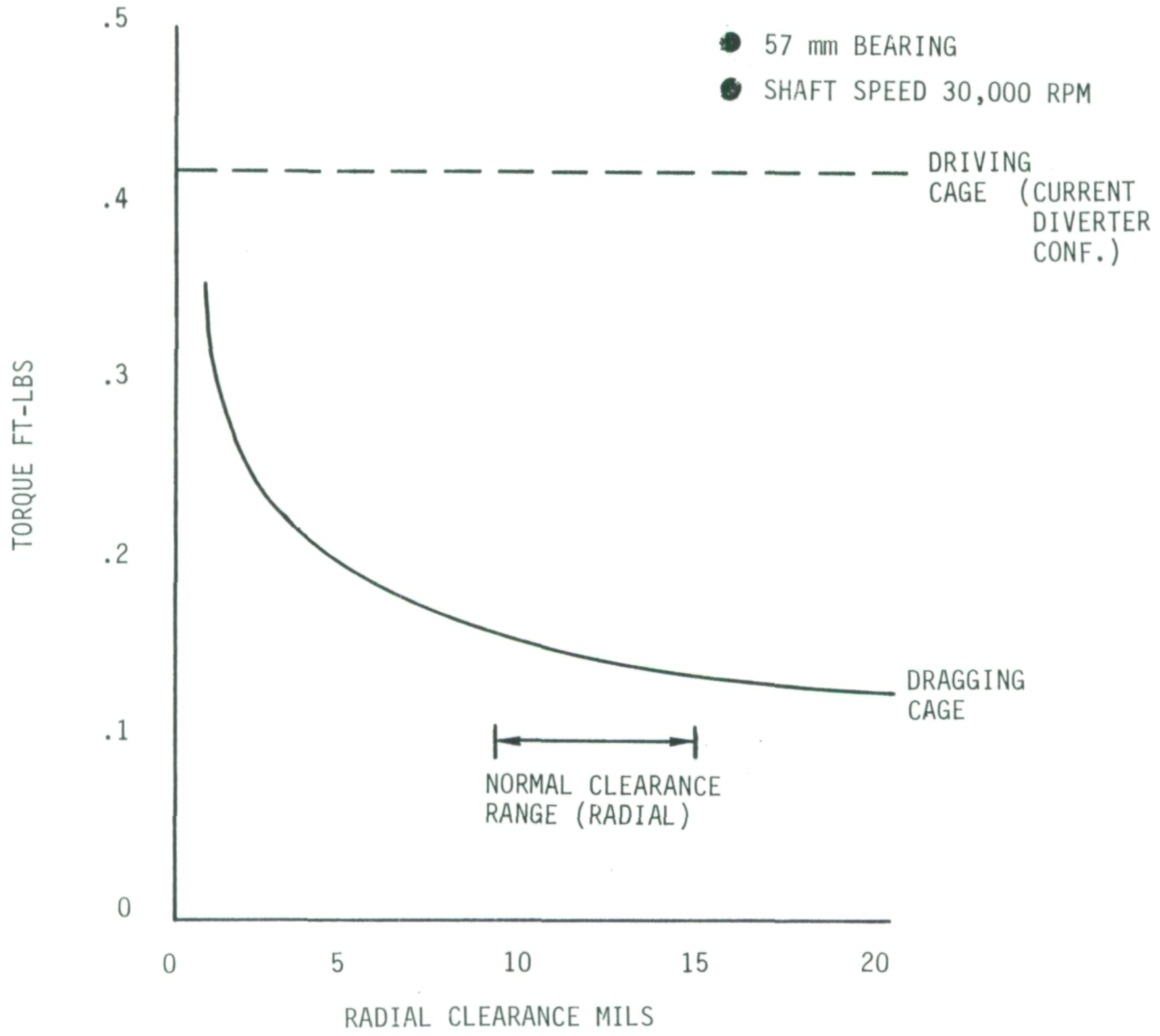

SRS TECHNOLOGIES

D = Orfice Diameter

U_o = Exit Velocity

X_o = Length of Irrotational Core

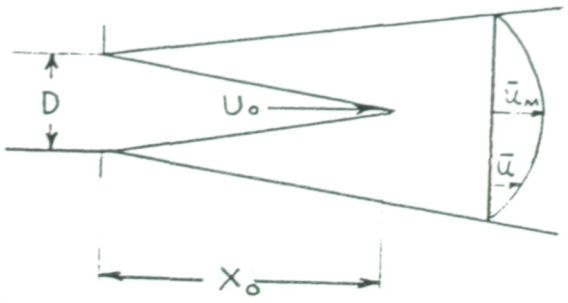

From Figure 127 of Reference 3:

$$\frac{X_o}{D} = 6.2$$

Therefore the length of the constant velocity zone for the 0.046" diameter orfice is: $X_o = (6.2)(0.046) = 0.285"$. At the time of jet impingement on the cage, the distance travelled by the fluid is estimated to be 0.269 inches. Therefore, the irrotational core of the coolant jet impinges on the cage, with very little velocity dissipated over this distance, and the cage receives most of the available force in the jets.

The cage drag torque does not consider any direct contact between the cage and outer race. Coulomb friction due to these possible encounters is not considered. Even though not exact, these estimates are sufficient to identify characteristics that imply undesirable operating conditions for the bearing cage. As shown in Exhibit 3.8.1, the driving torque overcomes the dragging torque, which is conducive to ball driven cage excitation that could lead to cage instability. A more stable condition would be for the fluid jets to cause a dragging torque on the cage, allowing resultant fluid related torques to act against the direction of cage rotation.

This condition can be provided by minor modifications of the coolant diverter plate. By changing the hole angle from 51° to 60° and the hole size from 0.046 to 0.040, the torque produced from the impinging jets can be changed from -0.42 to +0.6 ft-lbs. This provides a net torque of -0.283 ft-lbs for the current configuration, compared to +0.737 ft lbs for the modified diverter. These data are summarized in Exhibit 3.8.2. Also shown are the effects of increasing the flow rate with the current diverter geometry. Previous tests with this flow and diverter configuration resulted in cage delamination, attributed to the high jet impingement forces on the cage. As shown, the forces produced by the alternate configuration are about one third of the forces believed to have caused cage damage. Therefore, by the

EXHIBIT 3.8.2 TORQUE AND FORCE COMPARISIONS

1. Current Flow Diverter Configuration

   - o Coolant Flow 4.6 lbs/sec
   - o 30 Hole -.046" Diameter Holes
   - o Hole Angle 51°

Source of Load	Torque (ft-lb)	Force (lbs)
o Cage/Outer Race Fluid Friction (radial clearance 15 mils)	0.137	0.96
o Coolant Jets	-0.42*	-3.32
TOTAL	-.283	-2.36

2. Alternate Flow Diverter Configuration

   - o Coolant Flow 4.6 lbs/sec
   - o 30 Hole - .040" Diameter Holes
   - o Hole Angle 60°

Source of Load	Torque (ft-lb)	Force (lbs)
o Cage/Outer Race Fluid Friction (radial clearance 15 mils)	0.137	0.96
o Coolant Jets	0.6	4.69
TOTAL	0.737	5.65

3. Current Flow Diverter Configuration

   - o Coolant Flow 8 lbs/sec

Source of Load	Torque (ft-lb)	Force (lbs)
o Cage/Outer Race Fluid Friction (radial clearance 15 mils)	0.137	0.96
o Coolant Jets	1.95	15.21
TOTAL	2.087	16.17

* Negative Sign Means Torques and Forces are Pushing the Cage.

SRS TECHNOLOGIES

modifications previously described, the net fluid torque on the cage can be tailored to act in the direction to retard cage speed and provide a stabilizing effect on potential ball excited cage instability. This can be done while keeping the jet impingement forces well below those that have previously caused cage damage.

3.9 COOLANT FLOW DIVERTER VELOCITIES

The SSME LOX turbopump turbine-end bearing coolant flow circuit includes a flow diverter plate upstream of the Number 4 bearing. The purpose of the diverter is to provide coolant directly to the bearing components (balls and inner race), and reduce the relative velocities between the coolant and the bearing balls and cage. The magnitude and direction of these velocities are dependent on diverter geometry , coolant flow, and shaft speed. The current diverter is a circular plate consisting of 30 - 0.046" diameter holes, angled 39° from a tangent to the outer circumference to the plate. The angle serves to reduce the relative tangential velocity between the coolant and bearing balls and cage.

An analysis was done to evaluate the coolant velocities as a function of coolant flow and shaft speed. Shown in Exhibit 3.9.1 is the relative tangential velocity between the coolant and balls as a function of shaft speed and coolant flow. The diverter is rotating at shaft speed, which is about 55% greater than ball or cage speed. The axial velocity of the coolant jets increases with coolant flow, and since they are angled back, the net result is to reduce the relative tangential velocity between the bearing balls and coolant. The tangential velocity of the coolant increases with shaft speed and as flow rate increases the fluid tends to oppose rather than push the balls, as shown in Exhibit 3.9.1.

Since the nominal coolant flow rate is about 4.6 lbs/sec for the LOX turbopump turbine end bearings, the coolant tries to speed up the balls and cage for this condition. In addition, the current flow rate is fairly close to flows that would make the relative tangential velocity zero. For example, a 30% increase in flow would provide 6 lbs/sec which would cause the flow to slightly oppose the ball speed. Slight variations in flow around the velocity zero point could cause an alternating tangential force on the balls and

EXHIBIT 3.9.1 RALATIVE TANGENTIAL VELOCITY VS. COOLANT FLOW FOR BRG. #4- LOX TURBO PUMP

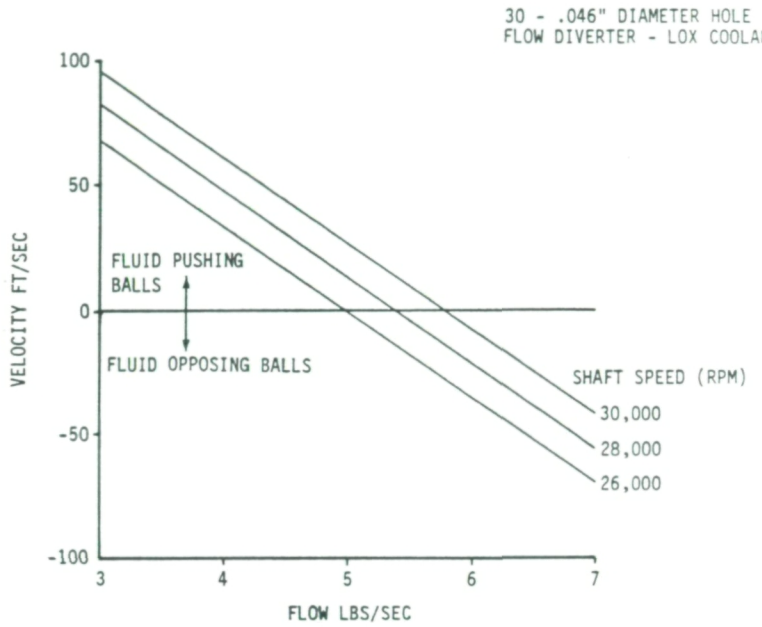

EXHIBIT 3.9.2 AXIAL VELOCITY VS. COOLANT FLOW FOR BRG. #4- LOX TURBO PUMP

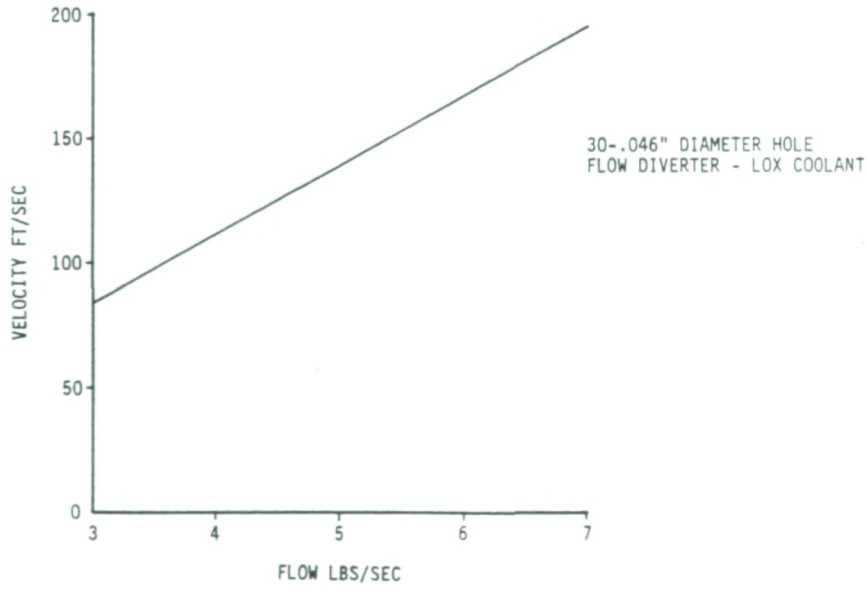

SRS TECHNOLOGIES

cage which could contribute to a forcing function, possibly causing cage instability.

Exhibit 3.9.2 provides the axial component of the coolant velocity as a function of coolant flow. Since this component is parallel to the bearing axis, it is independent of shaft speed.

The resultant velocity of the coolant impinging on the bearing balls and cage is shown in Exhibit 3.9.3 as a function of coolant flow and shaft speed. As indicated, the relative tangential velocity increases in the negative direction for higher flow rates, as the shaft speed decreases. Since the resultant velocity is the vector sum of the axial and relative tangential velocities, this causes the curves shown in Exhibit 3.9.3 to cross as the flow rate increases. The coolant flow that minimizes the resultant velocity can be expressed as:

$$w = \rho A \omega [r_h - .45 r_p] \cos\theta$$

where w = Coolant flow
A = Coolant flow area
ω = Shaft speed
r_h = Radius to coolant holes
r_p = Pitch radius
θ = Hole back angle.

The flow rates that minimize the resultant coolant velocities are noted on Exhibit 3.9.3. The above expression can also be used to select the diverter geometry that will minimize the resultant coolant velocity for given coolant flow rates and shaft speeds. For example the equation can be rearranged to give:

$$A \cos\theta = \frac{w}{\rho \omega [r_h - .45 r_p]}$$

This provides a choice of flow areas and diverter hole angles that provide a minimum resultant coolant velocity for a specified coolant flow rate and shaft speed.

EXHIBIT 3.9.3

RESULTANT VELOCITY VS COOLANT FLOW FOR BEARING #4 - LOX TURBO PUMP

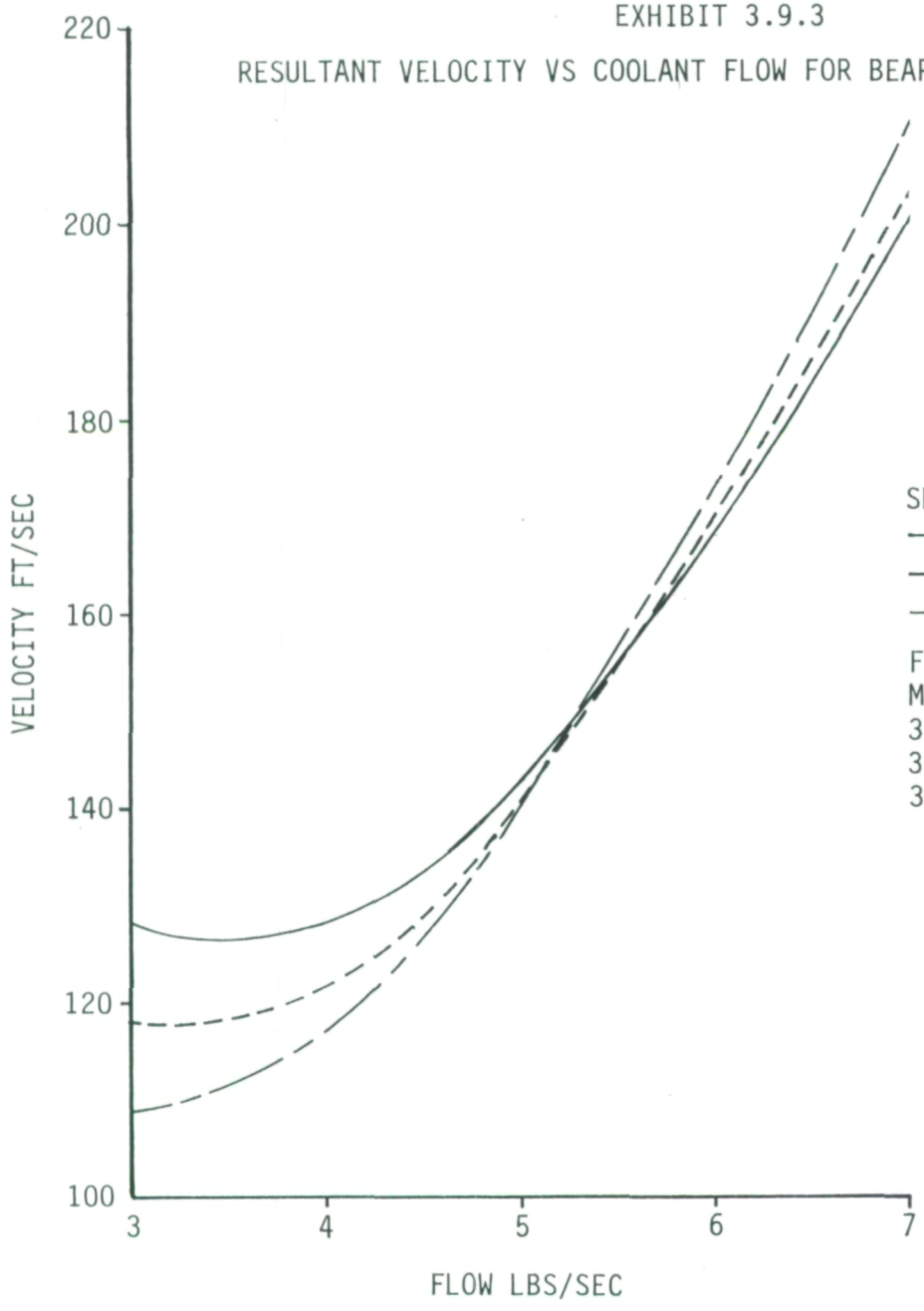

SHAFT SPEED (RPM)
——— 30,000
– – – – – 28,000
—— – —— 26,000

FLOW PRODUCING
MINIMUM VELOCITY (LBS/SEC)
3.49 FOR 30,000 RPM
3.26 FOR 28,000 RPM
3.02 FOR 26,000 RPM

SRS TECHNOLOGIES

3.10 CONTACT ANGLES AND BALL TRACKS AS FUNCTION OF BEARING LOAD

The 57 mm turbine-end LOX turbopump bearing model was used to provide parametric information on the effects of shaft speed and axial and radial loads on operating contact angles and inner race ball tracks. The axial loads ranged from 400 to 12000 lbs and the radial loads were from 100 to 5000 lbs. The contact angle data are provided in Exhibits 3.10.1 through 3.10.4, and the inner race track width data are provided in Exhibits 3.10.5 through 3.10.8. The track width data provides the width of the track caused by the ball excursions due to the azimuth change in contact angle as the ball rotates around the inner race. Since the track width data shown does not include the width of the contact area, the actual wear track should be wider by the length of the major axis of the contact ellipse. For the cases shown, the load is applied at an azimuth angle of 180° and the bearing reaction occurs at an azimuth angle of zero degrees. Since each ball has a different contact angle, only the two extremes were plotted.

3.11 LOX TURBOPUMP TURBINE-END BEARING THERMAL INVESTIGATION

The sensitivity of typical heat transfer coefficients to local pressure and boundary layer temperature in the turbine-end bearing of the LOX turbopump was investigated. The high rotational speed of bearing components (∿9000 rad/sec for balls) has generated interest concerning the potential effects of local centrifugal acceleration on fluid boundary characteristics such as pressure, temperature, and thickness. Since the ball translates at a velocity proportional to cage speed (∿1360 rad/sec), rotates at about 9000 rad/sec, and is partially shielded from the coolant flow by the cage, fluid heat transfer coefficients available in the literature for single or two phase flow do not adequately simulate these conditions. The objective of this investigation is to evaluate the pressure and temperature effects on heat transfer coefficients determined from typical correlations taken from the literature. This addresses primarily the effects of fluid property variations due to temperature and pressure changes.

A literature survey was conducted in an attempt to locate heat transfer data from two phase fluid systems involving rotating components. No such information was found; however, data on heat transfer from rotating cylinders in air was found. The data contained in Reference 4 is for rotating

EXHIBIT 3.10.1 CONTACT ANGLES VS. RADIAL LOADS - 57mm BEARING

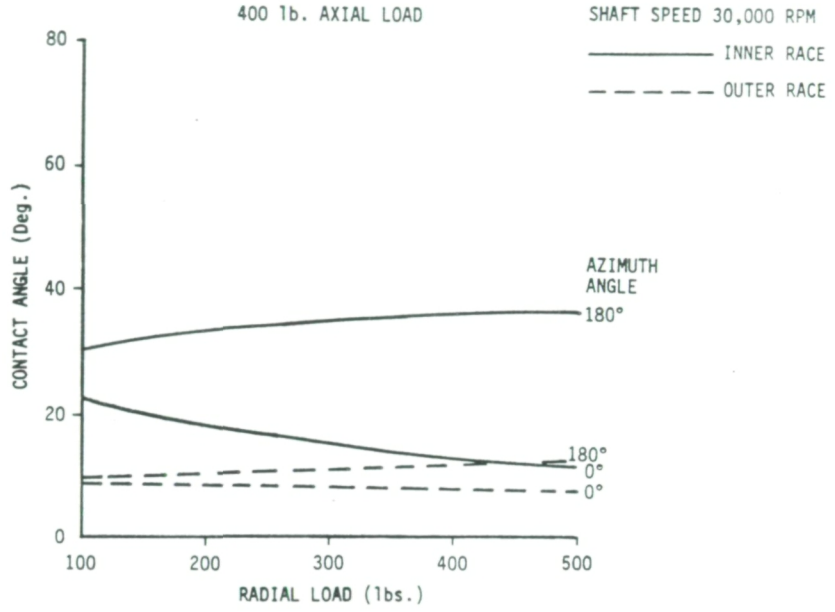

EXHIBIT 3.10.2 CONTACT ANGLE VS. RADIAL LOAD- 57mm BEARING

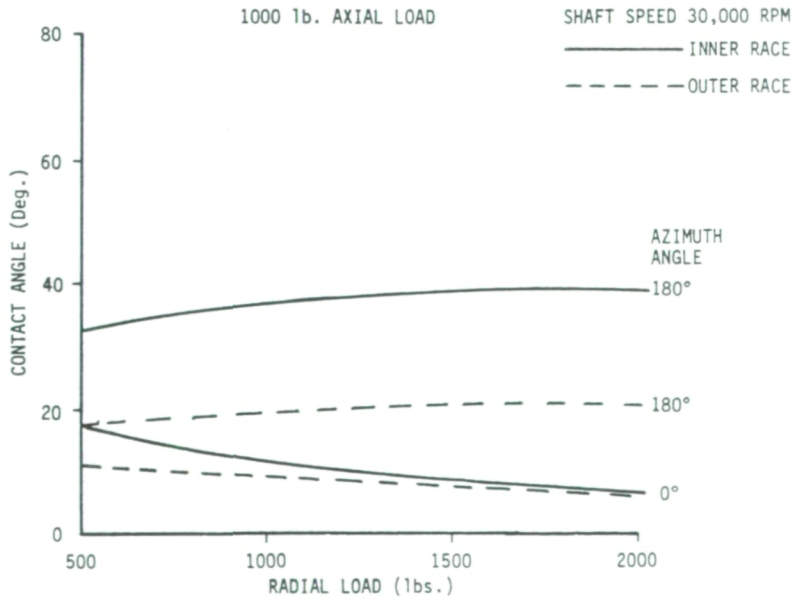

SRS TECHNOLOGIES

EXHIBIT 3.10.3 CONTACT ANGLE VS. RADIAL LOAD

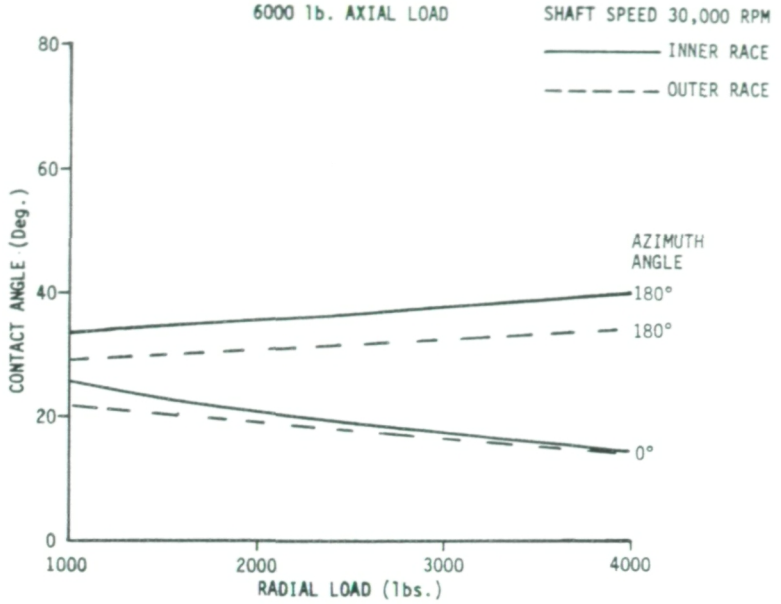

EXHIBIT 3.10.4 CONTACT ANGLE VS. RADIAL LOAD_ 57mm BEARING

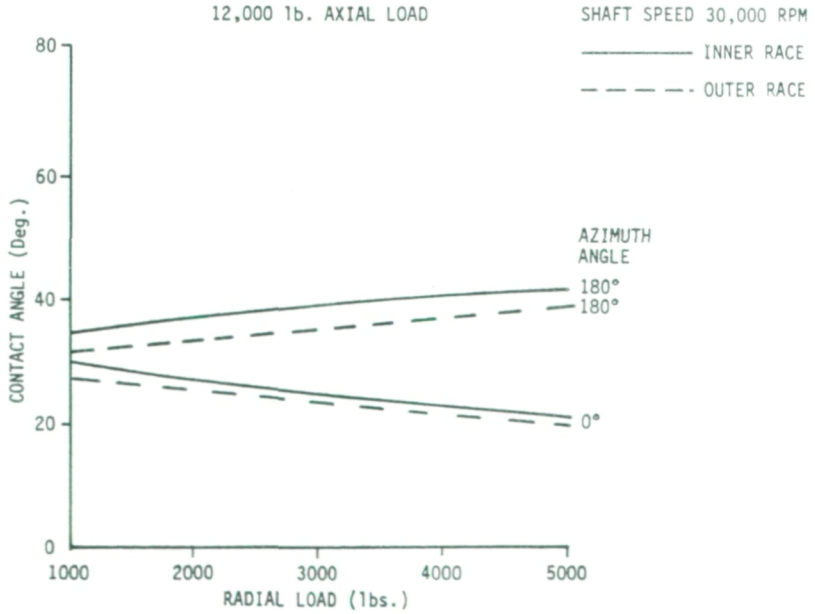

SRS TECHNOLOGIES

EXHIBIT 3.10.5 TRACK WIDTH VS. RADIAL LOAD- 57mm BEARING

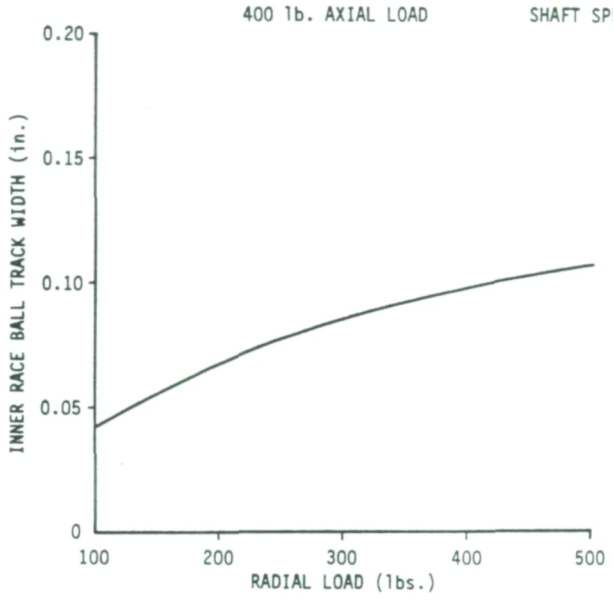

EXHIBIT 3.10.6 TRACK WIDTH VS. RADIAL LOAD- 57mm BEARING

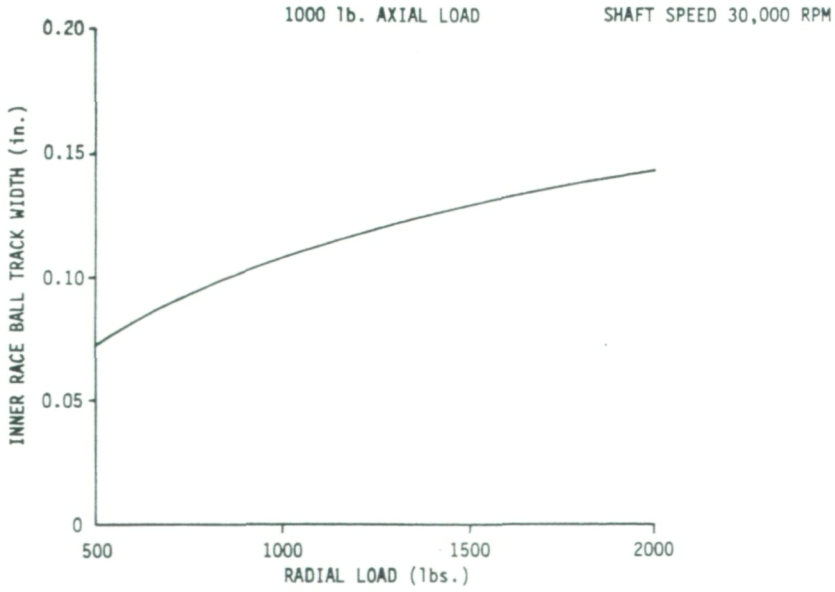

EXHIBIT 3.10.7 TRACK WIDTH VS. RADIAL LOAD- 57mm BEARING

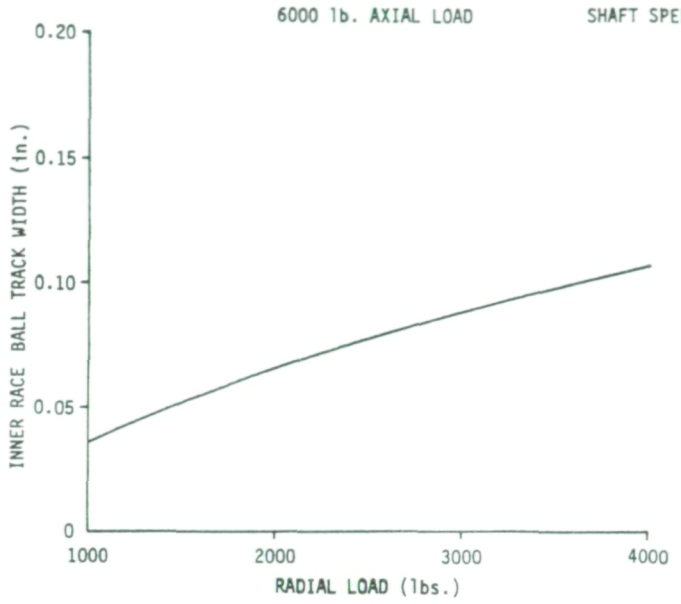

EXHIBIT 3.10.8 TRACK WIDTH VS. RADIAL LOAD- 57mm BEARING

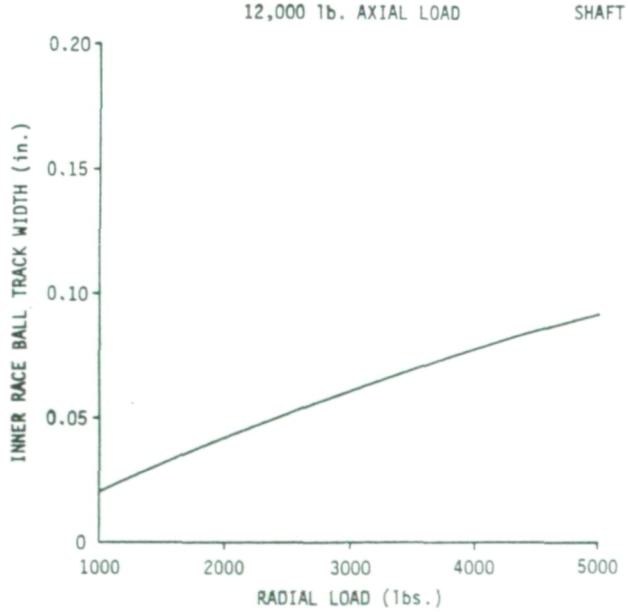

SRS TECHNOLOGIES

cylinders heated in air. It was reported that free convection influences on heat transfer from the cylinder were not important for rotational Reynolds numbers greater than 8000. For Reynolds numbers above this value, the heat transfer was correlated by the following expression.

$$1) \quad \frac{hD}{k} = .0863(N_{re})^{.7} (N_{pr})^{.35}$$

Where h ∿ heat transfer coefficient
D characteristic dimension
k ∿ thermal conductivity
N_{re} ∿ Reynolds Number based on relative speed between surface and fluid
N_{pr} ∿ Prandtl Number

This expression is similar to the one currently being used in the turbopump bearing thermal model, which is as follows:

$$2) \quad \frac{hD}{k} = .023(N_{re})^{.8} (N_{pr})^{.4}$$

The Reynolds numbers characteristic of the bearing inner race are on the order of 10^5, and Prandtl numbers are on the order of 1, for the vapor phase, the equations agree within about 6% for this range of conditions.

Interference photographs of the flow field (Reference 4) showed no significant density gradients due to pressure variations around the cylinder, up to a Reynolds number of 14,600.

Although the results of Reference 4 indicate that no significant pressure gradients exist in the boundary layer of rotating components due to centrifugal acceleration, there is a possibility of a radial pressure gradient in the rotating fluid external to the boundary layer. This could reduce the pressure at the edge of the boundary layer below the mean pressure in the rotating fluid. The pressure effect on the heat transfer coefficient is shown in Exhibit 3.11.1. These data show about a 16% reduction in heat transfer coefficient for a 50 psi reduction in pressure. Furthermore, the saturation temperature is reduced about 7°R which means vapor will form on the surfaces at a lower surface temperature. Another problem associated with

EXHIBIT 3.11.1 FLUID PRESSURE EFFECTS on INNER RACE HEAT TRANSFER COEFFICIENTS for LOX VAPOR

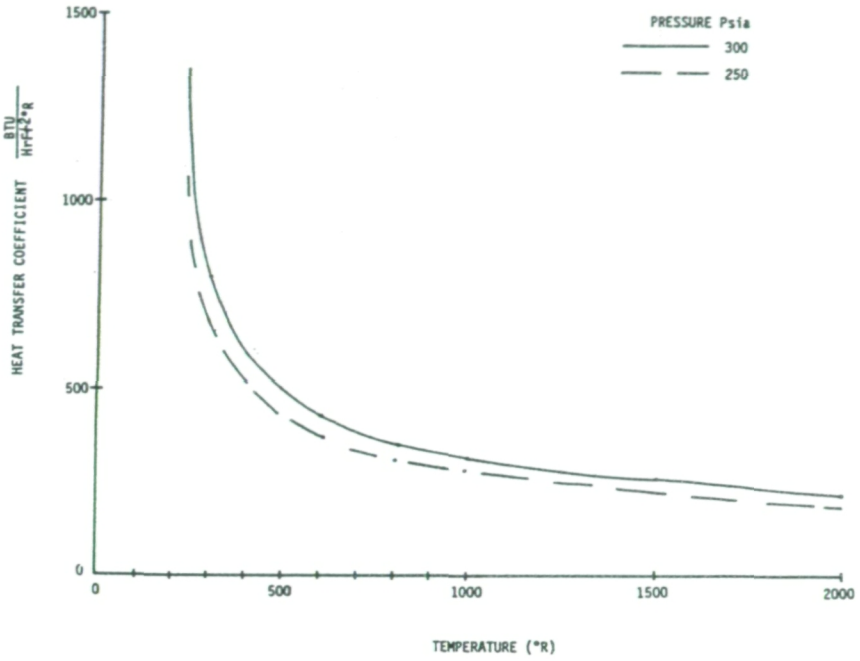

EXHIBIT 3.11.2 VARIATION OF INNER RACE HEAT TRANSFER COEFFICIENTS DUE TO THE ASSUMED BOUNDARY LAYER TEMPERATURE

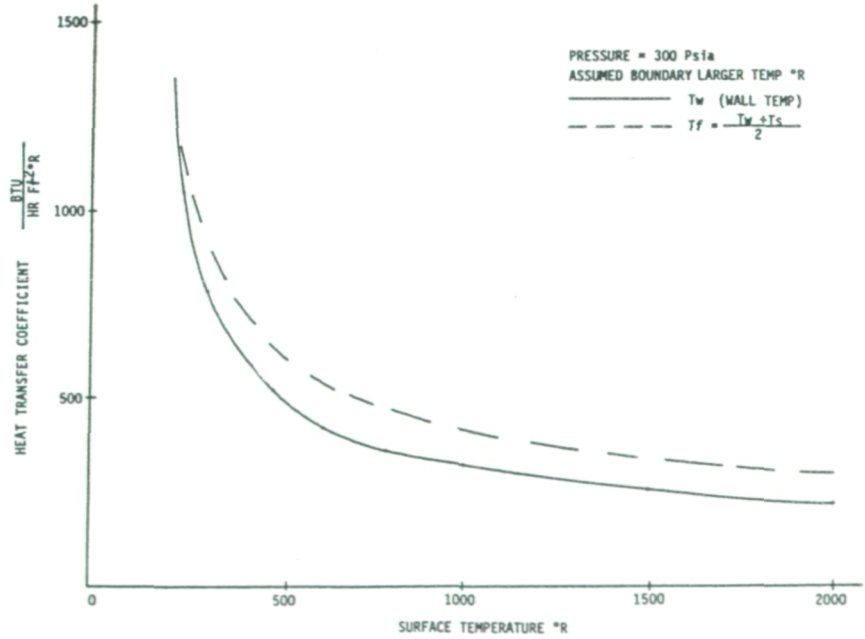

the application of typical heat transfer relationships is selecting the appropriate temperature for evaluation of the thermodynamic and transport properties. These are usually determined at the fluid bulk temperature or the average of the surface and fluid temperature (film temperature). The larger the temperature difference between the surface and fluid the greater the property variation and the more significant the temperature at which the properties are evaluated becomes. An example of this effect on heat transfer coefficients is shown in Exhibit 3.11.2. The evaluation of properties at the surface temperature provides a lower limit for the heat transfer coefficient and consequently a "worst case" for bearing component temperatures. As shown, there is approximately 28% decrease in heat transfer coefficient when the properties are evaluated at the surface, rather than film, temperature.

The 57 mm bearing thermal model developed for the BSMT was modified to simulate the SSME LOX turbopump turbine-end flow conditions. For example, the coolant flow through the shaft and the diverter velocity effects specific to the pump were incorporated into the BSMT model. The model was run to determine the sensitivity of heat transfer coefficients on the average temperature of the bearing components. The vapor film coefficients were estimated for different assumed boundary layer temperature distributions and pressures. The high rotational speed of the bearing components could affect local coolant temperature and pressure. The 57 mm bearing model was run for the following conditions:

- Axial Loads (lbs) 3000, 4000, and 5,000
- Local Coolant Pressure (psia) 250 and 300
- Local Fluid Properties Evaluated at Film and Surface Temperatures
- Coolant Flow Rate 4.6 lbs/sec
- Coolant Inlet Temp = -240°F.

The results of the analysis are given in Exhibits 3.11.3 and 3.11.4 in terms of average component temperatures and maximum temperatures in the bearing tracks. These data were used to determine the percentage change in temperature for the various conditions, as shown in Exhibits 3.11.5 and 3.11.6. At the higher loads, the component average temperatures appear to be more sensitive to variations in heat transfer coefficients, especially the inner and outer races. Exhibit 3.11.7 shows the component average and track temperatures as a function of axial load for a coolant pressure of 300 psia.

EXHIBIT 3.11.3 BEARING COMPONENT TEMPERATURES 57mm BEARING 3000 LB. AXIAL LOAD

CONDITION	COMPONENT	TEMPERATURE OF	
		AVERAGE	MAX TRACK
o 300 PSIA o FILM TEMP	BALL INNER RACE OUTER RACE	167 -136 -115	448 325 146
o 300 PSIA o WALL TEMP	BALL INNER RACE OUTER RACE	223 -110 -100	546 378 184
o 250 PSIA o FILM TEMP	BALL INNER RACE OUTER RACE	219 -108 -107	539 371 166
o 250 PSIA o WALL TEMP	BALL INNER RACE OUTER RACE	273 -90 -91	596 424 203

EXHIBIT 3.11.4 57mm BEARING COMPONENT TEMPERATURES

CONDITIONS (HEAT TRANSFER PROPERTIES EVALUATED AT FILM TEMP.)	COMPONENT	TEMPERATURE(^{o}F)	
		AVERAGE	MAX TRACK
o 4000lb AXIAL LOAD o 300 PSIA	BALL INNER RACE OUTER RACE	352. -61. 12.	772. 562. 349.
o 4000lb AXIAL LOAD o 250 PSIA	BALL INNER RACE OUTER	430. -31. 31.	847. 625 380
o 5000lb AXIAL LOAD o 300 PSIA	BALL INNER RACE OUTER RACE	624. 13. 160.	1205. 859. 629.
o 5000lb AXIAL LOAD o 250 PSIA	BALL INNER RACE OUTER RACE	867 135 285	1508 1082 815

SRS TECHNOLOGIES

C-2

EXHIBIT 3.11.5 PERCENTAGE INCREASE IN COMPONENT TEMPERATURE 3000 LB. AXIAL LOAD

CONDITION	COMPONENT	% INCREASE IN TEMP	
		AVERAGE	MAX TRACK
o 300 PSIA o FILM TO WALL COMPARISON	BALL INNER RACE OUTER RACE	33 18 13	12 16 26
o 250 PSIA o FILM TO WALL COMPARISON	BALL INNER RACE OUTER RACE	25 17 16	11 14 22
o FILM 300 TO 250 COMPARISON	BALL INNER RACE OUTER RACE	31 20 7	10 14 13
o WALL 300 TO 250 COMPARISON	BALL INNER RACE OUTER RACE	22 18 9	9 12 11

EXHIBIT 3.11.6 PERCENTAGE INCREASE IN COMPONENT TEMPERATURE

CONDITIONS (HEAT TRANSFER PROPERTIES EVALUATED FILM TEMP)	COMPONENT	% INCREASE IN TEMP(^{o}F)	
		AVERAGE	MAX TRACK
o 40001b AXIAL LOAD o 300 TO 250 PSIA COMPARISON	BALL INNER RACE OUTER RACE	22 49 158	10 11 9
o 50001b AXIAL LOAD o 300 TO 250 PSIA COMPARISON	BALL INNER RACE OUTER RACE	40 938 78	25 26 30

EXHIBIT 3.11.7 TEMPERATURE VS. LOAD

- 57 mm BEARING
- SHAFT SPEED 30,000 RPM
- COOLANT FLOW & PRESSURE (4.6 LBS/SEC 300 PSIA)
- HEAT TRANSFER PROPERTIES EVALUATED @ FILM TEMP.

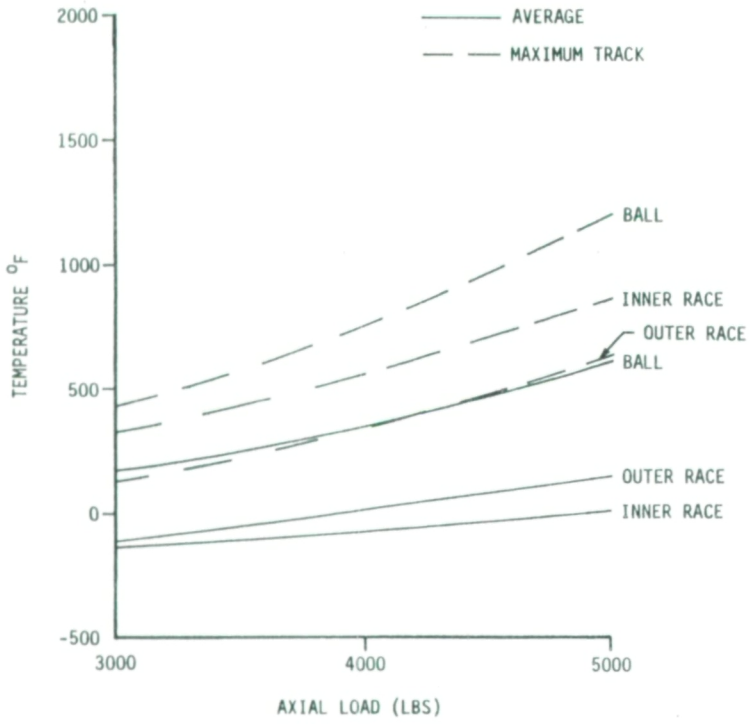

EXHIBIT 3.11.8 TEMPERATURE VS. LOAD

- 57 mm BEARING
- SHAFT SPEED 30,000 RPM
- COOLANT FLOW & PRESSURE 4.6 LBS/SEC 250 PSIA
- HEAT TRANSFER PROPERTIES EVALUATED @ FILM TEMPERATURE

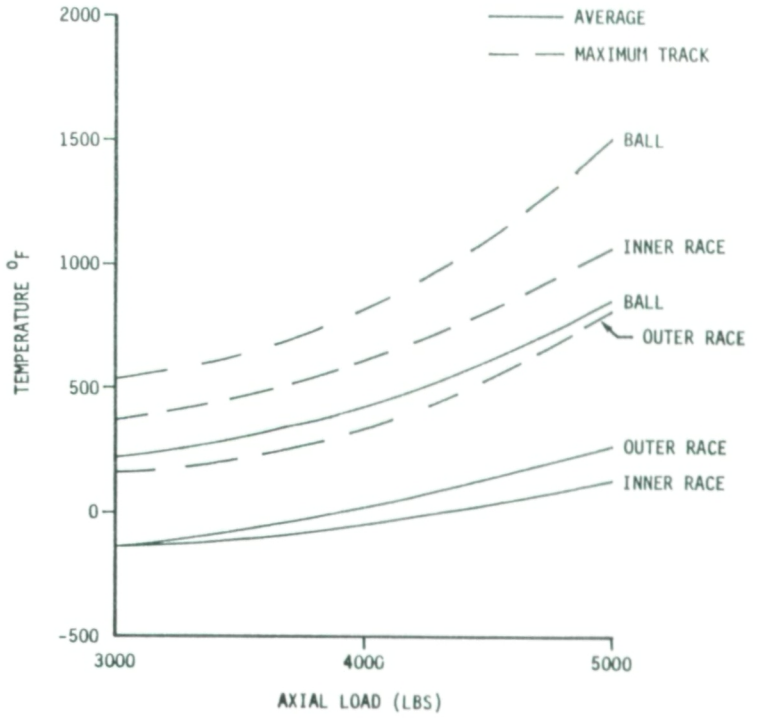

SRS TECHNOLOGIES

Exhibit 3.11.8 shows similar information for a coolant pressure of 250 psi. A 6000 lb axial load condition was attempted but the solution failed to converge, indicating a thermally unstable condition. This agrees with the increasing slope of the temperature curves as the load is increased.

3.12 SENSITIVITY OF 57 MM BEARING TEMPERATURE TO INCREASED FRICTIONAL HEATING

The 57 mm pump turbine-end bearing was evaluated to determine the sensitivity of bearing component temperatures to the variation in frictional heat generation. Three cases were investigated for axial loads of 1,000, 2,000, and 3,000 lbs. These cases were converged using a technique similar to that used with the 45 mm bearing analysis. The heat rates for each of these cases were doubled and tripled and used as input to the 57 mm bearing thermal model to determine the effect on bearing temperatures. A summary of the results is shown in Exhibit 3.12.1. Shown in Exhibits 3.12.2, 3.12.3, and 3.12.4 are plots of component temperatures vs. axial load for the different levels of heat generation.

3.13 BALL EXCURSIONS AS A FUNCTION OF LOADING FOR 57MM LOX PUMP BEARING

The objective of this effort is to estimate the ball excursions of the 57mm Lox pump turbine-end bearing as a function of axial and radial loads.

The cage pocket to ball diametrical clearance necessary to prevent cage interference with ball orbital speed depends on the relative speed of the cage and balls. The diametrical clearance necessary to prevent the cage from influencing the ball orbital speed is determined as follows.

1) $ds_b/dt = Rm_i \; W_b$

Where ds_b = distance traveled by ball in time dt
Rm_i = instantaneous radius to ball center
W_b = instantaneous ball orbital speed.

EXHIBIT 3.12.1 CHANGES IN HEAT RATE FOR 57mm BEARING

APPLIED AXIAL LOAD																				
1000 Lbs.							2000 Lbs.							3000 Lbs.						
TOTAL HEAT RATE (BTU/HR)	AVERAGE TEMPERATURE (°F)			MAXIMUM TRACK TEMPERATURE (°F)			TOTAL HEAT RATE (BTU/HR)	AVERAGE TEMPERATURE (°F)			MAXIMUM TRACK TEMPERATURE (°F)			TOTAL HEAT RATE (BTU/HR)	AVERAGE TEMPERATURE (°F)			MAXIMUM TRACK TEMPERATURE (°F)		
	INNER RACE	BALL	OUTER RACE	INNER RACE	BALL	OUTER RACE		INNER RACE	BALL	OUTER RACE	INNER RACE	BALL	OUTER RACE		INNER RACE	BALL	OUTER RACE	INNER RACE	BALL	OUTER RACE
10282	-184	-80	-207	39	38	-138	18854	-136	75	-139	206	292	25	27965	-89	240	-46	396	565	220
20565	-107	130	-153	353	358	-33	37708	7	474	4	722	901	337	55930	120	835	218	1144	1482	762
30847	-16	358	-95	690	696	122	56562	167	900	162	1275	1540	566	83895	356	1476	514	1950	2454	1348

EXHIBIT 3.12.2 57mm BEARING COMPONENT TEMPERATURES VS. APPLIED AXIAL LOAD

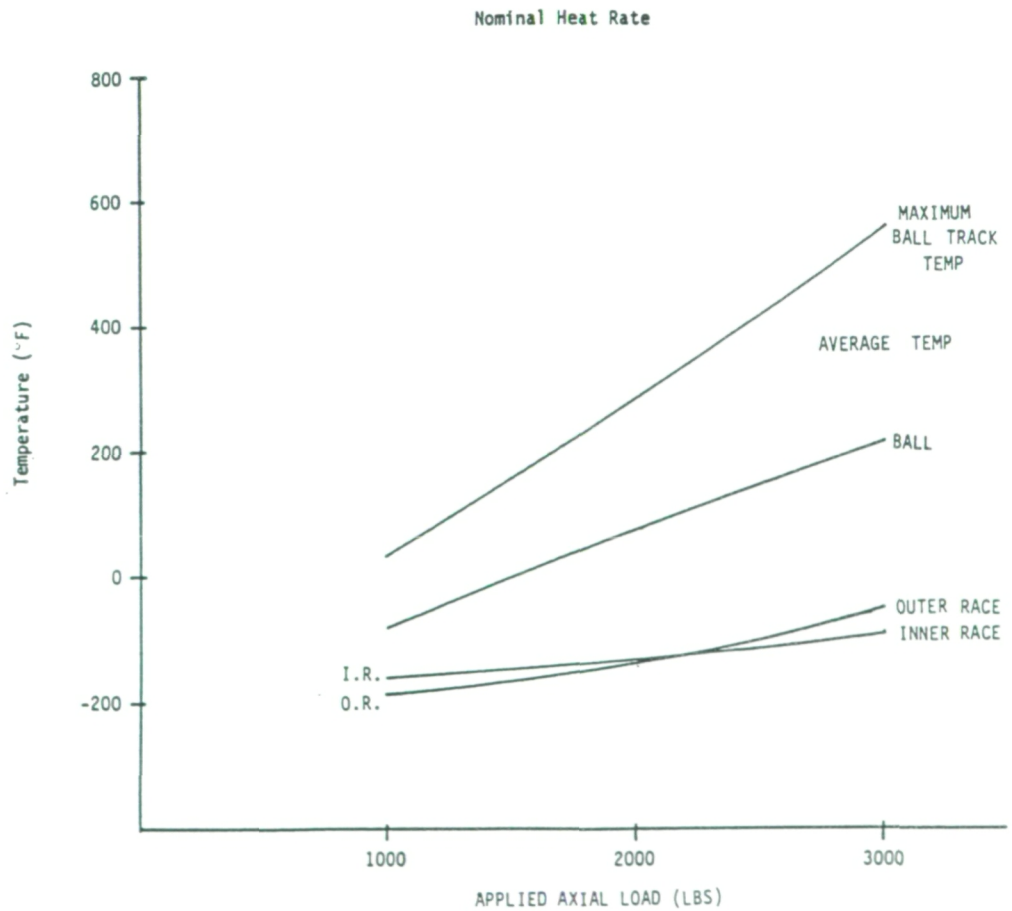

EXHIBIT 3.12.3 57mm BEARING COMPONENT TEMPERATURES VS. APPLIED AXIAL LOAD

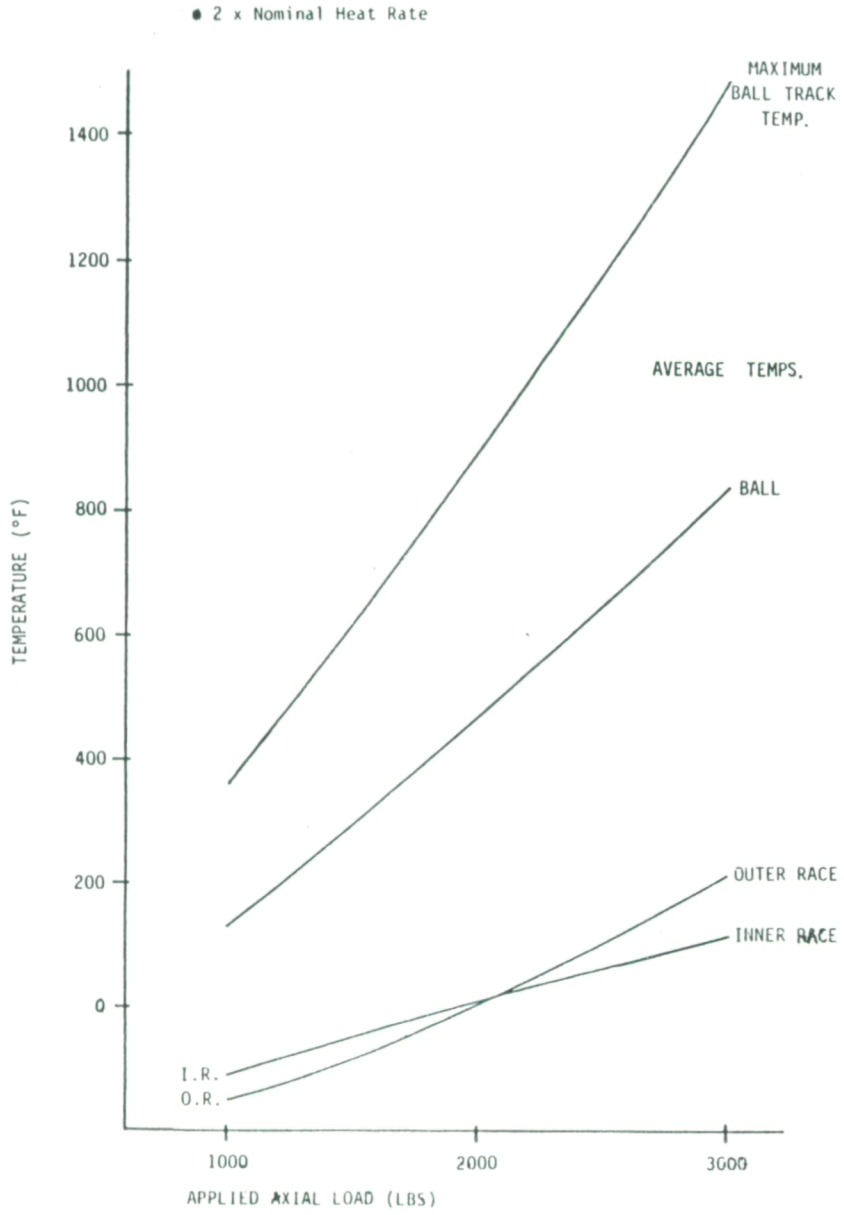

EXHIBIT 3.12.4 57mm BEARING COMPONENT TEMPEARTURES VS. APPLIED AXIAL LOAD

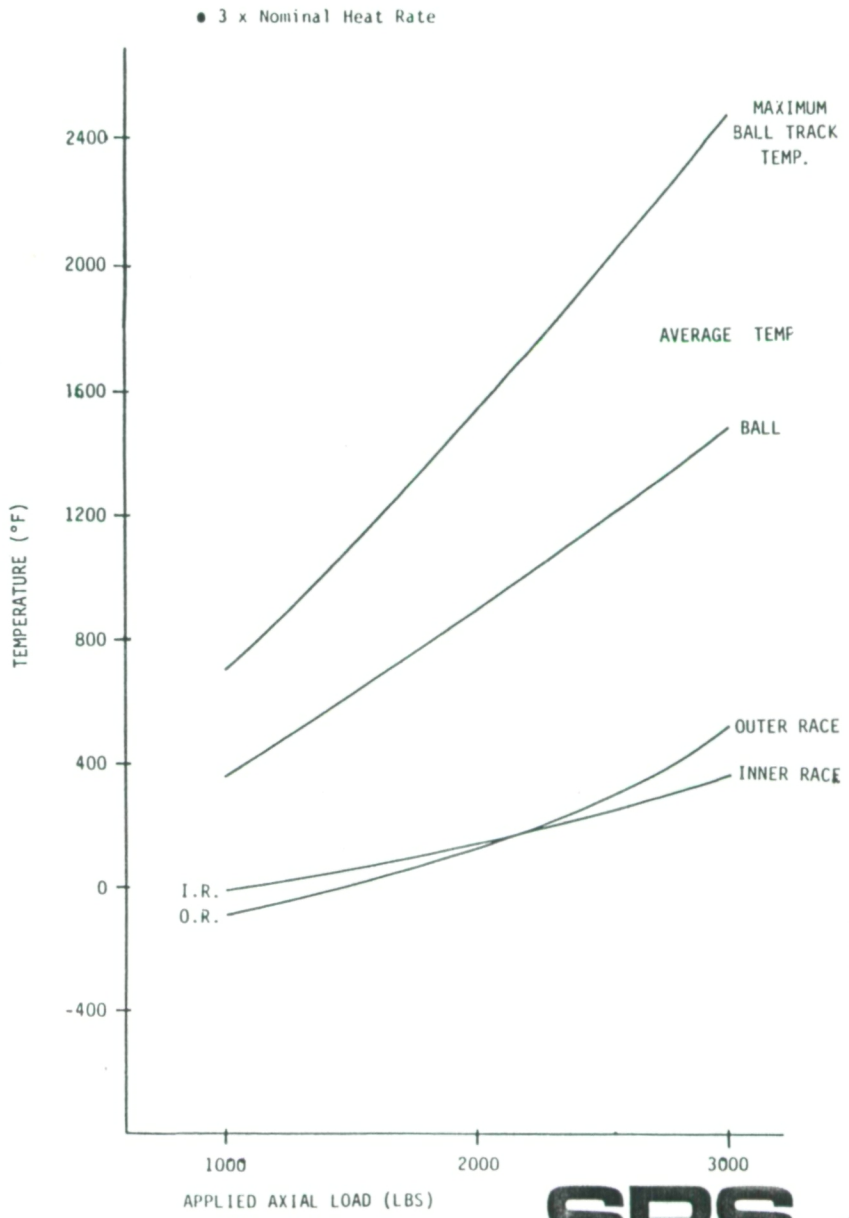

SRS TECHNOLOGIES

2) $ds_c/dt = R_c W_c$

Where ds_c = distance traveled by cage in time dt
R_c = radius to cage pocket center
W_c = cage speed

The distance between cage pocket centers is

$$ds_c = \frac{2\pi R_c}{13}$$

The time dt for the cage to rotate this distance is:

$$dt = \frac{2\pi}{13\ W_c}$$

The distance the ball travels in the same time is:

$$ds_b = (Rm_i\ W_b)\left(\frac{2\pi}{13W_c}\right)$$

The relative distance between ball and cage pocket center is

$$ds_b - ds_c = \frac{2\pi}{13}\left(Rm_i\ \frac{W_b}{W_c} - R_c\right)$$

$R_c = Dp/2$ Where Dp = Pitch diameter

$$ds_b - ds_c = \frac{2\pi}{13}\left(Rm_i\ \frac{W_b}{W_c} - \frac{Dp}{2}\right)$$

The net relative distance between the ball and cage is therefore:

$$3) \qquad Z = \frac{2\pi}{13} \sum_{i=1}^{13} \frac{Rm_i \; W_{bi}}{W_c} - Dp/2$$

Rm_i is the instantaneous radius to the ball center, and is a function of outer race contact angle and ball loading.

Rm_i is determined from the following geometrical representation:

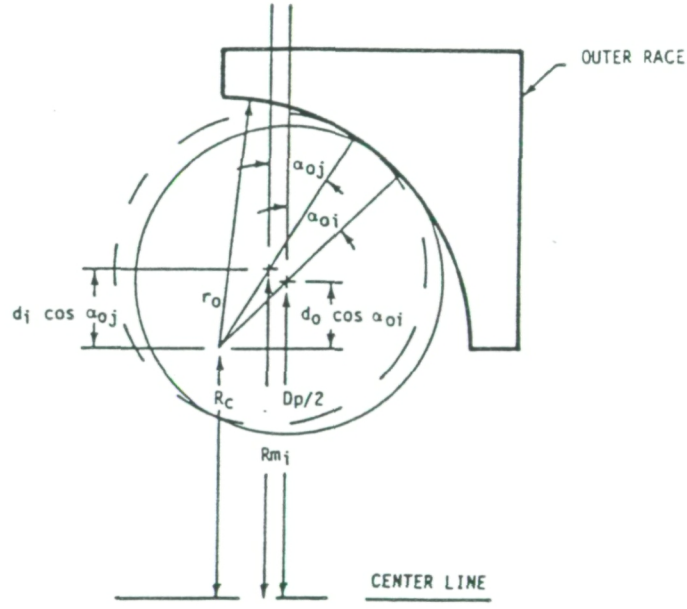

The distance from the outer race center line to the outer race curvature center (R_c) is

$$R_c = Dp/_2 - d_o \, Cos\alpha_{oi}$$

α_{oi} = free contact angle

$$d_o = r_o - D/_2 \quad ; D = \text{ball diameter}$$

$$R_c = Dp/_2 - r_o - D/_2 \, Cos\alpha_{oi}$$

$$f_o = r_o/D$$

$$R_c = Dp/_2 - (f_o - .5) \, D \, Cos\alpha_{oi}$$

then

$$Rm_i = R_c + d_i \, Cos \, \alpha_{oj} \quad ; \alpha_{oj} = \text{operating contact angle}$$

$$d_i = r_o - D/_2 + \delta_{oj} \quad ; \delta_{oj} = \text{elastic deformation at the outer race contact}$$

4) $$Rm_i = \frac{D_p}{2} - (f_o - .5) \, D \, Cos \, \alpha_{oi} + [(f_o - .5)D + \delta_{oj}] \, Cos \, \alpha_{oj}$$

The ball speeds, contact angles, and contact loads for the various axial and radial loading conditions were determined using the SHABERTH bearing code. The elastic deformation for each ball race contact was calculated for the outer race loads. Equations 3 and 4 were solved for the net distance required between ball and cage to prevent cage influences on ball speed.

Shown in Exhibit 3.13.1 are the results of the analysis. For example, a bearing preload of 1000 lbs and a ball/pocket diametrical clearance of 25 mils shows that a radial load of about 350 lbs will cause cage/ball interference. Reducing the preload to 800 lbs reduces the corresponding radial load to 250 lbs. Although higher preloads reduce ball excursions they induce higher contact stresses. Therefore there are opposing factors in evaluating the trades between increased ball pocket clearance with lower preloads vs. higher preloads and less clearance. Increased clearance tends to weaken the

EXHIBIT 3.13.1 BALL EXCURSION VS. LOAD

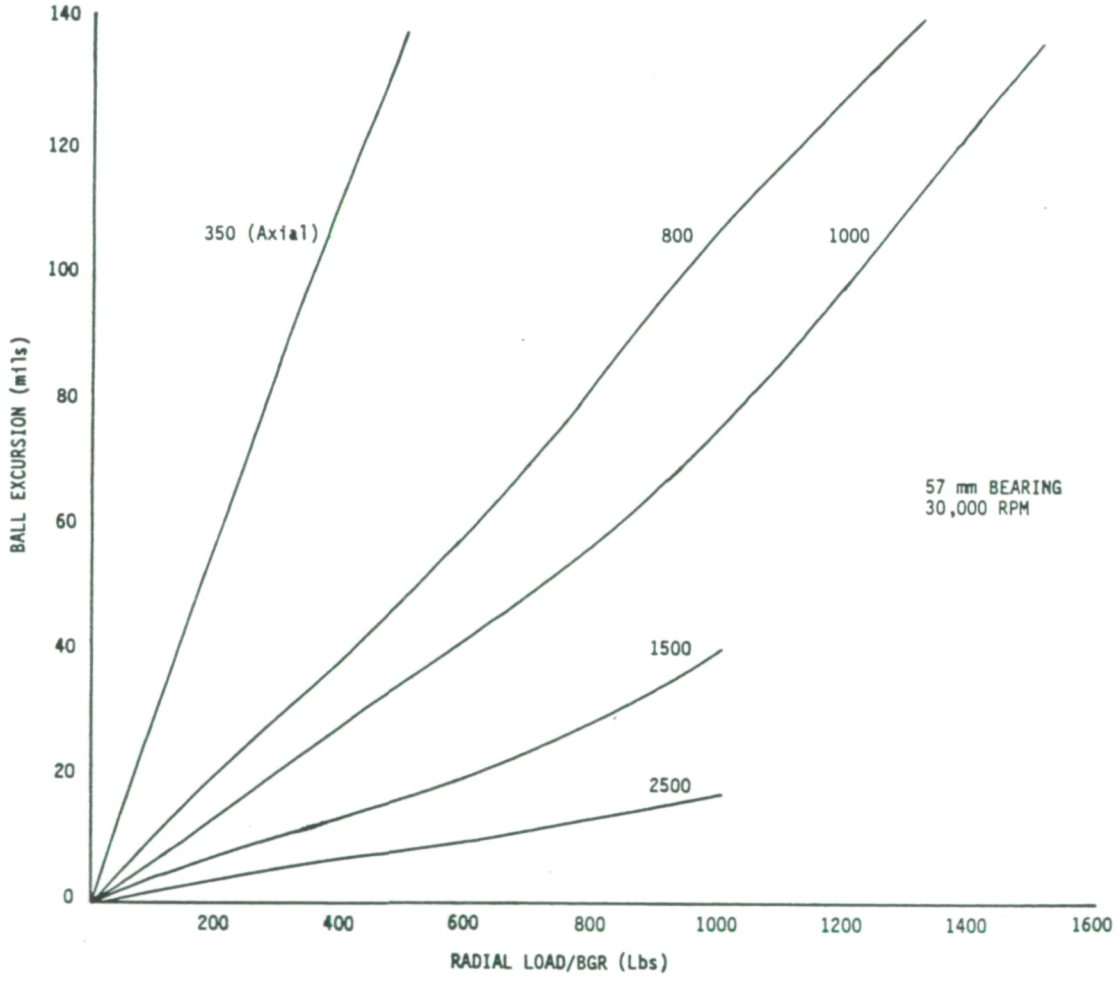

cage and perhaps reduce the number of balls with corresponding higher ball loads. Reducing the preloads without increasing the ball/pocket clearance causes ball/cage interference which causes increased cage pocket wear, ball skid, increased heat generation, and ball wear. The following section provides a quantitative estimate of the loads and stresses introduced into the 57 mm bearing cage as related to axial and radial loads for a specific value of ball to pocket diametrical clearance.

3.14 CAGE WEB STRESSES FOR 57MM LOX PUMP BEARING

An analysis was performed to estimate the cage pocket stresses induced by cage/ball interference for the 57mm bearing. The loads induced by cage speed and coolant pressure drop across the cage were included. The individual stress for each load was estimated and superimposed as an estimate of the total stress. The estimated cage pocket loads due to cage/ball interference are shown in Exhibit 3.14.1. These loads were determined by an iterative procedure that balanced the forces of the balls pushing the cage with the force required to drag the balls orbiting at speeds less than the cage speed. These are steady loads, and therefore do not account for loads that can occur due to transient characteristics such as cage instabilities. Shown in Exhibit 3.14.2 are the stresses estimated based on cage geometry and the loads discussed. Also shown, in Exhibit 3.14.3, are the safety factors based on an ultimate tensile stress of 30,000 PSI @ - 200°F. for the cage material. The critical buckling load based on a compressive modulus of 1.25×10^6 PSI is estimated to be 1063 pounds. Since this is considerably larger than the estimated compressive loads, buckling should not be a concern.

3.15 DEVELOPMENT OF BEARING MODELING PROGRAM ADORE FOR LOX TURBOPUMP BEARING

In 1985, NASA/MSFC purchased a computer program called ADORE to acquire the capability of simulating, in real-time, the dynamic performance of bearings used in the SSME turbopumps. This program was installed on the MSFC UNIVAC 1100/80 computer system.

ADORE is an advanced FORTRAN computer program for the real-time simulation of the dynamic performance of rolling bearings. The analytical foundation of ADORE essentially consists of the classical differential equations of motion, and the analytical models for the interaction between

EXHIBIT 3.14.1 ESTIMATED CAGE POCKET LOADS DUE TO CAGE/BALL INTERFERENCE

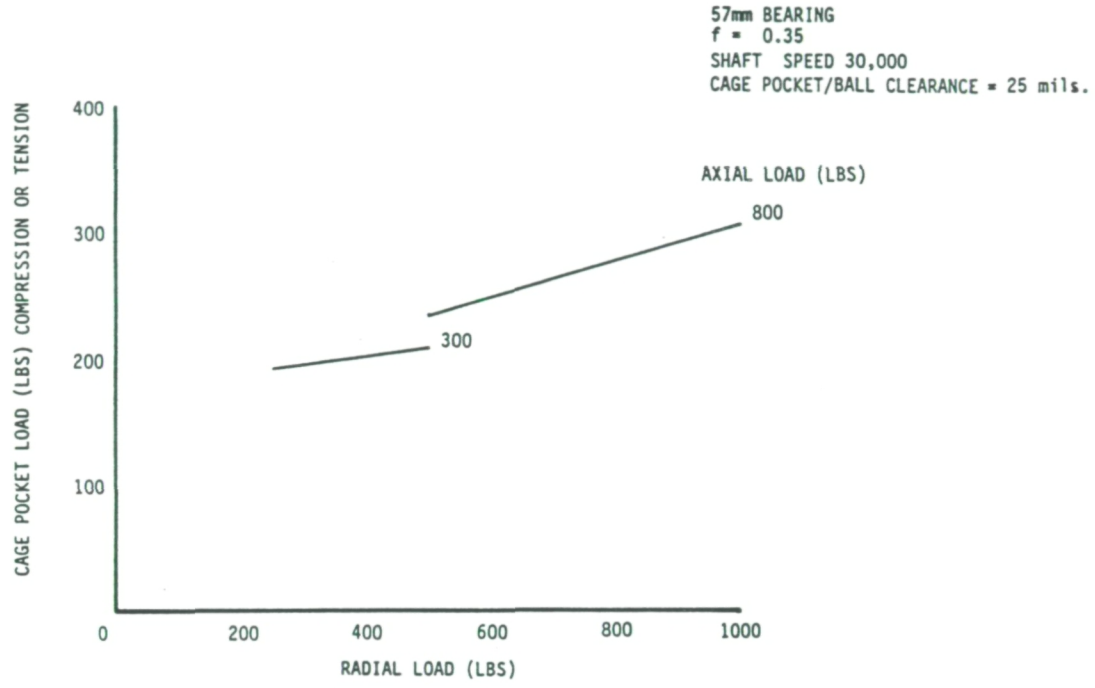

EXHIBIT 3.14.2 ESTIMATED CAGE TENSILE STRESSES

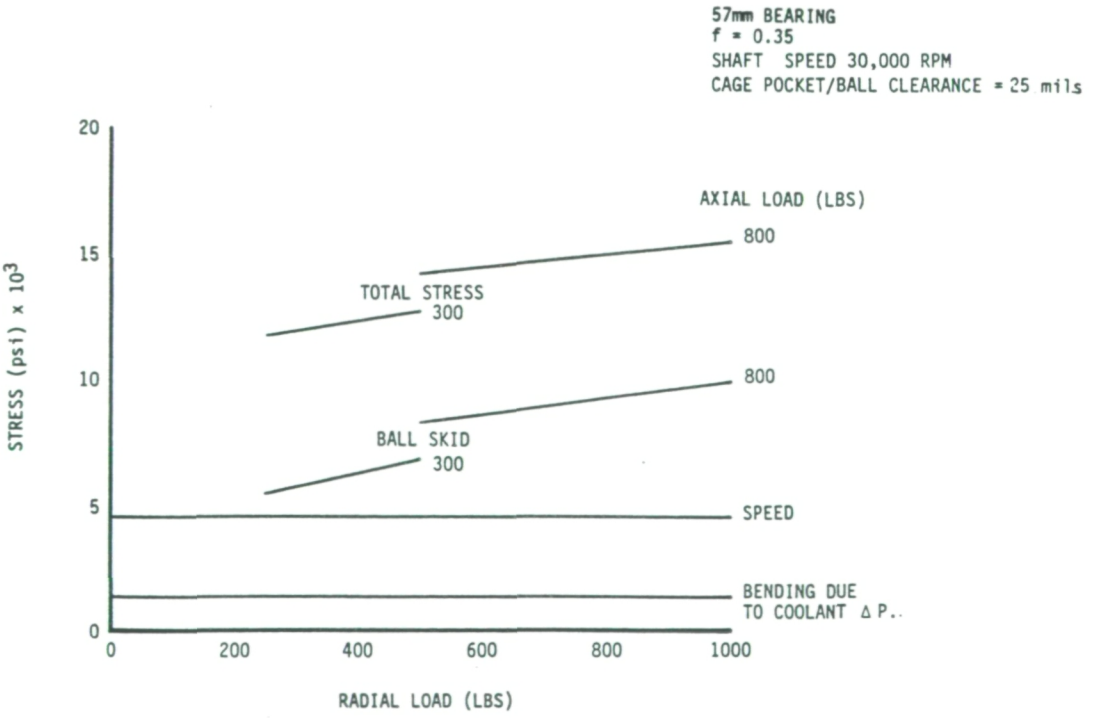

SRS TECHNOLOGIES

EXHIBIT 3.14.3 SAFETY FACTORS BASED ON TOTAL TENSION STRESS

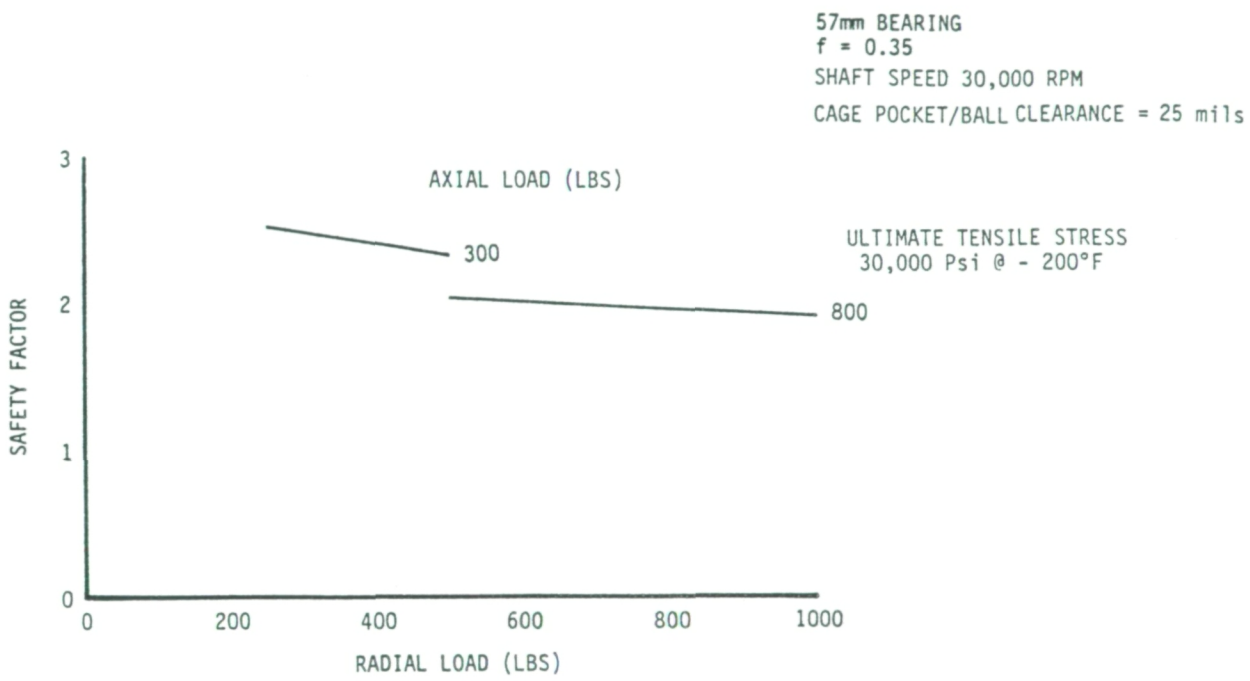

the various bearing elements. The equations of motion are formulated in a generalized six-degree-of-freedom system and the interaction models allow for arbitrary geometry of the bearing elements. Thus, any arbitrary variation in bearing geometry, such as geometrical imperfections or manufacturing tolerances, can be modeled and the influence of time dependent operating conditions on the general stability of bearing elements can be investigated.

The types of rolling bearings considered in ADORE include ball, cylindrical roller, tapered roller, spherical tapered roller and radially loaded single row spherical roller bearings. The bearings may be with or without cage, and the cage may be either a one-piece element or it may be segmented into several pieces. The analytical models in ADORE consist of the following:

(1) Rolling element/race interactions
(2) Rolling element/cage interactions
(3) Cage/race interactions
(4) Race flange interactions for rolling bearings
(5) External system interactions and constraints.

The rolling element/race interaction provides a model for the computation of normal and tractive forces at the rolling element to tract interface. The classical theories of elasticity and elastohydrodynamic lubrication provide the foundations of this model. Rolling element to cage and the cage/race contacts are modeled in terms of the geometrical interaction and an arbitrary constitutive relation for the computation of normal and friction forces. External system interactions and constraints include models for the applied forces and moments exerted on the bearing elements as a result of their interaction with the operating environment. This catgeory includes churning and drag effects as a function of lubricant flow through the bearing, geometrical distortion of the bearing elements due to thermal gradients, shrink fits and centrifugal expansion of the races, and any prescribed loads and/or geometrical constraints on the bearing.

The general motion of any bearing clement as a function of the applied forces and moments, computed from the interactions noted above, is considered in two parts:

(1) Motion of the mass center
(2) Rotation of the element about its mass center.

The mass center motion is generally considered in an inertial coordinate frame, while the rotational motion is treated in a body-fixed coordinate frame. The three coordinates which locate the mass center, and the three angles which define the angular orientation of the bearing element, constitute the six degrees of freedom available for the simulation of the general motion of the bearing element. These six fundamental coordinates, when combined with the six corresponding velocities, result in twelve differential equations of motion for each bearing element. Thus, for a bearing with N rolling elements, a one-piece cage, and outer and inner races, the model consists of a system of 12(N+3) simultaneous first order differential equations. The set of differential equations is numerically integrated to obtain the real-time simulation of the bearing performance.

ADORE is highly modular in structure. The entire code is divided into a large number of subprograms. Exhibit 3.15.1 shows the basic segments of ADORE, and the function of each subprogram or segment. A schematic overview of the program is presented in Exhibit 3.15.2. As evident from this figure, the program essentially has three modes of operation: the quasi-static mode, the dynamic mode, and the post-processing or plot mode. Each mode may be executed independently. Other features of the program are:

(1) The material properties of any element in the bearing may be specified arbitrarily.

(2) Either a force or a displacement may be prescribed along the (X,Y,Z) axes of the bearing races. Similarly, the rotational motion of the races may be specified by either specifying a moment or an angular displacement or acceleration.

(3) In order to account for the roughness of interacting surfaces, a "critical film thickness" is defined for each local interaction. At the rolling element/race interface, the critical film thickness corresponds to the value of the lubricant film thickness below which the elastohydrodynamic traction model is no longer valid. The rolling element/cage and cage/race contacts, the critical film thickness denotes a separation between the interacting surfaces below which the asperity interactions become significant and a fully metallic contact may be assumed.

EXHIBIT 3.15.1 BASIC SEGMENTS OF ADORE

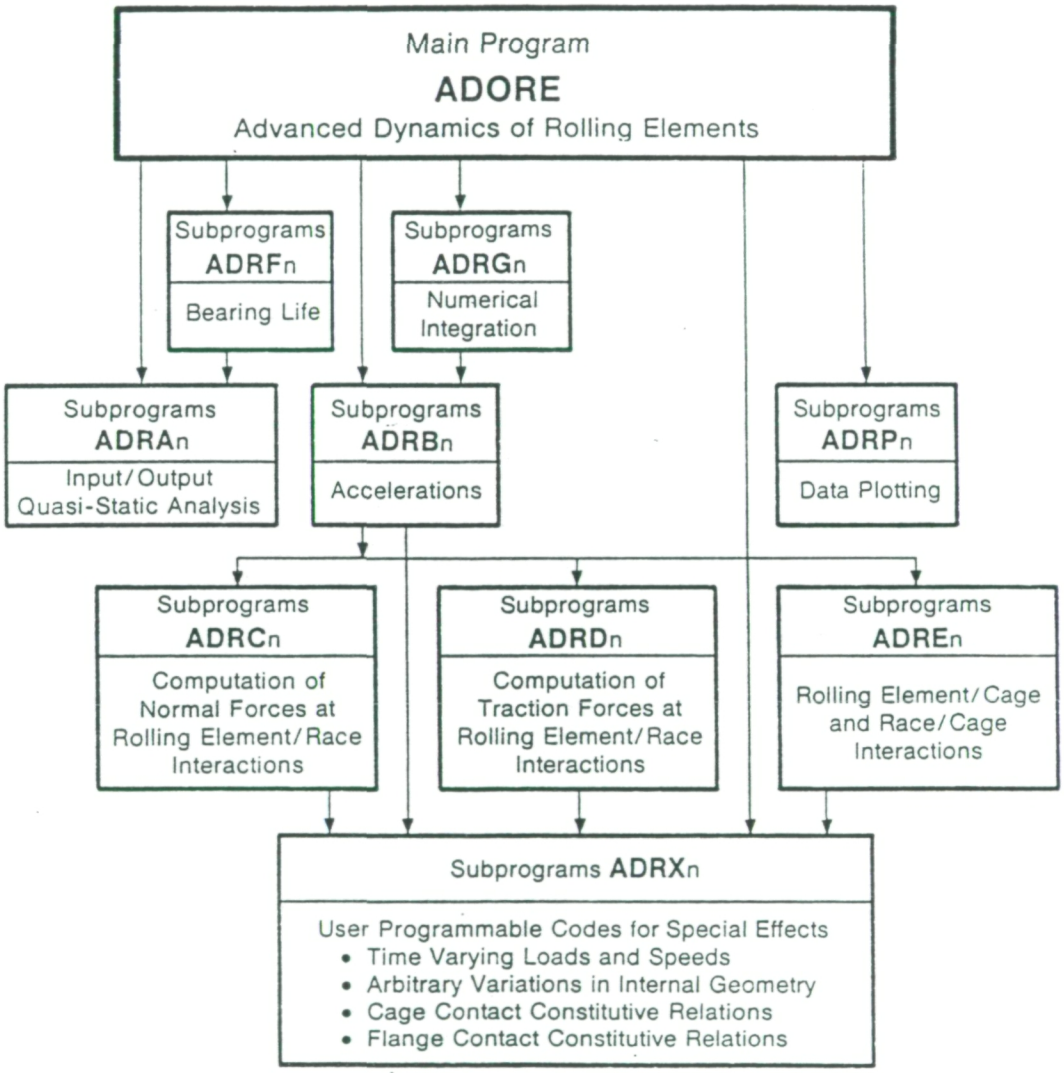

EXHIBIT 3.15.2 A SCHEMATIC OVERVIEW OF THE ADORE PROGRAM

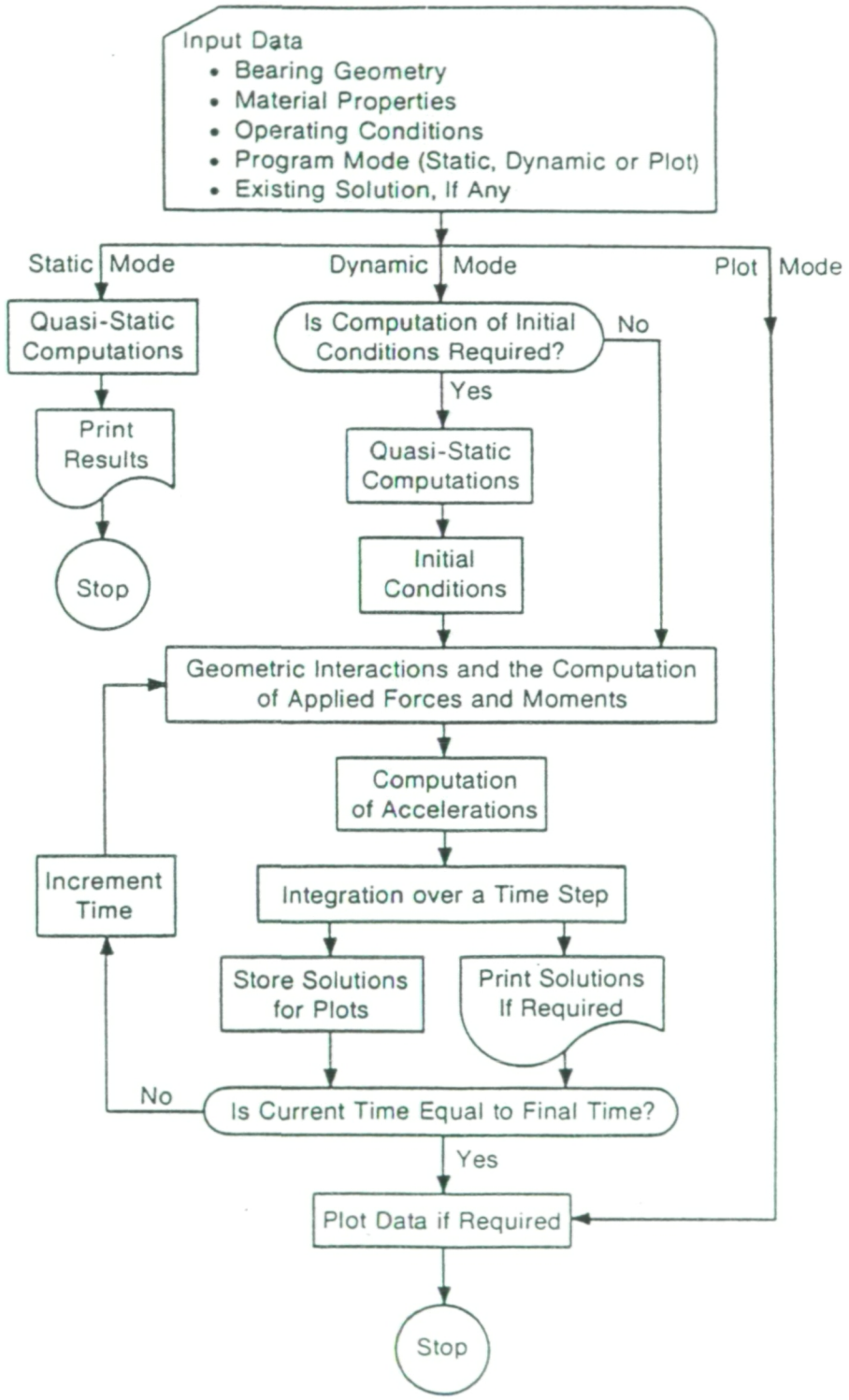

(4) For an oil lubricated bearing, the traction at the rolling element/ract interface is determined by elastohydrodynamic traction models based on the theological behavior of the lubricant. In the case of a solid lubricated bearing, or under conditions when an elastohydrodynamic traction model is no longer valid, an arbitrary traction curve may be used.

(5) The classical theories of laminar or turbulent flow are used to simulate the churning and drag effect. The essential inputs are the effective lubricant viscosity and density. Generally, a volume averaged density (which is taken to be equal to the lubricant density multiplied by the fraction of bearing cavity filled with the lubricant) is used to estimate the churning and drag effects.

STATUS OF THE BEARING MODELING PROGRAM ADORE

ADORE was purchased by NASA/MSFC to enable it to perform the dynamic analysis of bearing systems used in the SSME turbopumps, and has been installed on the MSFC UNIVAC 1100/80 computer system.

ADORE had been developed on a CDC CYBER computer system, and as such, some code modification was necessary to install the program on the UNIVAC. Specifically, the UNIVAC version required double precision variables because the default size of a UNIVAC 'word' is one half that of the CDC 'word'. Dr. Gupta, the author of ADORE, stipulated the use of double precision variables to avoid truncation errors. This conversion required changing all trigonometric function calls to their double precision equivalent, e.g., COS(X) was changed to DCOS(X). All constant numbers used in the CALL statement were converted to their corresponding double precision equivalents, e.g., 1.23E-10 was changed to 1.23D-10. All DATA statements that contained constant numbers had to be converted as well. However, the use of double precision variables doubles the size of memory required to store program data and the program then becomes too large. For this reason, ADORE was 'segmented' into two segments to reduce the amount of memory required. The first segment contains the analytical routines of ADORE, while the second segment contains the plotting routines. Because these two segments do not need to run at the same time, they can overlay each other in memory, thus reducing memory requirements considerably. The conversions outlined here required considerable editing, compilation, and debugging of the FORTRAN source code.

Once the modifications mentioned above had been completed and the program made operational, several tests runs were made to check the program and its output. Test cases given as examples in the "ADORE" manual were run to conduct checks on the program.

Next, input records necessary for modeling the 57 mm bearings used on the turbine-end of the SSME LOX turbopump were prepared for making preliminary runs with ADORE. The case of pure axial loading was considered first, with all balls in the bearing being of equal size. The case of unequal ball sizes will be run later on, after the simpler cases have been computed. Several problems were encountered and solved while making these preliminary runs. The program was successfully executed for 150 time steps for the case of axial loading.

4.0 REFERENCES

1. Bearing Tester Data Compilation, Analysis, and Reporting and Bearing Math Modeling, Final Report. SRS Technologies, (TR84-022); Contract NAS8-34687, May 1984.
2. Assessment of the Operating Characteristics of the SSME LOX Turbopump Pump-End Bearing, Final Report. SRS Technologies (TR85-009); Purchase Order H-78194B; December 1984.
3. Rouse, Hunter, Advanced Mechanics of Fluids. John Wiley and Sons, Inc., New York, 1959, pp. 390-394.
4. Free Convection Heat Transfer from a Rotating Horizontal Cylinder to Ambient Air with Interterometric Study of Flow, G. A. Etemad, Trans ASME, Vol. 77, 1955, pp. 1283-1289.
5. Vasta, Joseph A., Understanding Data Base Management Systems. Wadsworth Publishing Company, Belmont, CA, 1985.
6. Freund, John E., Statistics. Prentice-Hall, Inc., Englewood Cliffs, NJ, 1970.